UNIVERSIDADE FEDERAL DE MINAS GERAIS
Programa de Pós-Graduação em Engenharia Metalúrgica, Materiais e de Minas

Tese de Doutorado

Desenvolvimento e aplicação de revestimentos nanocerâmicos de zircônia em ligas níquel-titânio

Autora: Natália Isabel de Azevedo Lopes
Orientador: Prof. Vicente Tadeu Lopes Buono

Maio/2018
Natália Isabel de Azevedo Lopes

Natália Isabel de Azevedo Lopes

Desenvolvimento e aplicação de revestimentos nanocerâmicos de zircônia em ligas níquel-titânio

Tese de Doutorado apresentada ao Programa de Pós-Graduação em Engenharia Metalúrgica, Materiais e de Minas da Escola de Engenharia da Universidade Federal de Minas Gerais.

Área de Concentração: Ciência e Engenharia de Materiais

Orientador: Prof. Vicente Tadeu Lopes Buono

Belo Horizonte
Universidade Federal de Minas Gerais
Escola de Engenharia
2018

Lopes, Natália Isabel de Azevedo.
L864d Desenvolvimento e aplicação de revestimentos nanocerâmicos de zircônia em ligas níquel-titânio [manuscrito] / Natália Isabel de Azevedo Lopes. – 2018.
xiii, 103 f., enc.: il.

Orientador: Vicente Tadeu Lopes Buono.

Tese (doutorado) - Universidade Federal de Minas Gerais, Escola de Engenharia.

Inclui bibliografia.

.

1. Materiais - Teses. 2. Ciência dos materiais - Teses. 3. Biomateriais - Teses. 4. Ligas de níquel-titânio - Teses. I. Buono, Vicente Tadeu Lopes. II. Universidade Federal de Minas Gerais. Escola de Engenharia. III. Título.

CDU: 620(043)

Ao meu eterno orientador, professor Vicente Buono, pelo apoio, pela amizade, pelo carinho e pela confiança que me acompanham desde os tempos mais longínquos. O que você me ensinou não cabe em uma tese.

AGRADECIMENTOS

Ao CNPq, à Capes e à Fapemig pelo apoio financeiro na realização desse projeto e ao Erasmus Mundus pela oportunidade de aprendizado na Université de Lille.

Aos membros da banca de qualificação, professor Leandro Arruda e professora Vanessa Lins, e da banca de defesa, professora Ana Cecília Viana, professora Dalila Sicupira, professor Eduardo Nunes e professor Nicolau Castro, pelas valiosas contribuições para o desenvolvimento e para o aprimoramento deste trabalho.

Agradeço ao professor Alexandre Legris e aos membros do UMET/Université de Lille pelo acolhimento afetuoso. Ao engenheiro Nicolas Nuns, do UCCS, pelas análises por ToF-SIMS. Ao Damien Creton pelo bom humor cotidiano e pelos *carambar scientifique*. Ao Addad Ahmed pelas discussões sempre enriquecedoras e agradáveis. Ao professor Franck Béclin pela disponibilidade durante toda minha estadia e pelos valiosos ensinamentos.

À professora Vanessa Lins e à equipe do Laboratório de Corrosão-DEQ/UFMG, particularmente à Renata Soares e à Luíza Esteves, pela ajuda e pela disponibilidade em momentos essenciais. Ao LAQ-DEMET/UFMG, INCT-Acqua, principalmente à Patrícia Freitas, pela realização das análises por ICP-OES. Aos professores e funcionários do DEMET, especialmente ao professor Dagoberto Brandão, à professora Andreia Bicalho e à Patrícia Azevedo, por serem parte fundamental da minha história e do meu crescimento, e pelo cuidado ao longo desses anos.

Ao Dr. Evandro Alvarenga pelo privilégio da convivência, pelo precioso aprendizado em superfícies e corrosão e pelo entusiasmo compartilhado pela pesquisa.

Ao LabTerm pelo companheirismo ilimitável e pelos cafés incontáveis. Leandro, Ciça, Bebel, Bárbara e Laís, a convivência com vocês foi um prazer e um aprendizado. Ao Pedro e ao Nelson pela ajuda, pela companhia em madrugadas e feriados, e pelas discussões produtivas. Pelas improdutivas também.

Meu agradecimento afetuoso a minha mãe e meu irmão, pelo incentivo e pelo carinho durante toda minha vida, e por serem exemplos de força e dedicação. À Jéssica pelo apoio incondicional e a todos os amigos que tornaram essa caminhada mais leve.

SUMÁRIO

LISTA DE FIGURAS

LISTA DE TABELAS

LISTA DE NOTAÇÕES

ΔT	Histerese térmica entre as transformações martensítica e reversa
Af	Temperatura final da transformação reversa
AFM	Microscopia de força atômica
As	Temperatura de início da transformação reversa
DRX	Difração de raios X
DSC	Calorimetria exploratória diferencial
EDX	Espectroscopia de energia de raios X
FIB	Focused ion beam
Md	Temperatura limite de formação da martensita induzida por tensão
MEV	Microscopia eletrônica de varredura
MET	Microscopia eletrônica de transmissão
Mf	Temperatura de término da transformação martensítica
Ms	Temperatura de início da transformação martensítica
Nf	Número de ciclos até fratura
NiTi	Ligas equiatômicas de níquel e titânio
OCP	Potencial de circuito aberto
PDDA	Poli(cloreto de dialildimetilamônio)
polyDADMAC	Poli(cloreto de dialildimetilamônio)
Ra	Rugosidade média
Rf	Temperaturas final de formação da fase R
Rpv	Rugosidade pico-vale
Rs	Temperaturas de início de formação da fase R
SCE	Eletrodo saturado de calomelano
TEM	Microscopia eletrônica de transmissão
TTT	Tempo-temperatura-transformação
ToF-SIMS	Time of Flight Secondary Ion Mass Spectrometry

RESUMO

A corrosão e a degradação das ligas NiTi utilizadas como biomateriais representam uma preocupação constante, devido aos efeitos alergênicos, de toxicidade e carcinogenicidade associados à liberação de íons níquel no organismo. Falhas prematuras causadas por corrosão e fadiga também são críticas nas aplicações biomédicas dessas ligas. Nesse trabalho, estudou-se a aplicação de um revestimento nanoestruturado de zircônia e seus efeitos nas propriedades das ligas NiTi. Inicialmente, estudou-se a preparação superficial de ligas NiTi usando polimento eletrolítico. Os resultados mostraram que o polimento eletrolítico reduz a rugosidade superficial, remove camadas externas ricas em níquel e aumenta a resistência à corrosão das ligas. Em seguida, foram definidas as melhores condições para aplicação do revestimento de zircônia, a partir de eletrólitos constituídos por sais de zirconila, com adições de metanol e de um polímero catiônico. Os melhores resultados foram obtidos usando uma solução metanólica de $ZrOCl_2$ com adição de polyDADMAC. Uma caracterização mais completa do revestimento, obtido nessas condições, foi realizada em sequência, comparando as propriedades dos depósitos formados com e sem preparação superficial usando polimento eletrolítico. Realizou-se ainda análises da resistência e da estabilidade do revestimento submetido a ambientes corrosivos e solicitações mecânicas, simulando condições fisiológicas. Os resultados mostraram que o revestimento obtido no fio de NiTi após polimento eletrolítico não apresenta defeitos e é mais homogêneo e espesso do que o obtido sem polimento. Após teste de imersão em solução fisiológica artificial, durante 12 meses, o teor de níquel liberado em solução foi insignificante e a superfície dos fios foi totalmente coberta por uma camada de fosfato de cálcio, um indicador da bioatividade do material. Após testes de dobramento e fadiga, foram observadas algumas trincas no revestimento. Não houve, entretanto, delaminação expressiva e o revestimento de zircônia manteve suas propriedades protetivas. De um modo geral, o revestimento de zircônia obtido nesse estudo pode ser considerado bom candidato para melhoria das propriedades superficiais de ligas NiTi para aplicações biomédicas, incluindo implantes, *stents*, fios ortodônticos, instrumentos endodônticos e outros.

Palavras-chave: *ligas níquel-titânio; biomateriais; modificação de superfícies; nanorevestimentos; resistência à corrosão.*

ABSTRACT

Corrosion and degradation of NiTi alloys used as biomaterials remain a concern due to toxicity, carcinogenicity, and allergenic effects associated with the release of nickel ions in the human body. Premature failures caused by corrosion and fatigue are also critical in biomedical applications of these alloys. In this work, the application of a nanostructured zirconia coating and its effects on the fracture and corrosion resistance of NiTi alloys were evaluated. Initially, the surface preparation of NiTi alloys was studied using electrolytic polishing. The results showed that electrolytic polishing reduces surface roughness, removes nickel-rich external layers and increases corrosion resistance of NiTi alloys. Subsequently, the optimal conditions for application of the zirconia coating were defined, using electrolytes containing zirconyl salts, with additions of methanol and a cationic polymer. The best results were obtained using a methanolic solution of $ZrOCl_2$ with the addition of polyDADMAC. Then, a more complete characterization of the coating, obtained under these conditions, was performed, comparing the characteristics of the deposits formed on wires with and without surface preparation using electrolytic polishing. Analyzes of coating resistance and stability when submitted to corrosive environments and mechanical stresses, simulating physiological conditions, were also performed. The results showed that the coating obtained on the NiTi wire after electrolytic polishing is free of defects, more homogeneous and slightly thicker than that obtained without prior polishing. After immersion test in artificial physiological solution, for 12 months, the solubilized nickel was negligible, and the surface of the wires was covered by a layer of calcium phosphate, an indication of the bioactivity of the material. After bending and fatigue tests, cracks were observed in the coating, however, there was no significant delamination and the zirconia deposit maintained its protective properties. In general, the zirconia coating obtained in this study can be considered a good candidate for the improvement of surface properties of NiTi alloys for biomedical applications, including implants, stents, orthodontic wires, endodontic instruments, and others.

Keywords: *nickel-titanium alloys; biomaterials; surface modification; nanocoatings; corrosion resistance.*

1. Introdução

1.1 Relevância da pesquisa

Desde sua descoberta, em 1963, o uso das ligas equiatômicas de níquel e titânio (NiTi) tem se expandido para as mais diversas aplicações industriais, especialmente nas áreas de estruturas, automotiva, aeroespacial, robótica e biomédica. Suas propriedades de superelasticidade e efeito memória de forma, aliadas a uma boa resistência à corrosão e biocompatibilidade, tornam a aplicação dessas ligas particularmente importante na área biomédica, sendo usadas, por exemplo, na confecção de implantes ortopédicos, cateteres, *stents*, fios ortodônticos e instrumentos endodônticos.

A superelasticidade confere ao material um comportamento elástico não linear, permitindo que ele sofra grandes deformações, decorrentes do carregamento mecânico, com baixa deformação plástica residual após a retirada da carga. Este comportamento é associado a uma transformação de fase martensítica induzida por tensão, em que são formadas variantes de martensita convenientemente orientadas em relação à força aplicada, causando a deformação do material. Com a retirada da carga, o material retorna ao estado austenítico e, consequentemente, à sua forma original. Já no efeito memória de forma, uma deformação pseudoplástica no estado martensítico, que ocorre por um mecanismo de reorientação/demaclação, é recuperada por meio da transformação reversa da martensita deformada em austenita, ocasionada pelo aquecimento acima de uma temperatura crítica.

Em aplicações biomédicas, além de propriedades mecânicas adequadas, as ligas NiTi devem apresentar excelente biocompatibilidade e resistência à corrosão em meio fisiológico. Estudos sobre corrosão e liberação de íons níquel — reconhecidamente citotóxicos, mutagênicos e alergênicos — nessas ligas são limitados e controversos, uma vez que sua resistência à corrosão é extremamente dependente de suas condições superficiais. Embora uma boa resistência à corrosão seja esperada, devido à formação espontânea de uma camada passivadora de óxido de titânio, defeitos e irregularidades na superfície agem como sítios iniciais de corrosão e como concentradores de tensão, podendo iniciar a nucleação de trincas e causar falhas prematuras.

De um modo geral, a resistência à fratura e à corrosão de uma liga NiTi estão interligadas e dependem fortemente de sua qualidade superficial. A aplicação de um revestimento uniforme, coeso e com boa aderência ao substrato pode suavizar a heterogeneidade de sua superfície, atenuando os efeitos dos concentradores locais de tensão, diminuindo a nucleação de trincas e o risco de fratura por fadiga e, ainda, melhorar sua resistência à corrosão.

A zircônia apresenta reconhecida biocompatibilidade, aliada à excelente resistência à corrosão e à abrasão. Recobrimentos de zircônia possuem boa aderência e têm sido bastante utilizados com o objetivo de melhorar as propriedades superficiais de substratos metálicos para as mais diversas aplicações. Dessa forma, a aplicação de um revestimento nanocerâmico de zircônia em ligas NiTi pode aumentar sua resistência à corrosão e à fratura, sem afetar a superelasticidade e o efeito memória de forma. Neste projeto, estudou-se a aplicação de revestimentos nanoestruturados de zircônia por eletrodeposição, avaliando seus efeitos nas propriedades das ligas NiTi.

1.2 Objetivos

Este trabalho teve como objetivo geral melhorar as propriedades superficiais de ligas NiTi por meio da aplicação de revestimento nanocerâmico de zircônia. Para tanto, foram estabelecidos os seguintes objetivos específicos:

i. Definir as melhores condições para preparação da superfície das ligas NiTi antes da deposição, usando polimento eletrolítico;

ii. Comparar diferentes condições de aplicação de revestimento, buscando a obtenção de um filme mais uniforme, com menor rugosidade superficial e que resulte em uma maior resistência à corrosão;

iii. Avaliar a estabilidade e a aderência do revestimento por meio de testes fadiga e de dobramento em três pontos e testes de imersão e de resistência à corrosão em solução fisiológica artificial.

1.3 Estrutura da tese

Essa tese se divide em seis capítulos, que foram estruturados da seguinte forma: No capítulo 1 são apresentadas as justificativas para o desenvolvimento do projeto e seus objetivos. No capítulo 2 é feita uma breve revisão da literatura referente às ligas NiTi, suas aplicações e limitações, e sobre conceitos envolvidos na eletrodeposição de zircônia. Os capítulos 3, 4 e 5 são constituídos pelos trabalhos publicados durante a realização desta tese, na forma em que foram submetidos. Finalmente, no capítulo 6 são apresentadas as considerações finais, incluindo as principais conclusões, que integram os resultados dos trabalhos publicados, e as sugestões para trabalhos futuros.

2. Revisão Bibliográfica

2.1 Ligas NiTi

As ligas NiTi, pertencentes ao grupo dos materiais inteligentes (*smart materials*), apresentam duas propriedades extraordinárias: o efeito memória de forma e a superelasticidade. O efeito memória de forma foi observado pela primeira vez em 1932 por Arne Ölander, em uma liga de ouro e cádmio, mas o termo "memória de forma" só foi utilizado em 1941, e o uso das ligas se popularizou somente a partir da descoberta das ligas equiatômicas de níquel e titânio, em 1963, por Buehler e colaboradores, no *Naval Ordenance Laboratory* em Silver Springs, Maryland – EUA [1].

No efeito memória de forma, uma deformação não elástica, ou pseudoplástica, de até 8%, na fase de baixa temperatura, pode ser recuperada por meio de uma transformação reversa causada pelo aquecimento a uma temperatura acima de uma temperatura crítica. Já a superelasticidade apresenta-se na fase de alta temperatura das ligas, em que grandes deformações não lineares, de até 18%, decorrentes de um carregamento mecânico, podem ser recuperadas ao se retirar a carga aplicada. Estes dois efeitos estão relacionados à transformação martensítica, uma transformação de fase adifusional, na qual os átomos se movem cooperativamente por um mecanismo de cisalhamento, sem alterar a composição química da matriz, e se rearranjam em uma nova estrutura cristalina mais estável [2]. Os mecanismos envolvidos na transformação martensítica nas ligas NiTi serão discutidos na seção 2.1.2.

As ligas NiTi são utilizadas nos mais diversos segmentos, principalmente automotivo, aeroespacial e biomédico. A primeira bioaplicação de uma liga NiTi foi em 1971, em fios ortodônticos superelásticos. Seu uso passou por uma expansão significativa quando começaram a ser empregadas em cirurgias minimamente invasivas e após a aprovação de uma âncora de NiTi para cirurgias ortopédicas pela *US Food and Drug Administration*, em 1989. Embora dispositivos fabricados com ligas NiTi sejam consideravelmente mais caros do que os de aço inoxidável, essas ligas possuem comportamento superior em aplicações biomédicas, tais como resistência à corrosão e biocompatibilidade, além de apresentarem propriedades físicas únicas, que replicam

ossos e tecidos humanos. Atualmente, as ligas com memória de forma são usadas na fabricação de diversos dispositivos, principalmente em *stents*, suturas, pinças cirúrgicas, clipes para aneurisma, fios guia, âncoras ortopédicas, limas endodônticas, fios ortodônticos e armações para óculos [1].

2.1.1 Sistemas Ni-Ti

O diagrama de equilíbrio de fases Ni-Ti é mostrado na Figura 2.1. Para o estudo das ligas NiTi com efeito memória de forma, a região de interesse do diagrama é aquela delimitada pelas fases Ti_2Ni e $TiNi_3$. Observa-se pelo diagrama que a fronteira no lado rico em titânio da região correspondente à fase TiNi é praticamente vertical, enquanto no lado rico em níquel, sua solubilidade diminui significativamente com o decréscimo da temperatura. Em temperaturas abaixo de 650°C a fase TiNi é encontrada apenas em uma faixa estreita de composição, entre 50,0 e 50,5 %at. Ni [3].

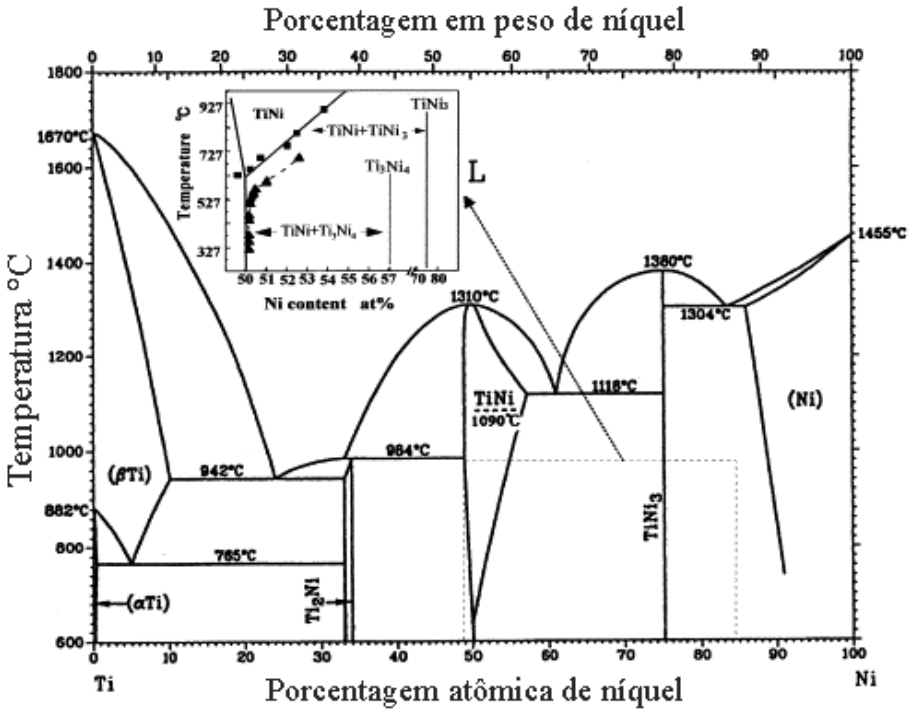

Figura 2.1 – Diagrama de equilíbrio de fases Ni-Ti [2].

A fase TiNi, ou fase β, correspondente à fase austenítica, possui uma estrutura cúbica do tipo B2 (CsCl), do grupo espacial Pm-3m, com parâmetro de rede de 0,3015 nm à temperatura ambiente [4]. A fase Ti_2Ni é cúbica, pertencente ao grupo espacial Fd3m,

com parâmetro de rede de 1,132 nm. O óxido que aparece predominantemente nessa liga é o Ti_4Ni_2O, que possui estrutura muito semelhante à do Ti_2Ni. A fase $TiNi_3$ possui estrutura hexagonal do tipo DO_{24}, grupo espacial $P6_3/mmc$, com parâmetros de rede a = 0,51010 nm, c = 0,83067 nm e c/a = 1,6284 [2].

2.1.2 Transformação martensítica

Conforme mencionado anteriormente, nas ligas NiTi, a austenita (B2) — fase β ou de alta temperatura — possui estrutura cúbica de corpo centrado ordenada. Durante a transformação martensítica, a austenita se transforma em martensita B19' — fase de baixa temperatura e de simetria inferior — que possui estrutura monoclínica e é pertencente ao grupo espacial $P2_1/m$. Os parâmetros de rede são dependentes da composição química e, por exemplo, para uma liga 49,2%$_{at.}$Ni, são: a = 0,2898 nm, b = 0,4108 nm, c = 0,4646 nm e β = 97,78 [3].

Em ligas NiTi trabalhadas a frio e recozidas em temperaturas apropriadas (cerca de 400°C), nas quais existe alta densidade de deslocações remanescentes, ou em ligas NiTi ricas em níquel envelhecidas, causando a precipitação de Ti_3Ni_4, um outro tipo de transformação pode ocorrer para a chamada fase R. A fase R foi identificada, inicialmente, como uma estrutura romboédrica e essa transformação era considerada como um efeito precursor da transformação martensítica para a fase B19'. Posteriormente, foi estabelecido que a fase R é trigonal — pertencente ao grupo P3 com parâmetros de rede de a = 0.738 nm e c = 0.532 nm, sem centro de simetria — e que a transformação B2 → R é uma transformação martensítica que compete com a transformação B2 → B19'. Se a transformação para a fase R aparece primeiro, ocorre uma transformação sucessiva B2 → R → B19'. No entanto, se a transformação para a fase B19' ocorre primeiro, a transformação para a fase R é suprimida. Os indicativos de que a transformação de B2 para R é mesmo uma transformação martensítica são:

i. placas de fase R são claramente observadas em microscópios eletrônicos;

ii. a transformação direta de B2 para B19' ocorre sem efeitos precursores, dependendo das condições; e

iii. o efeito memória de forma e a superelasticidade, característicos da transformação martensítica termoelástica, também são observados associados à transformação da fase R [2].

Tanto a fase R como a fase B19’ são afetadas pela distorção de rede ocasionada pela precipitação e por campos de tensões gerados por deslocações. No entanto, o efeito é maior na fase B19’ do que na fase R, o que faz com que suas temperaturas de transformações sejam separáveis. Na Figura 2.2 é mostrada uma curva obtida por Calorimetria Exploratória Diferencial (DSC - *Differential Scanning Calorimetry*) típica de uma liga NiTi em que a transformação martensítica ocorre em duas etapas: B2 → R → B19’. Na curva superior, correspondente ao resfriamento do material, o primeiro pico de transição exotérmica corresponde à transformação da fase B2 para a fase R, sendo Rs e Rf as temperaturas de início e fim de formação da fase R, respectivamente. O segundo pico exotérmico da curva é devido à transformação da fase R para a fase B19’, que começa na temperatura indicada por Ms e termina em Mf. Já a transformação reversa de B19’ para B2, que ocorre em apenas uma etapa, durante o aquecimento, é vista no pico endotérmico da curva inferior, com início em As e término em Af.

Do ponto de vista termodinâmico, sabe-se que a transformação martensítica tem como força motriz a diferença de entropia entre as fases austenítica e martensítica. A magnitude da variação de entropia dessa transformação é proporcional à distorção da rede cristalina associada a ela. Como a distorção na transformação para a fase R (~1%) é pequena em comparação à da fase B19’ (10%), a mudança na entropia também é menor. Isso indica que a transformação em dois estágios ocorre na sequência do aumento da distorção da rede cristalina, ou seja, da entropia [2].

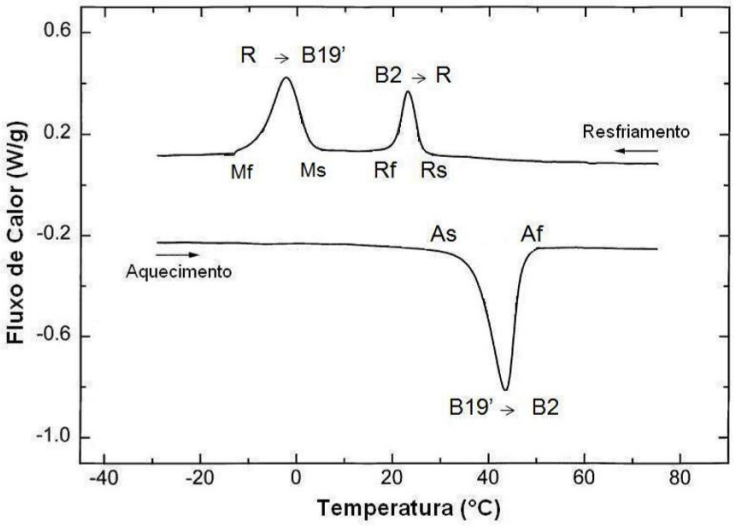

Figura 2.2 – Representação de uma curva DSC de uma liga NiTi equiatômica com transformação martensítica em duas etapas [5].

A transformação martensítica está associada a uma mudança de forma, ilustrada na Figura 2.3a, que gera uma zona de alta deformação ao redor da variante de martensita formada na matriz de austenita. Como essa transformação é de primeira ordem, ela acontece pelo processo de nucleação e crescimento e, para esse processo, é muito importante que a deformação gerada seja amenizada. As duas maneiras possíveis para a acomodação dessa deformação são por escorregamento ou por maclação — Figura 2.3b e Figura 2.3c, respectivamente. Estes mecanismos são conhecidos como deformações invariantes de rede, já que não causam qualquer alteração na estrutura cristalina da martensita. O mecanismo de acomodação depende do tipo de liga, mas a maclação é a deformação invariante de rede de interesse em ligas com memória de forma, já que o escorregamento é um processo irreversível.

No processo de maclação são originadas duas regiões simétricas em relação a um eixo de rotação, denominado contorno de macla [4]. O termo contorno de macla também pode se referir aos contornos de variantes individuais de martensita, que se comportam como maclas em relação às variantes adjacentes. Como os mecanismos de deformação invariante de rede não são suficientes para aliviar completamente a deformação ocasionada pela transformação martensítica, variantes múltiplas de martensita se combinam em um processo de autoacomodação. Em função do processo de autoacomodação, não há mudança na forma em decorrência da transformação

martensítica durante o resfriamento. Quando a martensita autoacomodada é deformada, a deformação se dá por movimento dos contornos de macla, que é equivalente à conversão de uma variante de martensita à outra [2].

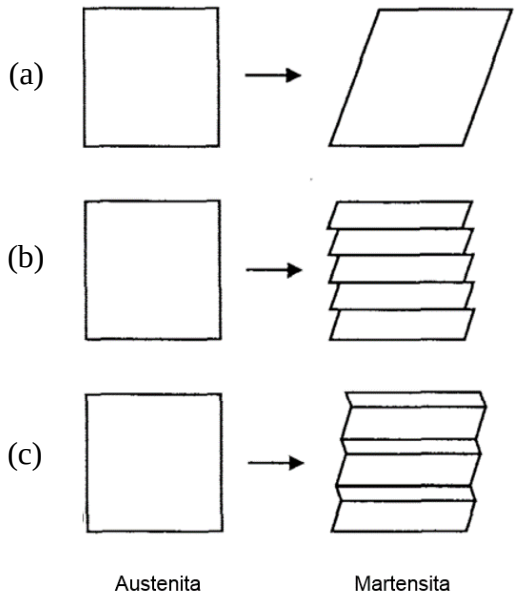

Figura 2.3 – Ilustração dos tipos de deformação invariante de rede da transformação martensítica: (a) mudança de forma na transformação martensítica; (b) acomodação por escorregamento; (c) acomodação por maclação [4].

Existe entre as transformações martensítica e reversa uma histerese térmica ($\Delta T = Af - Ms$), associada ao atrito gerado pelo movimento dos contornos de macla e variantes, que pode ser interpretada como a energia dissipada pelo sistema durante um ciclo de transformação. A magnitude dessa histerese varia de acordo com a liga, mas valores de 20 a 40°C são comuns em ligas com memória de forma [6]. A histerese associada à transformação da fase R é muito pequena (1 a 2°C), provavelmente pela baixa deformação que ocorre nessa transformação.

A martensita também pode ser formada, mesmo em temperaturas acima de Ms, pela aplicação de tensão, dando origem à chamada martensita induzida por tensão. Ao contrário da transformação martensítica induzida termicamente — onde variantes com diferentes orientações se autoacomodam (Figura 2.4a) — na transformação induzida por tensão somente as variantes orientadas no sentido da força aplicada irão crescer (Figura 2.4b) [4]. Nesta situação, a deformação da martensita ocorre pelo mecanismo de

reorientação/demaclação e, ao se retirar a carga aplicada, a martensita torna-se instável e a transformação reversa para a austenita ocorre, resultando na recuperação da forma do material.

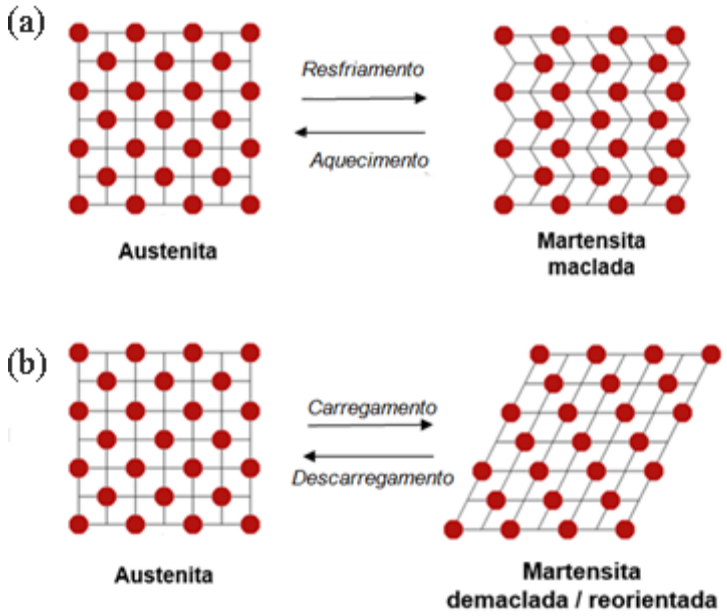

Figura 2.4 – Representação esquemática da transformação martensítica: (a) Induzida termicamente; (b) induzida por tensão.

2.1.3 Efeitos memória de forma e superelasticidade

Uma vez compreendidos os mecanismos envolvidos na transformação martensítica em ligas NiTi, o entendimento dos efeitos memória de forma e superelasticidade se torna mais claro. Tais efeitos podem ser categorizados em: efeito memória de forma, efeito memória de forma reversível e superelasticidade; conforme ilustrado na Figura 2.5.

No efeito memória de forma, um material no estado austenítico é resfriado abaixo de Mf, se tornando completamente martensítico. Nesse momento, não ocorre mudança em sua forma macroscópica, pois são formadas variantes de martensita autoacomodadas. No entanto, ao se aplicar uma tensão no material, em uma temperatura inferior a Mf, o material sofre uma deformação pseudoplástica, por mecanismos de reorientação/demaclação, formando uma martensita deformada. Essa deformação pseudoplástica resulta na alteração de forma no material. No entanto, ao se aquecer o

material a temperaturas acima de Af, faz-se com que ele retorne ao estado austenítico, e à sua forma original, pela transformação reversa.

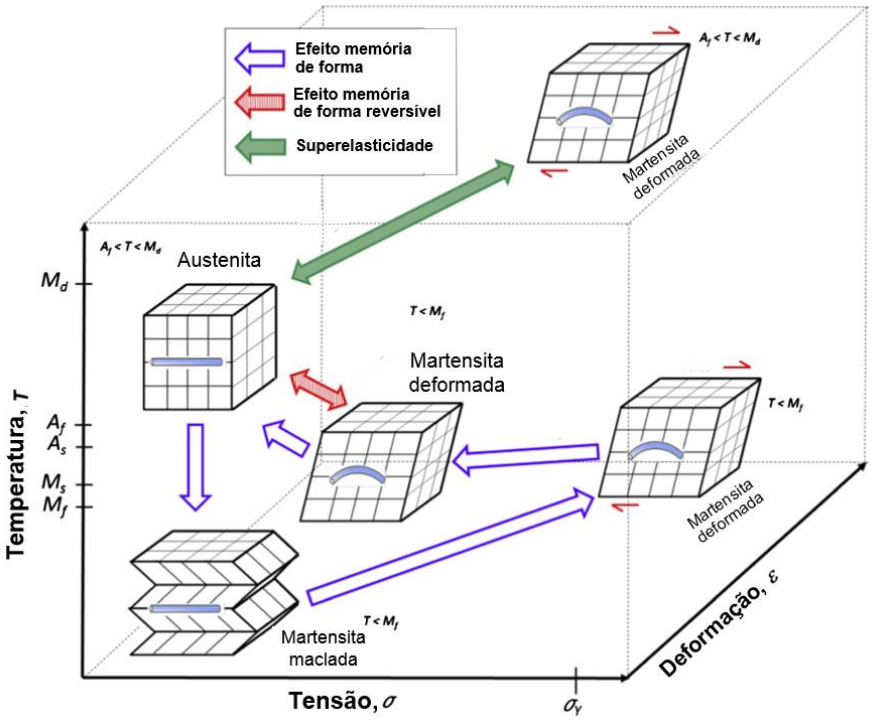

Figura 2.5 – Esquema ilustrativo dos efeitos memória de forma e memória de forma reversível e superelásticos [1].

O efeito memória de forma reversível (*two-way shape memory effect*) se difere do efeito memória de forma (*one-way shape memory effect*) por sua capacidade em "memorizar a forma" tanto no estado austenítico como no martensítico. Essa liga é menos utilizada comercialmente devido às dificuldades no tratamento térmico para aquisição da memória de forma. Além disso, o percentual de deformação recuperado é aproximadamente metade do recuperado em ligas com memória de forma [1].

Já a superelasticidade ocorre em temperaturas superiores à Af, quando se aplica tensão em uma liga que se encontra em seu estado completamente austenítico, dando origem à martensita induzida por tensão. Na transformação induzida por tensão, variantes favoravelmente orientadas em relação à força aplicada são formadas, causando a deformação do material. Ao retirar-se a carga, o material retorna ao estado austenítico e, consequentemente, à sua forma original. A temperatura limite na qual a martensita pode

ser induzida por tensão é denominada M_d — acima dessa temperatura, o material apresenta comportamento elasto-plástico característico de metais convencionais e a aplicação de uma tensão acima do limite de escoamento da austenita passa a resultar em uma deformação plástica [6].

2.1.4 Processos de fabricação

A fabricação das ligas NiTi envolve as seguintes etapas: fundição, forjamento, laminação a quente, trefilação a frio, conformação e tratamento de memória de forma. Devido à alta reatividade do titânio com o oxigênio, a liga é geralmente fundida em alto vácuo, por indução de alta frequência. Outros métodos de fusão também podem ser aplicados, tais como fusão por feixe de elétrons, fusão a arco com proteção de argônio e fusão a arco de plasma. A principal vantagem da fusão por indução está no controle mais preciso da composição química da liga, uma vez que as temperaturas de transformação são extremamente sensíveis a variações no teor de níquel. Se a operação for conduzida com os devidos cuidados, a variação na temperatura Ms pode ser controlada em ± 5°C. Para o controle mais preciso do processo, o forno de indução pode operar com um sistema a vácuo, que retira uma amostra da liga fundida e mede rapidamente sua temperatura Af. Em seguida, adiciona-se titânio ou níquel, conforme a necessidade, até que a temperatura Af desejada seja atingida [7].

Após o processo de fundição, a liga solidificada é forjada e laminada a quente, na forma de barras ou placas. A liga é facilmente trabalhada em temperaturas superiores a 527°C, contudo, embora a usinabilidade das ligas NiTi melhore com o aumento da temperatura, a dureza da superfície também aumenta devido à oxidação. Assim, a temperatura ideal para o trabalho a quente está em torno de 800°C. Comparado com o trabalho a quente, o trabalho a frio das ligas NiTi é muito mais difícil. Sua usinabilidade depende da composição química da liga, sendo que quanto maior o teor de níquel, pior a usinabilidade. O trabalho a frio torna-se especialmente difícil em ligas com teores de níquel superiores 51%at. [7].

Para se processar ligas NiTi de maneira satisfatória, uma linha combinando etapas de trefilação e recozimento é necessária. Problemas de aderência entre os fios de NiTi e as ferramentas são frequentes, sendo necessário o uso de lubrificantes adequados. Embora

uma camada de óxido mais espessa na superfície do fio diminua o atrito com as ferramentas, ela afeta suas características de memória de forma. A usinagem das ligas NiTi é muito difícil e, geralmente, exige o uso de ferramentas de carboneto de tungstênio. Após trefilação, o NiTi é conformado e fixado na forma final desejada e passa, então, pela última etapa de processamento, o tratamento de memória de forma. Nessa etapa, o material é, usualmente, aquecido entre 350 e 450°C, por tempos que variam de 10 a 100 minutos, de acordo com o tamanho do produto. Como a temperatura de tratamento afeta as temperaturas de transformação e outras características do efeito memória de forma, a temperatura do forno é controlada com precisão e a circulação de ar dentro dele deve ser suficiente para garantir a homogeneidade da temperatura em todo o material. Quando o aquecimento é finalizado, os materiais são retirados do forno e resfriados. Existem ainda diversos outros métodos para revelar o efeito memória de forma, entre eles o envelhecimento, aplicável em ligas com alto teor de níquel (superior a 50,5%at.), no qual a liga é tratada em alta temperatura e envelhecida a 400°C, por até cinco horas. O tratamento térmico para a superelasticidade é, basicamente, o mesmo utilizado para o efeito memória de forma [7].

Recentemente, vêm sendo desenvolvidas técnicas alternativas para a produção de ligas NiTi empregando-se a metalurgia do pó. Em rotas de processamento via metalurgia do pó, alguns problemas associados à fundição, tais como segregação e crescimento rápido dos grãos durante as etapas de trabalho a quente, são evitados. Além disso, tais rotas permitem um controle mais preciso da composição química e a produção de componentes com formas variadas, minimizando o número de etapas subsequentes de usinagem [8].

2.1.5 Comportamento mecânico

O comportamento mecânico das ligas NiTi está diretamente relacionado às suas temperaturas de transformação e à temperatura de teste, ou temperatura de deformação (Td), podendo ser dividido em três regimes principais [3,9,10]:

i. Td < Mf – A liga encontra-se, inicialmente, com estrutura completamente martensítica e a deformação ocorre pelo movimento dos contornos de maclas e variantes, com o crescimento da variante melhor orientada em relação à tensão

aplicada. A Figura 2.6a mostra um exemplo de uma curva tensão-deformação típica para uma liga NiTi abaixo de Mf.

ii. Af < Td < Md – A estrutura inicial da liga é completamente austenítica e a martensita induzida por tensão, formada no ciclo de carregamento, é instável na ausência de tensão e, consequentemente, se reverterá à austenita no descarregamento. Uma curva tensão-deformação típica para uma liga NiTi nessa condição é mostrada na Figura 2.6b.

iii. Td > Md – A tensão crítica requerida para induzir a transformação martensítica nesta faixa de temperatura torna-se tão alta que a deformação plástica pelo movimento de deslocações ocorre antes da indução de martensita.

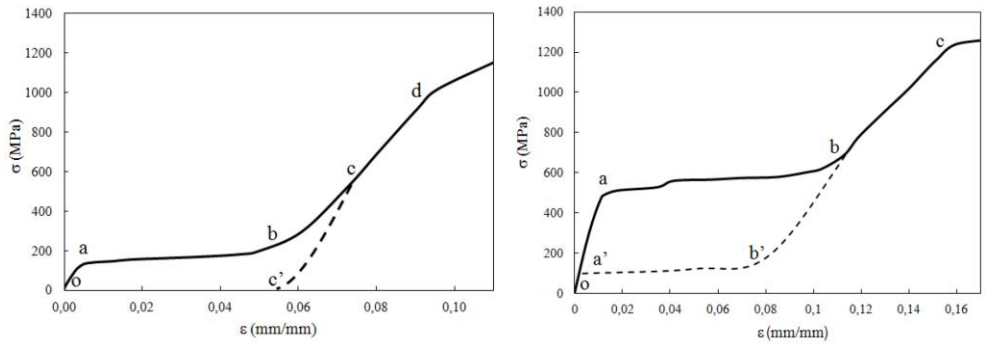

Figura 2.6 – Curvas tensão-deformação típicas de uma liga NiTi com estrutura: (a) martensítica – Td < Mf; (b) austenítica – Af < Td < Md [5].

2.2 Fratura por fadiga em ligas NiTi

A fratura por fadiga nos metais envolve três estágios: a nucleação de trincas, o seu crescimento lento e progressivo e a fratura final rápida. A nucleação de trincas está relacionada a um fluxo plástico não homogêneo, em nível microscópico, podendo ocorrer mesmo quando a estrutura se encontra, macroscopicamente, sob tensões elásticas. Estes fatores podem resultar em um fluxo plástico localizado, produzindo "intrusões" e "extrusões" superficiais que, sob a ação de tensões cíclicas, culminam na nucleação de trincas [11].

Diversas aplicações das ligas NiTi envolvem carregamento cíclico e a fratura por fadiga é uma preocupação constante. A fadiga em ligas NiTi é, usualmente, causada pela nucleação e crescimento de trincas, a partir de regiões de não homogeneidade e de defeitos superficiais, que funcionam como concentradores locais de tensão. A fadiga está, ainda, relacionada a fenômenos adicionais, como mudanças nas temperaturas de transformação e perda do efeito memória de forma e da superelasticidade [12].

Em instrumentos endodônticos rotatórios, por exemplo, o risco de fratura inesperada permanece um problema significativo na sua aplicação em tratamentos de canal. Durante a instrumentação, especialmente na preparação de canais radiculares curvos, os instrumentos podem fraturar por fadiga, quando o instrumento é submetido a um número excessivo de ciclos de tração e compressão, na região de curvatura máxima do canal [13].

Em um estudo usando limas endodônticas Miltex NiTi files, Silva *et al.* [14] avaliaram o efeito do eletropolimento na resistência à fadiga das limas. Os resultados obtidos indicaram que o eletropolimento aumentou a resistência à fadiga das limas, sem afetar sua eficiência de corte. Tal efeito foi explicado pela redução das irregularidades presentes na superfície que atuam como concentradores locais de tensão.

2.3 Biocompatibilidade e resistência à corrosão de ligas NiTi

A biocompatibilidade pode ser definida como a capacidade de um material de ter uma resposta adequada em uma aplicação específica, com o mínimo de reações alérgicas, inflamatórias ou tóxicas, quando em contato com os tecidos vivos ou fluidos orgânicos. Além da resposta induzida pelo material no organismo, um fator determinante na biocompatibilidade do material é a degradação que este sofre durante sua aplicação. No caso das ligas NiTi, existe a constante preocupação com efeitos alergênicos, de toxicidade e carcinogenicidade associados à dissolução e à liberação de íons níquel no organismo [15–17].

Em ligas NiTi, uma camada protetora de óxido estável (TiO_2) tende a se formar espontaneamente em sua superfície, passivando-a. Entretanto, durante o recozimento da liga, uma camada complexa composta de uma mistura de óxidos de titânio e de fases

ricas em níquel é formada. O TiO_2 é extremamente estável e inerte, enquanto fases ricas em níquel apresentam baixa biocompatibilidade [16]. Uma liga NiTi biocompatível deve apresentar uma camada superficial livre de níquel, com apenas TiO_2 exposto ao ambiente. Embora a camada de TiO_2 garanta boa biocompatibilidade e resistência à corrosão às ligas NiTi, algumas limitações devem ser observadas [18,19]:

i. Camadas muito espessas de TiO_2 não fornecem uma proteção adequada em materiais sujeitos a deformações, mesmo moderadas, e a presença de trincas e outros defeitos serve como caminho para a difusão de íons, levando à corrosão;

ii. um potencial elétrico suficientemente elevado, originado por uma fonte externa ou por metais dissimilares próximos, em ambientes condutores, pode levar à ruptura da camada de TiO_2; e

iii. a presença de pequenas falhas na camada de TiO_2 pode levar à corrosão localizada do material e acelerar a nucleação de trincas, causando falhas prematuras.

Alguns tratamentos de superfície tradicionalmente aplicados em biomateriais são: polimento mecânico, polimento eletroquímico, ataque químico por soluções ácidas, tratamentos térmicos, e outros. As superfícies de ligas NiTi com polimento mecânico apresentam comportamento incerto em relação à resistência à corrosão, causado pela presença de heterogeneidades, arranhões e de contaminantes na superfície. Tratamentos térmicos em ar, argônio e atmosferas parcialmente redutoras também são aplicados para favorecer a formação de óxidos na superfície e prevenir a liberação de íons níquel [16]. Processamentos químicos e eletroquímicos, que dissolvem seletivamente fases ricas em níquel e formam camadas finas de TiO_2, produzem o melhor acabamento superficial, com camadas de óxido resistentes e suficientemente finas para aguentar deformações no substrato sem trincar [18].

Camadas finas de TiO_2 formadas por processamentos químicos, em que as fases ricas em níquel são removidas, são mais resistentes à corrosão e às deformações impostas ao substrato do que aquelas formadas por oxidação. Em geral, uma camada fina de TiO_2 é bastante eficiente como barreira para a difusão de oxigênio e, se as superfícies dos

componentes de NiTi forem cuidadosamente preparadas, existe pouco risco de corrosão e de liberação de níquel no organismo [16].

Alguns polimentos eletrolíticos têm se mostrado bastante eficientes na melhoria da resistência à corrosão de dispositivos de NiTi, pois removem a camada exterior das ligas, que, usualmente, apresentam estruturas deformadas e defeitos superficiais, que aumentam a atividade eletroquímica na superfície e diminuem sua resistência à corrosão. A preparação superficial exerce, ainda, uma grande influência nas propriedades e na estrutura de recobrimentos aplicados aos materiais. Além disso, eletropolimentos evitam a formação de martensita induzida por tensão na superfície durante tratamentos superficiais mecânicos [16,20,21].

Pohl *et al.* [22] estudaram os efeitos do eletropolimento na rugosidade superficial de uma liga NiTi com memória de forma nos estados austenítico e martensítico. Nesse trabalho, os melhores resultados de eletropolimento nas estruturas austeníticas foram obtidos usando um eletrólito constituído de ácido perclórico e ácido acético. Para as amostras no estado martensítico, foi utilizado um eletrólito de ácido nítrico e metanol. Tanto no estado austenítico como martensítico, foi observado o aumento da resistência à corrosão do material e a diminuição da rugosidade.

Simka *et al.* [23] avaliaram a influência da composição do eletrólito e das condições de operação na qualidade da superfície de uma liga NiTi. Superfícies uniformes foram obtidas apenas quando foram usados eletrólitos contendo ácidos hidrofluorídrico e sulfúrico. Também foi observado um aumento da resistência à corrosão após eletropolimento, esterilização e passivação das amostras, determinado por testes eletroquímicos em solução Tyrode.

A Figura 2.7 mostra uma comparação da resistência à corrosão entre uma liga NiTi com preparação superficial adequada, NiTi passivado, uma liga NiTi com camada de TiO_2 formada espontaneamente por oxidação ao ar, sem uma camada passivadora eficiente, NiTi oxidado, e um aço inoxidável 316L. A avaliação da resistência à corrosão foi feita por teste de polarização potenciodinâmica em solução salina tamponada de fosfato a 37°C. Segundo Duerig [24], após o teste de polarização observou-se que tanto o NiTi passivado como o aço inox mantiveram a integridade da camada passivadora. Já o NiTi

com camada de TiO_2 formada espontaneamente por oxidação ao ar sofreu corrosão severa. Além disso, a amostra NiTi oxidado apresentou liberação de íons níquel significativamente maior do que a amostra NiTi passivado em teste de imersão por até 90 dias em solução salina tamponada de fosfato a 37°C.

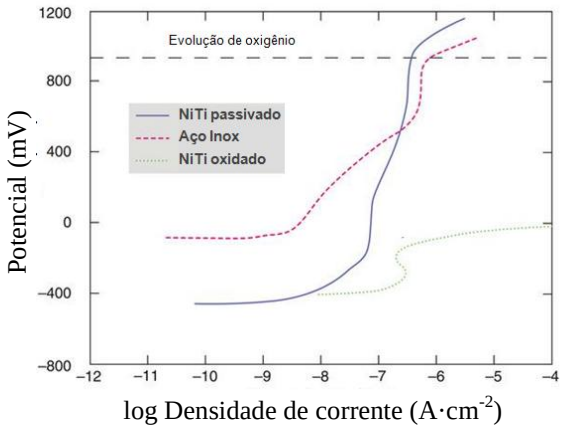

Figura 2.7 – Teste de polarização potenciodinâmica de uma liga NiTi passivada, uma liga NiTi com camada de TiO_2 formada por oxidação ao ar e um aço inoxidável [24].

De um modo geral, tanto a resistência à corrosão como a resistência à fadiga de um material de NiTi dependem fortemente de sua qualidade superficial e da integridade de sua camada de óxido. Fases duras e resistentes à abrasão, tais como carbonetos, são bastante usadas em recobrimentos, junto com metais resistentes à corrosão e elementos ligantes, buscando uma boa combinação de resistência à corrosão e à abrasão; e à propagação de trincas e à fadiga a ela associada. Uma área emergente de estudo é a aplicação de revestimentos nanoestruturados, que podem melhor a resistência à abrasão e à corrosão, sem afetar as propriedades mecânicas do substrato. Atualmente, pode-se destacar dentre os nanorecobrimentos mais aplicados os óxidos de silício, alumínio, titânio e zircônio — SiO_2, Al_2O_3, TiO_2 e ZrO_2 [25–27].

2.4 Eletrodeposição de zircônia

O zircônio e seus compostos, especialmente a zircônia, possuem excelentes biocompatibilidade e resistências à corrosão e à abrasão [28]. Além disso, a zircônia apresenta boa aderência a substratos metálicos e pode ser aplicada por diversos métodos, tais como imersão, deposição química a vapor, eletrodeposição, sol-gel, entre

outros [29–32]. A eletrodeposição catódica é um processo bastante difundido para a obtenção de filmes nanoestruturados, pois possui vantagens importantes, tais como: controle rígido da espessura, boa uniformidade e pureza dos filmes obtidos, e taxas de deposição elevadas. É, ainda, especialmente atrativo devido à possibilidade de aplicação em substratos com formas complexas, em baixas temperaturas e usando equipamentos de custo relativamente baixo [33].

Stefanov *et al.* [34] examinaram a estrutura e a composição de filmes de zircônia obtidos por eletrodeposição em substrato de aço inoxidável 316L, em diferentes condições. Foram avaliados eletrólitos aquosos e alcoólicos de vários sais de zircônio — $ZrCl_4$, $Zr(SO_4)_2$ e $ZrCl_2$. Os melhores resultados foram obtidos para o eletrólito de $ZrCl_4$ em álcool etílico. Foi estabelecido que, em contraste com eletrólitos aquosos, nos quais os melhores resultados eram obtidos para deposições entre 1,3 e 2,4 V, a melhor faixa de potencial para deposição usando eletrólitos alcoólicos era de 9 a 25 V e que potenciais superiores a 25 V deterioram a qualidade do filme, gerando muitas trincas e poros. Além disso, tratamentos térmicos a 550°C não resultaram em alterações na estrutura, na composição química ou na adesão dos filmes de zircônia. Embora o revestimento obtido pelos autores tenha apresentado boa aderência ao substrato e seja apropriado para a aplicação proposta no estudo, como suporte catalítico, ele não pode ser considerado como uma boa alternativa para proteção contra a corrosão, devido à sua porosidade.

Yen e Huang [35] realizaram o recobrimento de uma liga Ti-6AI-4V por eletrodeposição, usando uma solução de $ZrO(NO_3)_2$. Foi obtida uma camada de zircônia com estrutura monoclínica, que mostrou boa adesão ao substrato após recozimento a 700°C durante 5 minutos. A liga recoberta apresentou boa resistência à corrosão em testes de imersão em soluções ácidas de HCl e H_2SO_4 e solução aquosa de NaCl. Em um estudo realizado por Setare *et al.* [36], revestimentos de óxido de zircônio de cerca de 1,5 µm foram eletrodepositados em um aço inoxidável 316L, usando um eletrólito de $ZrOCl_2$. Foram obtidas camadas de ZrO_2 nanocristalinas, com estrutura cristalográfica tetragonal. Os autores compararam a diferença entre os revestimentos obtidos usando eletrodeposição por corrente contínua e por corrente pulsada e perceberam que os recobrimentos obtidos por corrente contínua se apresentavam quebradiços, enquanto o

método utilizando corrente pulsada produziu filmes mais densos e uniformes, com melhores propriedades mecânicas e melhor comportamento em relação à resistência à corrosão.

Zhitomirsky e Petric [29] produziram, por eletrodeposição, filmes finos de um compósito organocerâmico de hidróxido de zircônio e de poli(cloreto de dialildimetilamônio) — PDDA, em substratos de níquel. A eletrodeposição foi feita a partir de uma solução de $ZrOCl_2$ e PDDA e os experimentos mostraram que o peso da camada depositada aumenta com o aumento da concentração de $ZrOCl_2$ no eletrólito e com o aumento da densidade de corrente aplicada. Os autores concluíram que o uso do PDDA como aditivo contribui para a obtenção de filmes com melhor adesão ao substrato e com maior resistência ao aparecimento de trincas. Pang *et al.* [37] também estudaram a eletrodeposição de ZrO_2 com adição de PDDA. Nesse estudo, foram obtidos filmes constituídos de nanopartículas tetragonais aderentes ao substrato metálico de aço inoxidável 301. O peso da camada depositada pôde ser controlado pelo tempo de deposição e pela concentração de PDDA no eletrólito. Como pode ser visto na Figura 2.8, a adição de PDDA permitiu a obtenção de revestimentos de zircônia sem trincas.

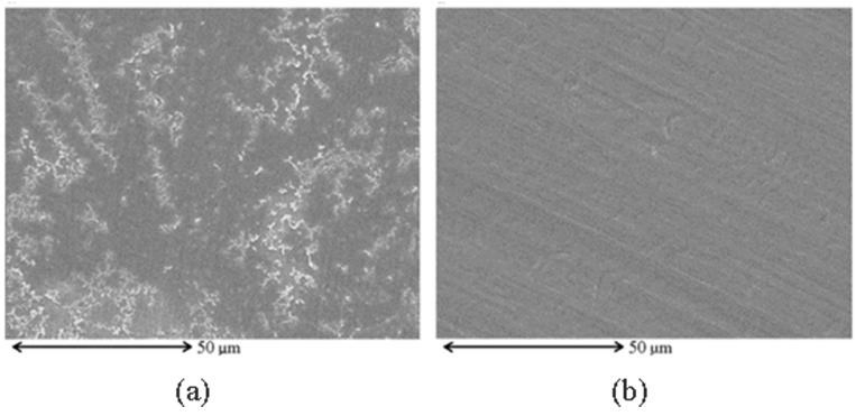

Figura 2.8 – Aspecto superficial do revestimento de zircônia depositado em substrato de aço inoxidável: (a) eletrodeposição a partir de $ZrOCl_2$; (b) adição de PDDA [37].

Giacomelli *et al.* [38] estudaram os efeitos da aplicação de um revestimento de zircônia no potencial de ruptura de um fio de NiTi usado em implantes endovasculares. Os fios foram, primeiramente, submetidos a um eletropolimento com solução de ácido

perclórico e ácido acético e, então, o revestimento foi eletrodepositado a partir de uma solução de $ZrOCl_2.8H_2O$. Embora tenha sido obtido um revestimento uniforme, nota-se a presença de várias trincas (Figura 2.9). Os resultados dos testes eletroquímicos de medida de potencial de circuito aberto e de polarização potenciodinâmica, em solução de saliva artificial, mostraram que o recobrimento aumentou a resistência à corrosão do fio.

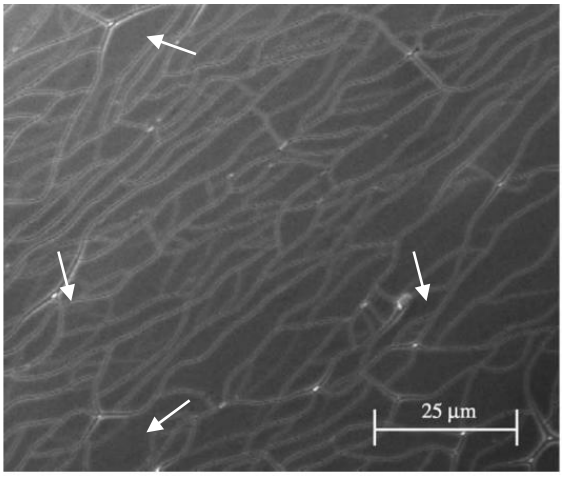

Figura 2.9 – Aspecto superficial de um revestimento de zircônia em fio de NiTi [38].

Em geral, o mecanismo proposto para a eletrodeposição de zircônia, em substratos metálicos, a partir de soluções de sais de zircônio, envolve as seguintes etapas [29,35]:

i. Dissociação do sal de zircônio:

$$ZrO(NO_3)_2 \rightarrow ZrO^{2+} + 2NO_3^-$$

ou

$$ZrOCl_2.8H_2O \rightarrow ZrO^{2+} + 2Cl^{-1} + 8H_2O$$

ii. Hidrólise do íon zirconila:

$$ZrO^{2+} + H_2O \rightarrow Zr(OH)_2^{2+}$$

iii. Precipitação do hidróxido de zircônio na superfície do substrato:

$$Zr(OH)_2^{2+} + 2OH^- \rightarrow Zr(OH)_4$$

iv. Desidratação do hidróxido – ao ar:

$$Zr(OH)_4 \rightarrow ZrO_2 + H_2O$$

As fontes mais prováveis de OH^- no catodo, a superfície do substrato, são:

i. Redução de O_2

$$O_2 + 2H_2O + 4e^- \rightarrow 4OH^-$$

ii. Redução de H_2O

$$2H_2O + 2e^- \rightarrow H_2 + 2OH^-$$

2.5 Referências

1. Mohd Jani J, Leary M, Subic A, Gibson MA. A review of shape memory alloy research, applications and opportunities. Materials & Design (1980-2015) 2014;56:1078–113. doi:10.1016/j.matdes.2013.11.084.
2. Otsuka K, Ren X. Physical metallurgy of Ti–Ni-based shape memory alloys. Progress in Materials Science 2005;50:511–678. doi:10.1016/j.pmatsci.2004.10.001.
3. Saburi T. Ti-Ni shape memory alloys. In: OTSUKA, K.; WAYMAN C, organizador. Shape Memory Materials. 1ed., Cambridge: Cambridge University Press; 1998, p. 49–96.
4. Otsuka K, Wayman CM. Shape Memory Materials. 1ed. Cambridge: Cambridge University Press; 1998.
5. Santos LA. Aplicação do método dos elementos finitos na análise do comportamento mecânico de instrumentos endodônticos de níquel-titânio. UFMG, 2013.
6. Wayman CM, Duerig TW. An Introduction to Martensite and Shape Memory. Engineering Aspects of Shape Memory Alloys, Elsevier; 1990, p. 3–20. doi:10.1016/B978-0-7506-1009-4.50005-6.
7. Suzuki Y. Fabrication of shape memory alloys. In: Otsuka, K.; Wayman CM, organizador. Shape Memory Materials. 1ed., Cambridge: Cambridge University Press; 1998, p. 133–48.
8. Bram M, Ahmad-Khanlou A, Heckmann A, Fuchs B, Buchkremer HP, Stöver D. Powder metallurgical fabrication processes for NiTi shape memory alloy parts. Materials Science and Engineering: A 2002;337:254–63. doi:10.1016/S0921-5093(02)00028-X.
9. Miyazaki S, Otsuka K, Suzuki Y. Transformation pseudoelasticity and deformation behavior in a Ti-50.6at%Ni alloy. Scripta Metallurgica 1981;15:287–92. doi:10.1016/0036-9748(81)90346-X.

10. Melton K., Mercier O. Fatigue of NiTi thermoelastic martensites. Acta Metallurgica 1979;27:137–44. doi:10.1016/0001-6160(79)90065-8.

11. Courtney TH. Mechanical behavior of materials. McGraw Hill; 1990.

12. Hornbogen E. Some effects of martensitic transformation on fatigue resistance. Fatigue & Fracture of Engineering Materials & Structures 2002;25:785–90. doi:10.1046/j.1460-2695.2002.00579.x.

13. Bahia MG de A. Resistência à Fadiga e Comportamento em Torção de Instrumentos Endodônticos de NiTi ProFile. UFMG, 2004.

14. Silva MAC, Gomes JAC., Ormiga F. Influence of electrochemical polishing on the mechanical behaviour of nickel-titanium rotary files. Australian endodontic journal : the journal of the Australian Society of Endodontology Inc 2013;39:73–7. doi:10.1111/j.1747-4477.2011.00308.x.

15. Denkhaus E, Salnikow K. Nickel essentiality, toxicity, and carcinogenicity. Critical Reviews in Oncology/Hematology 2002;42:35–56. doi:10.1016/S1040-8428(01)00214-1.

16. Shabalovskaya S, Anderegg J, Van Humbeeck J. Critical overview of Nitinol surfaces and their modifications for medical applications. Acta Biomaterialia 2008;4:447–67. doi:10.1016/j.actbio.2008.01.013.

17. Ryhänen J, Niemi E, Serlo W, Niemelä E, Sandvik P, Pernu H, et al. Biocompatibility of nickel-titanium shape memory metal and its corrosion behavior in human cell cultures. Journal of Biomedical Materials Research 1997;35:451–7. doi:10.1002/(SICI)1097-4636(19970615)35:4<451::AID-JBM5>3.0.CO;2-G.

18. Duerig T, Pelton A, Stöckel D. An overview of nitinol medical applications. Materials Science and Engineering: A 1999;273–275:149–60. doi:10.1016/S0921-5093(99)00294-4.

19. Duerig TW. Some unsolved aspects of Nitinol. Materials Science and Engineering A 2006;438–440:69–74. doi:10.1016/j.msea.2006.05.072.

20. Cissé O, Savadogo O, Wu M, Yahia LH. Effect of surface treatment of NiTi alloy on its corrosion behavior in Hanks' solution. Journal of Biomedical Materials Research 2002;61:339–45. doi:10.1002/jbm.10114.

21. Shabalovskaya SA, Rondelli GC, Undisz AL, Anderegg JW, Burleigh TD, Rettenmayr ME. The electrochemical characteristics of native Nitinol surfaces. Biomaterials 2009;30:3662–71. doi:10.1016/j.biomaterials.2009.03.034.

22. Pohl M, Heßing C, Frenzel J. Electrolytic processing of NiTi shape memory alloys. Materials Science and Engineering A 2004;378:191–9. doi:10.1016/j.msea.2003.11.080.

23. Simka W, Kaczmarek M, Baron-Wiecheć A, Nawrat G, Marciniak J, Żak J. Electropolishing and passivation of NiTi shape memory alloy. Electrochimica Acta 2010;55:2437–41. doi:10.1016/j.electacta.2009.11.097.

24. Duerig T. Shape Memory Alloys. In: Narayan R, organizador. ASM Handbook, Volume 23: Materials for Medical Devices. 1ed., ASM International; 2002, p. 237–50.

25. Gurrappa I, Binder L. Electrodeposition of nanostructured coatings and their characterization—A review. Science and Technology of Advanced Materials 2008;9:43001. doi:10.1088/1468-6996/9/4/043001.

26. Zhitomirsky I, Petric A, Niewczas M. Nanostructured ceramic and hybrid materials via electrodeposition. JOM 2002;54:31–4. doi:10.1007/BF02709090.

27. Dahotre NB, Sudarshan TS. Intermetallic and ceramic coatings. Marcel Dekker; 1999.

28. Chevalier J. What future for zirconia as a biomaterial? Biomaterials 2006;27:535–43. doi:10.1016/j.biomaterials.2005.07.034.

29. Zhitomirsky I, Petric A. Electrolytic deposition of zirconia and zirconia organoceramic composites. Materials Letters 2000;46:1–6.

30. Balamurugan A, Kannan S, Rajeswari S. Structural and electrochemical behaviour of sol-gel zirconia films on 316L stainless-steel in simulated body fluid

environment. Materials Letters 2003;57:4202–5. doi:10.1016/S0167-577X(03)00290-8.

31. Torres-Huerta AM, Domínguez-Crespo MA, Onofre-Bustamante E, Flores-Vela A. Characterization of ZrO2 thin films deposited by MOCVD as ceramic coatings. Journal of Materials Science 2012;47:2300–9. doi:10.1007/s10853-011-6044-0.

32. Espitia-Cabrera I, Orozco-Hernández H, Torres-Sánchez R, Contreras-García ME, Bartolo-Pérez P, Martínez L. Synthesis of nanostructured zirconia electrodeposited films on AISI 316L stainless steel and its behaviour in corrosion resistance assessment. Materials Letters 2004;58:191–5. doi:10.1016/S0167-577X(03)00443-9.

33. Zhitomirsky I, Gal-Or L. Cathodic Electrosynthesis of Ceramic Deposits. Journal of the European Ceramic Society 1996;16:819–24. doi:10.1016/0955-2219(96)00002-7.

34. Stefanov P, Stoychev D, Valov I, Kakanakova-Georgieva A, Marinova T. Electrochemical deposition of thin zirconia films on stainless steel 316 L. Materials Chemistry and Physics 2000;65:222–5. doi:10.1016/S0254-0584(00)00251-0.

35. Yen SK, Huang TY. Characterization of the electrolytic ZrO2 coating on Ti-6A1-4V. Materials Chemistry and Physics 1998;56:214–21. doi:10.1016/S0254-0584(98)00178-3.

36. Setare E, Raeissi K, Golozar MA, Fathi MH. The structure and corrosion barrier performance of nanocrystalline zirconia electrodeposited coating. Corrosion Science 2009;51:1802–8. doi:10.1016/j.corsci.2009.05.004.

37. Pang X, Zhitomirsky I, Niewczas M. Cathodic electrolytic deposition of zirconia films. Surface and Coatings Technology 2005;195:138–46. doi:10.1016/j.surfcoat.2004.08.216.

38. Giacomelli FC, Giacomelli C, De Oliveira AG, Spinelli A. Effect of electrolytic ZrO2 coatings on the breakdown potential of NiTi wires used as endovascular implants. Materials Letters 2005;59:754–8. doi:10.1016/j.matlet.2004.11.015.

3. Preparação superficial

CARACTERIZAÇÃO DA SUPERFÍCIE APÓS POLIMENTO ELETROLÍTICO DE LIGAS NITI SUPERELÁSTICAS E COM EFEITO MEMÓRIA DE FORMA

Nesse estudo, buscou-se definir os parâmetros mais adequados para o eletropolimento de ligas NiTi superelásticas e com efeito memória de forma, à temperatura ambiente, usando um eletrólito de H_2SO_4 em metanol. Foram realizadas avaliações da morfologia superficial por MEV e AFM, além de testes de resistência à corrosão em solução salina balanceada (*Hank's solution*), à 37°C, simulando condições fisiológicas. Os resultados mostraram que o eletropolimento é capaz de reduzir significativamente a rugosidade superficial, remover as camadas mais externas ricas em níquel, e aumentar a resistência à corrosão em ligas NiTi austeníticas e martensíticas. Observou-se, ainda, que o aumento da resistência à corrosão foi mais pronunciado para a liga martensítica, com efeito memória de forma.

Publicado em **Materials Research**

DOI: http://doi.org/10.1590/1980-5373-mr-2016-0933

SURFACE CHARACTERIZATION OF NITI SUPERELASTIC AND SHAPE MEMORY ALLOYS AFTER ELECTROLYTIC POLISHING

Natalia Isabel de Azevedo Lopes*, Laís Ávila de Oliveira Silva,
Leandro de Arruda Santos and Vicente Tadeu Lopes Buono

Department of Metallurgical and Materials Engineering,
Universidade Federal de Minas Gerais (UFMG), Belo Horizonte, MG, Brazil

ABSTRACT

For the biomedical application of NiTi alloys, an excellent surface finishing process is required to guarantee high corrosion resistance and biocompatibility, eliminating the allergenic and toxic effects associated with the release of nickel ions in the body. Electropolishing is a process that can reduce surface imperfections and form a thin protective layer of TiO_2, even in complex-shaped devices. The main objective of our study was to find and report suitable parameters for electrolytic polishing of NiTi wires, in both the superelastic and shape memory states. The results indicate that electropolishing in a 3.5 $mol \cdot L^{-1}$ methanolic H_2SO_4 electrolyte at 20°C can effectively reduce surface roughness, remove superficial nickel-rich layers and improve corrosion resistance for austenitic and martensitic NiTi alloys.

Keywords: *NiTi; superelasticity; shape memory effect; electrolytic polishing; biomaterial.*

3.1 Introduction

Nickel-titanium (NiTi) alloys have a wide range of prospective biomedical applications due to two extraordinary properties: shape memory effect and superelasticity [1]. These effects take place in NiTi alloys with near-equiatomic composition, and are related to the martensitic transformation, a diffusionless phase transformation in which atoms move cooperatively by a shear-like mechanism, rearranging themselves to form a more stable crystalline structure. The shape memory effect, or pseudoplasticity, is displayed when the low-temperature martensitic phase suffers an apparently plastic deformation upon loading, which is eliminated when the material is heated above its transformation temperature. Superelasticity, or pseudoelasticity, is characterized by large recoverable strains upon loading and unloading in the high-temperature austenitic phase [2].

Currently, most shape memory and superelastic biodevices are produced using NiTi alloys. However, there are allergenic, toxic, and carcinogenic effects associated with the release of nickel ions in the human body, which remain a concern in the application of these alloys [3]. In the production process, a coarse and complex layer consisting of a mixture of TiO_2 and nickel-rich phases is formed on the alloy surface. Moreover, conventional machining of NiTi alloys usually results in a surface with many defects and irregularities that can accelerate the corrosion and degradation of the material [1]. Additional surface processing is needed in order to promote the depletion of nickel in the outermost layers, to form a smooth and defect-free surface, and to ensure the formation of a protective layer of titanium oxide [4].

Among the treatments traditionally used for biomaterials, chemical and electrochemical processes generally lead to better surface finishing than mechanical routes. Electrolytic polishing can selectively dissolve surface irregularities and simultaneously form a thin protective layer of titanium oxide [5]. For this reason, and due to its easy and inexpensive application to objects of complex shapes, electropolishing has been applied commonly in the finishing of NiTi devices. Although electropolishing of NiTi is already used commercially, there are few descriptive papers on the electrolytic polishing processes and parameters of NiTi alloys. Most knowledge on this area is empirical [4] and few systematic studies have been published [6-8].

The aim of our study was to find and report suitable parameters for the electropolishing of NiTi alloys at 20°C, with martensitic or austenitic structures, to enable its application as a biomaterial. Furthermore, it is the purpose of the present work to investigate the electrolytic polishing effects on the surface morphology and the corrosion resistance of NiTi wires.

3.2 Experimental

3.2.1 Materials

Two commercial near-equiatomic NiTi wires (Stanford Advanced Materials, Irvine, CA, USA), with a diameter of 1 mm, were used in this study: a superelastic wire with an austenitic structure at room temperature (nominal austenite finish temperature, Af, of 0°C), and a shape memory wire with a martensitic structure (Af = 70°C).

3.2.2 Surface characterization

The superficial morphology of the materials was evaluated using scanning electron microscopy (SEM, Inspect S50, FEI, Hillsboro, USA). Roughness measurements were made in triplicate over an area of 30 μm × 30 μm using atomic force microscopy (AFM, XE-70, Park System, Suwon, Korea), operating in the tapping mode. Semi-quantitative microanalyses were performed by energy dispersive X-ray spectroscopy (EDX, Genesis, EDAX Inc., Mahwah, USA). The phase composition was analyzed by X-ray diffraction (XRD, Empyrean, PANalytical, Almelo, The Netherlands) using Cu-Kα radiation.

3.2.3 Electrolytic polishing

All the samples were initially pickled in a phosphoric acid solution [9] to remove the dark, coarse oxide layer, cleaned in an ultrasonic bath with acetone for 15 minutes and then with deionized water for an additional 15 minutes. This procedure was performed to avoid early saturation effects during electropolishing.

For the electrolytic polishing, a potentiostat (VersaSTAT 3, Princeton Applied Research, Berwyn, USA), a standard electrochemical cell with a platinum grid as the

counter electrode and an Ag/AgCl reference electrode, were used. All potential values in this work refer to this electrode. The electrolyte chosen was a 3.5 $mol \cdot L^{-1}$ methanolic sulfuric acid (H_2SO_4) solution at 20°C [6]. Anodic polarization curves were determined using a potentiodynamic scan from 0 V to 10 V at a scan rate of 0.1 $V \cdot s^{-1}$. The electropolishing was conducted at the corresponding current plateau in the anodic polarization curves for the superelastic and the shape memory wires, for four different lengths of time (30, 60, 120 and 240 s). A surface area of 0.95 cm^2 was exposed to the electrolyte, and the samples were weighed in a precision scale, before and after electropolishing, to determine the average mass removal. Measurements were made in triplicate.

3.2.4 Electrochemical characterization

The electrochemical evaluation was also performed using a standard three-electrode cell with a platinum grid and an Ag|AgCl electrode as counter and reference electrodes, respectively. Potentiodynamic polarization curves were obtained starting from the open circuit potential and progressing in the anodic direction up to 2 V at a scan rate of 0.001 $V \cdot s^{-1}$ at a constant temperature of 37°C. The electrolyte used was the Hank's simulated physiologic solution (composition given in Table 3.1), chosen as it has been shown to yield highly reproducible results when used to assess the corrosion behavior of NiTi alloys [10]. After the electrochemical test, additional surface morphology assessment of the wires was performed using SEM.

Table 3.1 – Chemical components of Hank's solution.

Component	**Concentration ($g \cdot L^{-1}$)**
NaCl	8.00
Glucose	1.00
KCl	0.40
$NaHCO_3$	0.35
$CaCl_2$	0.14
$MgCl_2 \cdot 6H_2O$	0.10
KH_2PO_4	0.06
$MgSO_4 \cdot 7H_2O$	0.06
$Na_2HPO_4 \cdot 2H_2O$	0.06

3.3 Results and discussion

3.3.1 Electrolytic polishing

The surface morphologies of the NiTi superelastic and shape memory wires in their as received condition are shown in Figure 3.1a and Figure 3.1b, respectively. Both samples display a coarse oxide layer, resulting from annealing during the manufacturing process. This thermally formed oxide layer is predominantly composed of TiO_2, but significant amounts of metallic nickel and Ni_3Ti were detected by the XRD analysis (data not shown). The presence of nickel and nickel-rich phases in the surface hinders biomedical applications, and thick, impure oxide layers are more susceptible to localized corrosion than thin, uniform TiO_2 layers [5,11]. After pickling, most of the thermally formed oxide layer was removed. However, remnants of the coarse layer and several surface irregularities are present, as shown in Figure 3.1c and Figure 3.1d.

As many factors influence the electropolishing quality, the process parameters should be adjusted based on the current-voltage relationship for each specific system [12]. Figure 3.2 shows the anodic potentiodynamic polarization curves for superelastic and shape memory NiTi wires in a 3.5 $mol \cdot L^{-1}$ methanolic H_2SO_4 electrolyte at 20°C. The optimum region for electropolishing is the limiting current plateau in the polarization curve. In this region, the process is mass-transport controlled, limited by the diffusion of cations dissolved from the metal surface through the passivated layer [6]. For our systems, the potentials chosen for electropolishing (indicated in Figure 3.2) were 7 V for the superelastic wire and 8 V for the shape memory wire. The corresponding limiting currents were 0.07 $A \cdot cm^{-2}$ and 0.22 $A \cdot cm^{-2}$ for the superelastic and the shape memory wires, respectively.

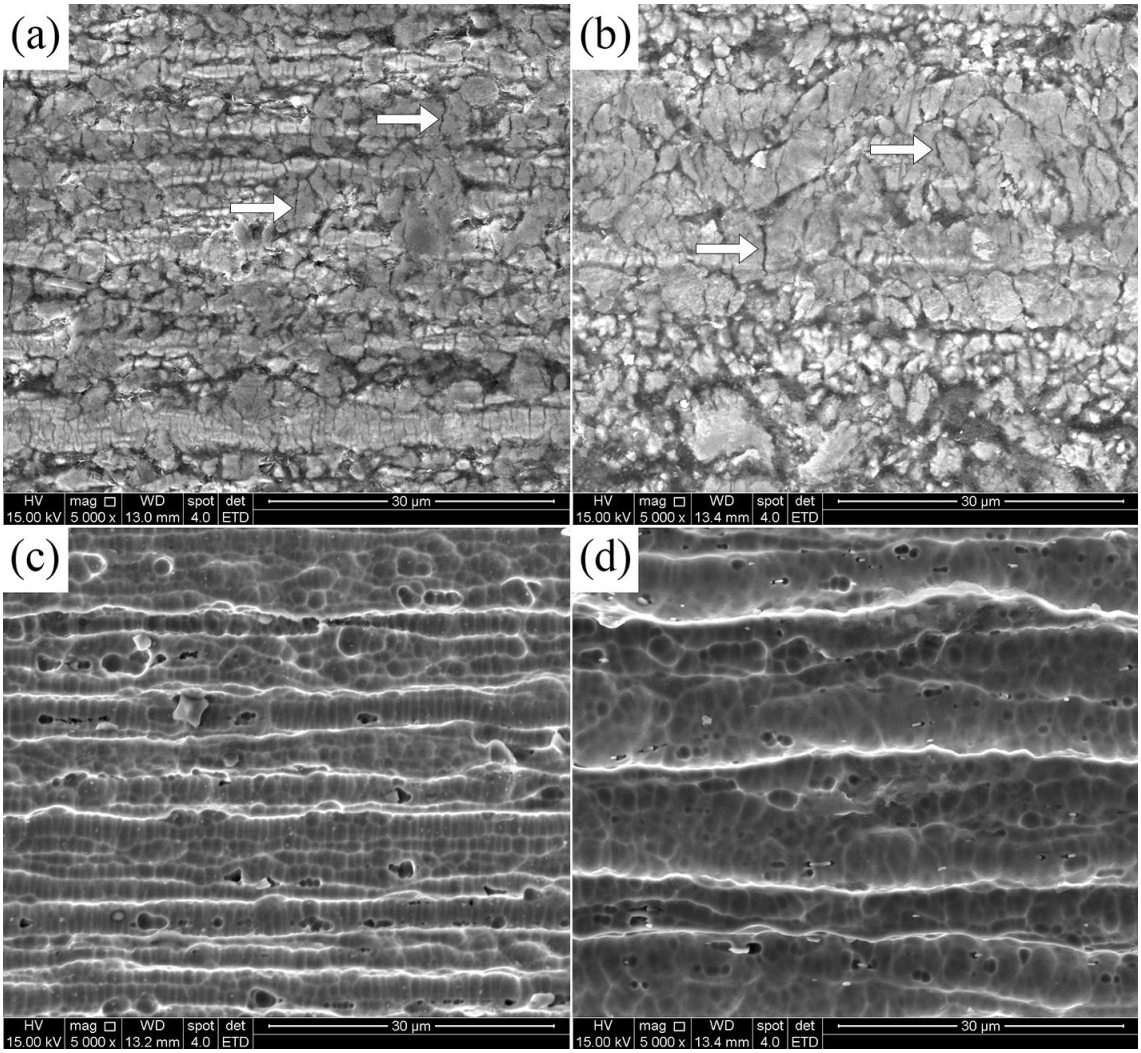

Figure 3.1 – SEM surface morphology images of NiTi wires: (a) superelastic and (b) shape memory, as received; (c) superelastic and (d) shape memory, after pickling. White arrows illustrate the presence of cracks in the oxide layer.

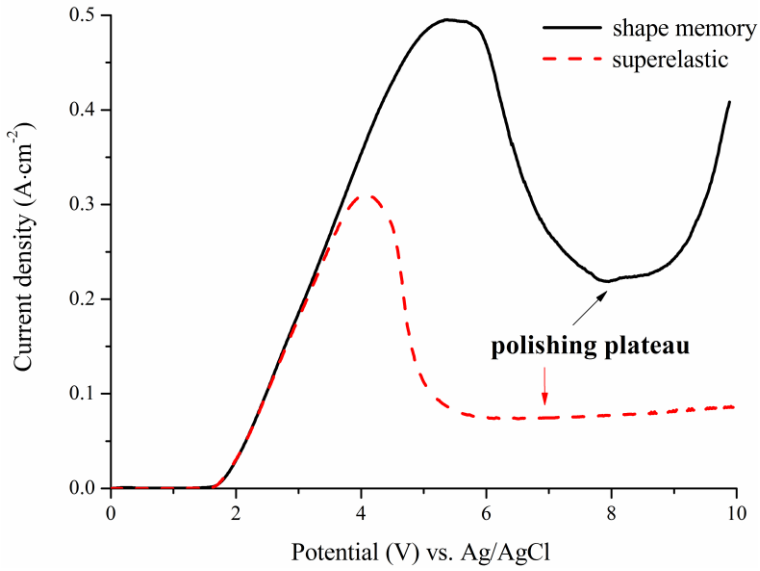

Figure 3.2 – Anodic polarization curves of NiTi wires in 3.5 mol·L^{-1} methanolic H_2SO_4 solution.

In one of the few systematic studies on the electropolishing of NiTi alloys, Fushimi *et al.* [8] investigated the polishing conditions of NiTi disks (50.5 at. % Ni and Af = 37°C) in methanolic H_2SO_4 solutions. The H_2SO_4 concentration was varied from 0.1 to 7 mol·L^{-1} and the electropolishing was carried out at -10°C, meaning that the alloy was in the shape memory martensitic state. They found that the limiting current decreased linearly with increasing H_2SO_4 concentration, and that for concentrations of up to 0.3 mol·L^{-1}, the reaction was under Ohmic control and electropolishing was not observed. They reported that the best results were obtained for a 3 mol·L^{-1} concentration and a potential of 8 V, which showed a limiting current of approximately 0.05 A·cm^{-2}. This current is four times lower than the one we obtained and reinforces the fact that temperature [8] and initial surface roughness [7] are among several factors affecting electrolytic polishing.

The average mass removal of NiTi during electrolytic polishing, determined for different times, is displayed in Figure 3.3. As expected, longer polishing times resulted in a larger removal of mass. It is also observed that the mass removal was more severe in the superelastic wires. This average mass removal corresponds to an average linear removal rate of 8.3 µm·min^{-1} for the austenitic state and of 5.5 µm·min^{-1} for the martensitic state. It is interesting to note that after 120 seconds the mass removal rate

apparently increased for the superelastic alloy and decreased for the shape memory alloy. In a similar study, Pohl *et al.* [7] investigated the surface topography of a NiTi alloy (50.5 at. % Ni and Af = 34°C). They conducted electropolishing of the alloy in the austenitic state at 20°C using an electrolyte of acetic acid and perchloric acid, at a potential of 10 V, which lead to a linear removal rate of 3.5 µm·min^{-1}. For the martensitic state, they used a methanolic nitric acid solution, at a temperature of -30°C and a potential of 5.5 V, and measured a removal rate of 2.1 µm·min^{-1}. Although they achieved an initial reduction in the surface roughness, longer polishing periods lead to waviness formation due to material segregation. Armitage and Grant [13] used a nitric acid solution, like that used by Pohl *et al.* [7], for the electropolishing at -30°C of a nominally equiatomic NiTi alloy with a martensitic start temperature of 92.1°C, using a potential of 15 V; they reported that the electrolytic polishing resulted in a rougher surface.

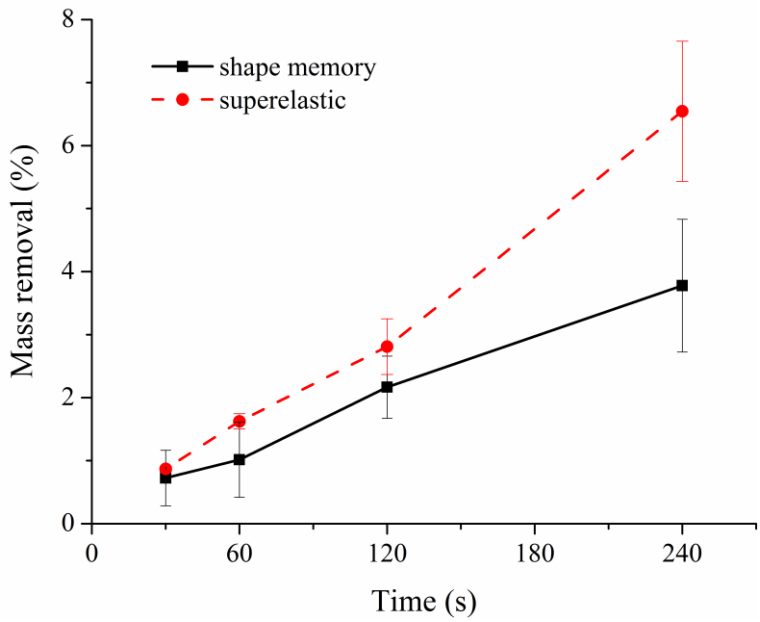

Figure 3.3 – Mass removal percentage after polishing NiTi wires in 3.5 mol·L^{-1} methanolic H_2SO_4 solution, at different times.

The average surface roughness (R_a) values of the specimens, measured by AFM, are presented in Figure 3.4. Longer polishing times represent a steady decrease in the surface roughness. After 240 s of electropolishing, the average surface roughness was 0.10 ± 0.09 µm for the superelastic wire and 0.17 ± 0.07 µm for the shape memory wire.

This represents a reduction of seven times in comparison with the pickled superelastic wire surface and almost four times in the shape memory wires.

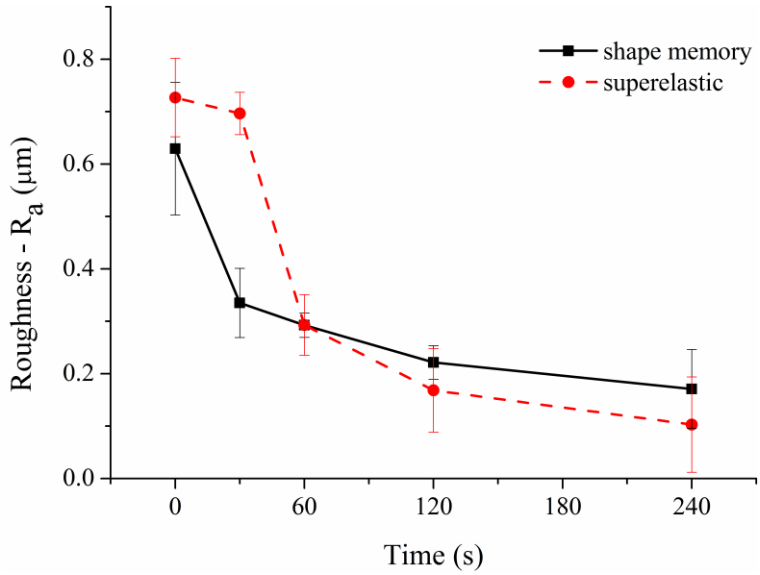

Figure 3.4 – Average surface roughness (R_a), measured by AFM, after polishing NiTi wires in 3.5 mol·L^{-1} methanolic H_2SO_4 solution, at different times.

Semi-quantitative microanalyses by EDX (Table 3.2) indicate that the nickel content in the outermost surface layers decreased with electropolishing and approached an equiatomic composition after 120 s. Figure 3.5 shows the diffractograms of NiTi wires that were electrolytically polished for 240 s. Only the phases stable at room temperature; martensite B19' for the shape memory wire, and austenite B2 for the superelastic wire, were identified for each sample.

Table 3.2 – Superficial nickel content after electrolytic polishing at different times determined by EDX.

Sample	Ni (at. %)				
	Time (s)				
	pickled	30	60	120	240
superelastic	54.8 ± 0.8	52.5 ± 1.2	51.6 ± 0.2	50.4 ± 0.4	50.1 ± 0.6
shape memory	55.5 ± 1.0	52.1 ± 0.3	50.6 ± 0.6	50.4 ± 0.5	50.8 ± 0.9

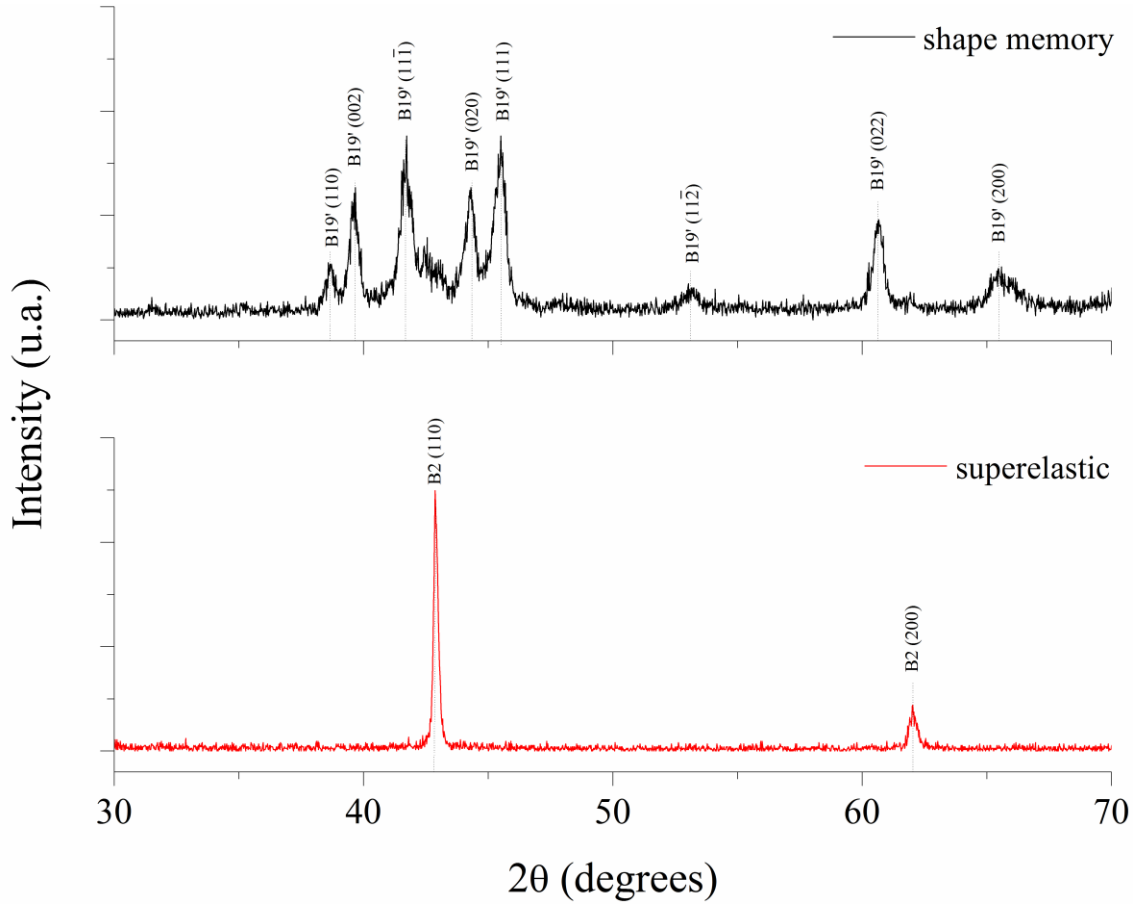

Figure 3.5 – X-ray diffraction profile of superelastic and shape memory NiTi alloys after 240 s of electrolytic polishing.

The surface morphologies of the NiTi surfaces after 240 s of polishing are shown in Figure 3.6. A considerable increase in the degree of uniformity can be seen in both the superelastic and the shape memory surfaces, and a number of inclusions randomly distributed throughout the surface are now evident. EDX microanalyses suggested that these particles are mainly titanium carbide, which usually forms during the melting process of NiTi alloys in carbon crucibles [14]. Although the SEM images of NiTi surfaces after 240 s of polishing suggest that a smoother surface was obtained on the martensitic wire, the values of average surface roughness measured by AFM were not statistically different, probably due to contributions from the titanium carbide particles.

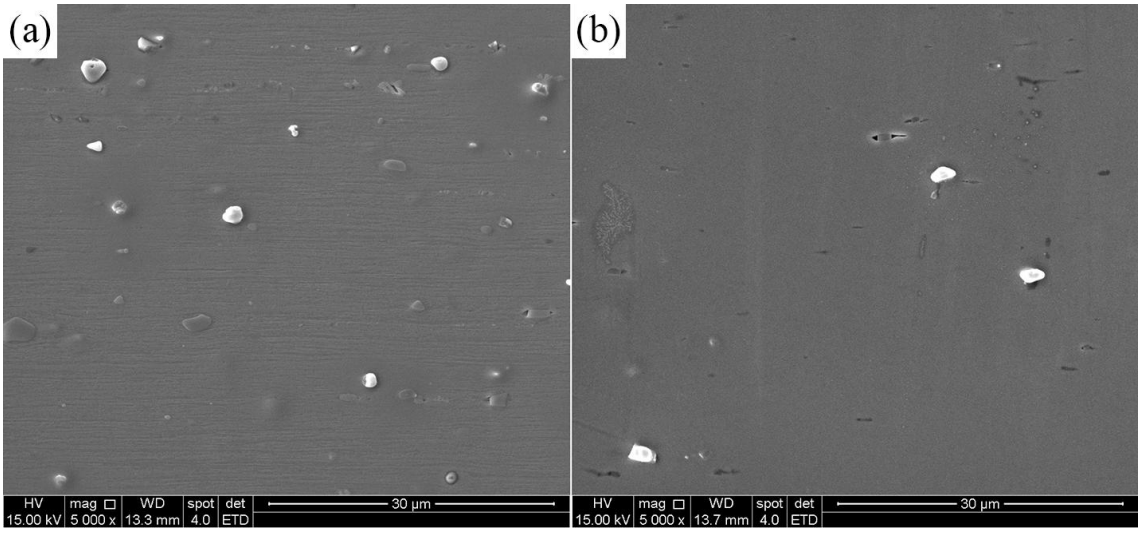

Figure 3.6 – Surface morphologies of NiTi wires after 240 s of electropolishing: (a) superelastic and (b) shape memory.

Smoother surfaces are usually associated with higher corrosion resistance [15] and longer fatigue life [16,17] in NiTi materials. A low surface roughness is desirable for many applications, such as in stents [18], orthodontic wires [19] and endodontic instruments [20]. However, a higher surface roughness might be required for other applications, such as in implants, where cell attachment and proliferation are important [21,22]. The final surface roughness can be adjusted accordingly by controlling the polishing times.

3.3.2 Electrochemical characterization

Potentiodynamic polarization was applied to study the corrosion behavior of the NiTi wires in Hank's solution, both as received and after electropolishing. The polarization curves for the superelastic and shape memory samples are shown in Figure 3.7. In the as received condition, both alloys showed similar corrosion potentials, and the superelastic alloy displayed a breakdown potential. According to the polarization curve, the corrosion mechanism of the shape memory wire in the as received condition appears to be uniform corrosion, while the superelastic wire presents localized corrosion with a low passivation current density of 10^{-7} A·cm^{-2}.

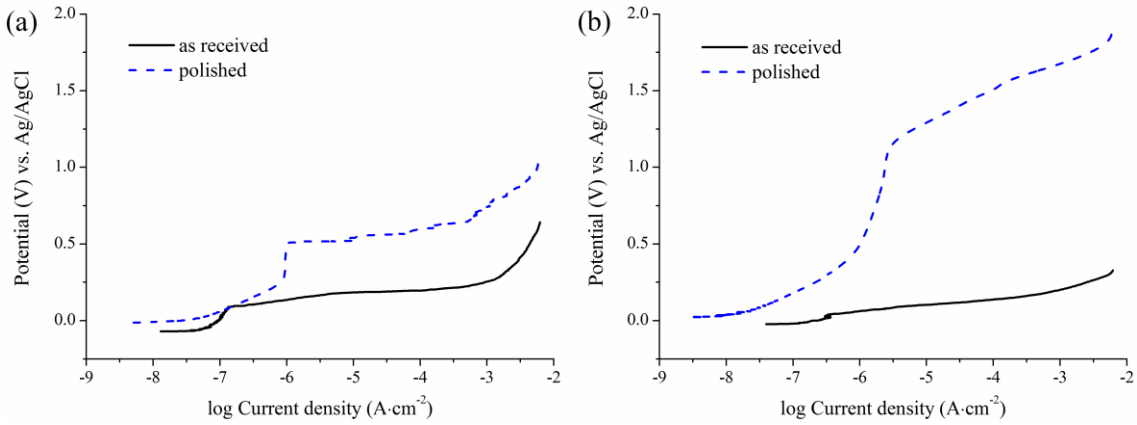

Figure 3.7 – Potentiodynamic polarization of NiTi wires in Hank's solution: (a) superelastic and (b) shape memory.

Since the corrosion resistance of NiTi alloys relies on the presence of a passivated TiO_2 layer, the film integrity and uniformity is of great importance [5]. In the as received condition, cracks on the oxide surface are evident, as exemplified by the arrows in Figure 3.1, which make it easier for the electrolyte to get into the substrate, and result in a lower corrosion resistance. The lower corrosion resistance of the shape memory alloy observed is a result of the different thermal treatments needed to control the transformation temperatures of the NiTi alloys, that also modify the surface oxide [2,11].

The condition of a surface strongly affects its corrosion resistance, which has lead to a wide range of data reported on the corrosion of NiTi devices, and so care should be taken when considering any results from the literature that do not explicitly state how the surfaces were prepared and tested [5,23-25]. As expected, in this study, the electrolytically polished superelastic and shape memory wires presented more noble corrosion potential values, when compared with their corresponding as received samples. Additionally, electropolishing resulted in a significant improvement to the breakdown potential and to the pitting corrosion resistance of the NiTi alloys. For the superelastic alloy, after electrolytic polishing, the passivation current density increased from 10^{-7} A·cm^{-2} to 10^{-6} A·cm^{-2}. The potentiodynamic polarization results also indicated that for the polished wires, the shape memory alloy showed higher corrosion resistance than the superelastic alloy. The surface morphologies after the polarization

tests of the superelastic and shape memory wires, shown in Figure 3.8 and Figure 3.9, respectively, support the above observations.

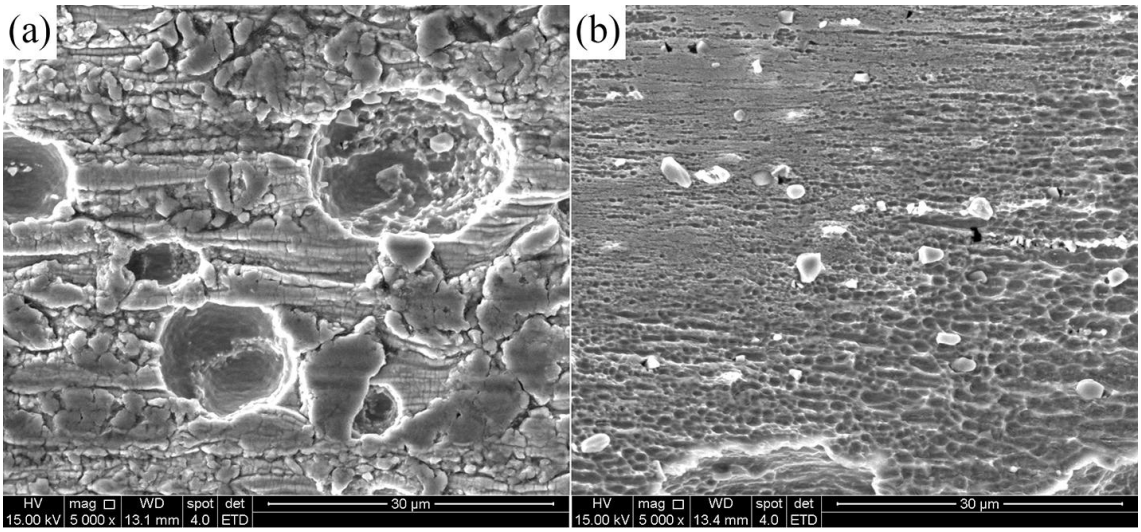

Figure 3.8 – Surface morphologies of superelastic NiTi wires after potentiodynamic polarization in Hank's solution: (a) as received and (b) polished.

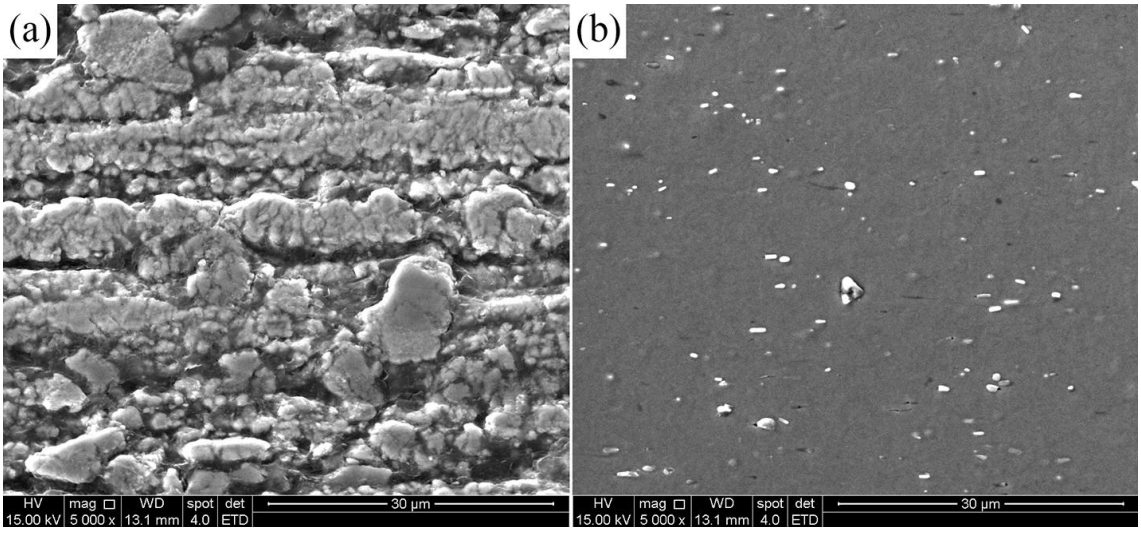

Figure 3.9 – Surface morphologies of shape memory NiTi wires after potentiodynamic polarization in Hank's solution: (a) as received and (b) polished.

The ASTM Standard F2129 does not establish the potential values that an implant must endure to define if its corrosion resistance is satisfactory, and recommends the use of an appropriate reference specimen with good *in vivo* corrosion resistance history [26]. Stainless steel 316L is widely used in biomedical applications, making it a suitable

reference material. Studies of its corrosion resistance report a breakdown potential of 0.35 V in Hank's solution at 37°C [21,25]. In our study, the electrolytic polishing elevated the breakdown potentials of the NiTi alloys to 0.52 V for the superelastic, and above 1.1 V for the shape memory. Therefore, electropolishing at the conditions reported is a suitable surface modification technique to be used in biomedical applications of NiTi devices, for superelastic and shape memory alloys.

The increase in corrosion resistance after electrolytic polishing is related to the smoothing of the surface and to the formation of a uniform TiO_2 protective layer on the surface [4,5]. A more pronounced improvement in corrosion resistance was observed in the shape memory martensitic alloy than in the superelastic austenitic alloy. Although their average surface roughness values after electropolishing were statistically similar, SEM images of the polished surfaces suggest that the shape memory alloy exhibits a smoother final surface, with less precipitated particles, most likely resulting in a superior corrosion resistance. The lower amount of precipitated particles and defects on the surface of the shape memory alloy is expected, given that the NiTi is more ductile and easier to deform in the martensitic than in the austenitic state [2], and the production route for NiTi devices is easier in that state.

3.3.3 Conclusions

The effects of electropolishing using a 3.5 $mol \cdot L^{-1}$ methanolic H_2SO_4 electrolyte at 20°C on the surface morphology of superelastic and shape memory NiTi wires were studied. The impact on their corrosion resistances in Hank's simulated physiological solution was also evaluated. The results showed that electrolytic polishing under the reported conditions can effectively reduce the surface roughness of both superelastic and shape memory NiTi alloys, and remove superficial nickel-rich layers. In the as received condition, the superelastic wire showed less corrosion susceptibility than the shape memory wire. The latter presented uniform corrosion, while the corrosion mechanism of the superelastic alloy was localized corrosion with a low passivation current density of 10^{-7} $A \cdot cm^{-2}$. After electropolishing, a significantly increase in their corrosion resistance in Hank's solution was observed, which was more pronounced in the shape memory alloy than in the superelastic alloy. In summary, electrolytic

polishing is a promising surface modification technique to be used in biomedical applications of superelastic and shape memory NiTi devices.

ACKNOWLEDGMENTS

This work was supported by Conselho Nacional de Desenvolvimento Científico e Tecnológico (CNPq), Brasília, DF, Brazil; and Coordenação de Aperfeiçoamento de Pessoal de Nível Superior (CAPES/PROEX), Brasília, DF, Brazil.

3.3.4 References

1. Duerig T, Pelton A, Stöckel D. An overview of nitinol medical applications. Materials Science and Engineering: A. 1999;273–275:149–160.
2. Otsuka K, Ren X. Physical metallurgy of Ti–Ni-based shape memory alloys. Progress in Materials Science. 2005;50:511–678.
3. Denkhaus E, Salnikow K. Nickel essentiality, toxicity, and carcinogenicity. Critical Reviews in Oncology/Hematology. 2002;42:35–56.
4. Hassel AW. Surface treatment of NiTi for medical applications. Minimally Invasive Therapy & Allied Technologies. 2004;13:240–247.
5. Shabalovskaya S, Anderegg J, Van Humbeeck J. Critical overview of Nitinol surfaces and their modifications for medical applications. Acta Biomaterialia. 2008;4:447–467.
6. Neelakantan L, Hassel AW. Rotating disc electrode study of the electropolishing mechanism of NiTi in methanolic sulfuric acid. Electrochimica Acta. 2007;53:915–919.
7. Pohl M, Heßing C, Frenzel J. Electrolytic processing of NiTi shape memory alloys. Materials Science and Engineering: A. 2004;378:191–199.
8. Fushimi K, Stratmann M, Hassel AW. Electropolishing of NiTi shape memory alloys in methanolic H_2SO_4. Electrochimica Acta. 2006;52:1290–1295.
9. Okazaki S, Ohhashi T, Nakao S, Hirose Y, Hitosugi T, Hasegawa T. Wet etching of amorphous TiO_2 thin films using H_3PO_4-H_2O_2 aqueous solution. Japanese Journal of Applied Physics. 2013;52:98002.
10. Hansen AW, Führ LT, Antonini LM, Villarinho DJ, Marino CEB, Malfatti C de F. The Electrochemical Behavior of the NiTi Alloy in Different Simulated Body Fluids. Materials Research. 2015;18:184–190.
11. Zhu L, Fino JM, Pelton AR. Oxidation of Nitinol. In: SMST-2003 Proceedings of the International Conference on Shape Memory and Superelastic Technologies; 2003 May 5-8; Pacific Grove, CA, USA. p. 357–366.

12. Yang G, Wang B, Tawfiq K, Wei H, Zhou S, Chen G. Electropolishing of surfaces: theory and applications. Surface Engineering 2016;0:1–18.
13. Armitage DA, Grant DM. Characterisation of surface-modified nickel titanium alloys. Materials Science and Engineering: A. 2003;349:89–97.
14. Frenzel J, Zhang Z, Neuking K, Eggeler G. High quality vacuum induction melting of small quantities of NiTi shape memory alloys in graphite crucibles. Journal of Alloys and Compounds. 2004;385:214–223.
15. ASM International. Materials and coatings for medical devices : cardiovascular. ASM International; 2009.
16. Patel MM, Gordon RF. An Investigation of Diverse Surface Finishes on Fatigue Properties of Superelastic Nitinol Wire. In: SMST-2006 Proceedings of the International Conference on Shape Memory and Superelastic Technologies; 2006 May 7-11; Pacific Grove, CA, USA. p. 1–6.
17. Silva MAC, Gomes JADCP, Ormiga F. Influence of electrochemical polishing on the mechanical behaviour of nickel-titanium rotary files. Australian Endodontic Journal. 2013;39:73–77.
18. Tepe G, Schmehl J, P Wendel H, Schaffner S, Heller S, Gianotti M, Reduced thrombogenicity of nitinol stents - In vitro evaluation of different surface modifications and coatings. Biomaterials. 2006;27:643–650.
19. Wichelhaus A, Geserick M, Hibst R, Sander FG. The effect of surface treatment and clinical use on friction in NiTi orthodontic wires. Dental Materials : Official Publication of the Academy of Dental Materials. 2005;21:938–945.
20. Gutmann JL, Gao Y. Alteration in the inherent metallic and surface properties of nickel-titanium root canal instruments to enhance performance, durability and safety: a focused review. International Endodontic Journal. 2012;45:113–128.
21. Chen Q, Thouas GA. Metallic implant biomaterials. Materials Science and Engineering R: Reports. 2015;87:1–57.

22. Wirth C, Grosgogeat B, Lagneau C, Jaffrezic-Renault N, Ponsonnet L. Biomaterial surface properties modulate in vitro rat calvaria osteoblasts response: Roughness and/or chemistry? Materials Science and Engineering: C. 2008;28:990–1001.

23. Simka W, Kaczmarek M, Baron-Wiecheć A, Nawrat G, Marciniak J, Żak J. Electropolishing and passivation of NiTi shape memory alloy. Electrochimica Acta. 2010;55:2437–2441.

24. Cissé O, Savadogo O, Wu M, Yahia LH. Effect of surface treatment of NiTi alloy on its corrosion behavior in Hanks' solution. Journal of Biomedical Materials Research. 2002;61:339–345.

25. Thierry B, Tabrizian M, Trepanier C, Savadogo O, Yahia L. Effect of surface treatment and sterilization processes on the corrosion behavior of NiTi shape memory alloy. Journal of Biomedical Materials Research. 2000;51:685–693.

26. ASTM Standard F2129–04. Standard Test Method for Conducting Cyclic Potentiodynamic Polarization Measurements to Determine the Corrosion Susceptibility of Small Implant Devices. ASTM International; 2004.

4. Eletrodeposição e caracterização do revestimento

DEPOSIÇÃO ELETROQUÍMICA E CARACTERIZAÇÃO DE NANO REVESTIMENTOS DE ZrO_2 EM LIGA NiTi SUPERELÁSTICA

Este estudo teve como objetivo avaliar condições distintas de deposição para obtenção de um revestimento nanoestruturado adequado para aplicações biomédicas. Eletrólitos a base de dois sais de zirconila, $ZrOCl_2$ e $ZrO(NO_3)_2$, como adições de metanol e de polyDADMAC foram testados para deposição em fios superelásticos de NiTi após preparação superficial usando polimento eletrolítico, nas condições reportadas no estudo mostrado no capítulo 3. No presente estudo, focou-se na deposição em ligas superelásticas, uma vez que seu uso em aplicações biomédicas é mais comum do que o uso de ligas martensíticas. Um fio superelástico comercial com melhor acabamento superficial e Af nominal igual a 20°C foi adquirido para este estudo e, desse modo, pequenos ajustes na temperatura e no tempo do polimento eletrolítico foram feitos. A caracterização das amostras antes e após deposição foi feita por meio de análises de morfologia e de composição química da superfície por MEV/EDX e AFM. A resistência à corrosão foi medida por meio de testes de polarização potenciodinâmica em solução fisiológica artificial (*Hank's solution*) a 37°C. Os resultados mostraram que a deposição usando soluções aquosas de $ZrOCl_2$ e $ZrO(NO_3)_2$ reduz a rugosidade superficial e melhora a resistência à corrosão de fios de NiTi superelásticos. Quando um eletrólito metanólico de $ZrOCl_2$ foi utilizado, a deposição é heterogênea e trincas são observadas no filme. A adição de polyDADMAC aos eletrólitos aquosos e metanólicos resulta em um revestimento mais uniforme e em uma maior resistência à corrosão. A maior resistência à corrosão e a menor rugosidade superficial é observada quando o revestimento é aplicado utilizando o eletrólito metanólico de $ZrOCl_2$ com adição de polyDADMAC.

Publicado em **Applied Surface Science**

DOI: http://doi.org/10.1016/j.apsusc.2018.04.154

ELECTROCHEMICAL DEPOSITION AND CHARACTERIZATION OF ZrO_2 CERAMIC NANOCOATINGS ON SUPERELASTIC NiTi ALLOY

Natalia Isabel de Azevedo Lopes*, Nelson Henrique Jardim Freire, Pedro Damas Resende, Leandro de Arruda Santos and Vicente Tadeu Lopes Buono

Department of Metallurgical and Materials Engineering,
Universidade Federal de Minas Gerais (UFMG), Belo Horizonte, MG, Brazil

ABSTRACT

This study aimed to develop an appropriate nano-sized coating to prevent premature failures of NiTi components and nickel release to the human body. Two zirconyl salts, $ZrOCl_2$ and $ZrO(NO_3)_2$, were evaluated for electrodeposition as well as the effects of methanol and polyDADMAC addition. The surface morphology and chemical composition of the coated samples were evaluated using scanning electron microscopy with energy dispersive X-ray spectrometry, X-ray diffraction, and atomic force microscopy. The corrosion resistance was evaluated using potentiodynamic polarization tests in Hank's simulated physiological solution at 37 °C. The results showed that deposition using both $ZrOCl_2$ and $ZrO(NO_3)_2$ aqueous solutions reduces the surface roughness and improves the corrosion resistance of superelastic NiTi wires. When a $ZrOCl_2$ methanolic electrolyte was used, the deposition was heterogeneous and cracks were observed in the film. The addition of PolyDADMAC to aqueous and methanolic electrolytes resulted in more uniform coating surface and higher corrosion resistance in Hank's solution. The deposition of ZrO_2 improved the corrosion resistance of NiTi wires even when no previous electrolytic polishing was applied.

Keywords: *nickel-titanium; corrosion; electrodeposition; nanocoating; zirconia; biomaterials.*

4.1 Introduction

NiTi alloys are widely used in biomedical applications and are preferred for specific applications over conventional implant materials such as titanium, stainless steel, and cobalt-based alloys because of their unique thermomechanical properties. Superelastic (or pseudoelastic) NiTi alloys have the ability to recover their original shape after large deformations only by load removal and have been used to produce orthodontic wires and distractors, self-expandable vascular stents, intraspinal implants, intramedullary nails, etc. [1]. Nevertheless, studies of the corrosion behavior and nickel release of NiTi devices exposed to simulated body fluid environments are still limited and controversial [2]. Some reports noted serious concerns over the systemic toxicity of nickel ion release [3,4]. However, other studies stated that NiTi has a corrosion resistance comparable to that of pure titanium and its nickel release is insignificant [5,6]. Ohtsu et al. [7] demonstrated that nickel ion concentration ranging from $0.05\ mg{\cdot}L^{-1}$ to $3\ mg{\cdot}L^{-1}$ results in a beneficial antibacterial effect without cytotoxicity.

Although a high corrosion resistance is expected owing to the spontaneous formation of a passive TiO_2 thin film on the surface of NiTi alloys, their corrosion stability is strongly dependent on the surface condition [8]. Defects and irregularities act as corrosion initiation sites and stress concentrators, which can initiate the nucleation of cracks and cause premature failure of the NiTi device. Several surface modification techniques have been investigated to improve the surface of NiTi alloys, such as electrochemical processes, ion implantation, and coating applications of different materials and compounds [9]. Among these compounds, ZrO_2 presents high mechanical strength, chemical inertness, thermal stability, and excellent wear and corrosion resistances [10]. It has been deposited on stainless steels [11-13] and other materials intended for biomedical applications such as titanium alloys [14-16] and cobalt-chromium-molybdenum alloys [17] with relative success.

Few attempts to coat NiTi alloys with ZrO_2 have been reported. Giacomelli et al. [18] performed electrodeposition using a $ZrOCl_2$ solution and obtained a uniform coating that improved the breakdown potentials of the NiTi wire but with numerous cracks in evidence. A study by Qiu et al. [19] showed that a 7-μm-thick hydroxyapatite/ZrO_2 composite coating electrodeposited on NiTi improved the corrosion resistance of the

alloy by approximately 60 times. The drawback is that the mechanical strength of hydroxyapatite is very low for use in load-bearing applications. To the best of our knowledge, the most successful attempt to deposit a ZrO_2 coating on NiTi alloy was made by Sui and Cai [20], using plasma immersion ion implantation and deposition. They obtained a 200-nm-thick coating that lowered the surface friction coefficient and improved the corrosion resistance of the alloy. Furthermore, Ng et al. [21] used laser alloying technique to modify the surface of a NiTi alloy with ZrO_2, successfully improving its wear and corrosion resistance.

This study aimed to obtain a uniform and crack-free nanoscaled ZrO_2 coating to minimize nickel release to the human body and avoid premature failures of NiTi components using electrodeposition — a low cost and rapid method to obtain high-purity deposits on substrates of complex shapes [22]. Electrodepositions were performed using electrolytes of two zirconyl salts, $ZrO(NO_3)_2$ and $ZrOCl_2$. The effects of the addition of methanol and polyDADMAC to the electrolyte were also evaluated. Characterizations were performed using scanning electron microscopy with energy dispersive X-ray spectrometry (SEM/EDX), X-ray diffraction (XRD), atomic force microscopy (AFM), and differential scanning calorimetry (DSC), and the corrosion resistance was assessed using potentiodynamic polarization tests in Hank's simulated physiological solution at a constant temperature of 37 °C.

4.2 Experimental procedure

4.2.1 Sample preparation and characterization

A superelastic NiTi wire with a diameter of 1 mm (supplied by NDC, Fremont, CA, USA) was used as the substrate. The phase transformation temperatures were obtained using DSC (DSC-60, Shimadzu, Kyoto, Japan) with the method of tangent interception. Measurements were carried out in triplicate, using specimens with a mass of 20 mg, at temperatures ranging from −100 °C to 100 °C under a controlled cooling/heating rate of 10 °C/min. *C*rystallographic phases were identified using XRD (Empyrean, PANalytical, Almelo, The Netherlands) with Cu-Kα radiation at 40 kV and 30 mA, step size of 0.01° and time per step of 3.0 s.

The surface morphology and semi-quantitative chemical composition were evaluated using SEM (Inspect S50, FEI, Hillsboro, USA) equipped with EDX (Genesis, EDAX Inc., Mahwah, USA). Additional superficial evaluation was performed using AFM (XE-70, Park System, Suwon, Korea) operating in the tapping mode with the scanning rate of 1 Hz. The surface roughness was measured over three areas of 30 μm × 30 μm per sample using the average surface roughness (Ra) parameter.

Prior to the deposition, the NiTi wires were electrolytic polished at the room temperature of 25 °C using a potentiostat (VersaSTAT 3, Princeton Applied Research, Berwyn, USA) and a standard electrochemical cell with a platinum grid as the counter electrode and a Ag|AgCl (3.0 $mol \cdot L^{-1}$ KCl) as the reference electrode. In this paper, all potentials refer to this electrode at 25 °C. A 3.5 $mol \cdot L^{-1}$ H_2SO_4 methanolic solution at room temperature of 25 °C was used as the electrolyte and the anodic polarization curve was determined via a potentiodynamic scan from 0 V to 10 V at a scan rate of 0.01 $V \cdot s^{-1}$. The electropolishing was conducted at the corresponding limiting current density plateau in the anodic polarization curve for different times. After electrolytic polishing, the samples were ultrasonically cleaned with acetone and deionized water.

4.2.2 Electrochemical deposition

Analytical grade chemicals from Sigma–Aldrich — zirconium oxynitrate hydrate ($ZrO(NO_3)_2 \cdot xH_2O$), zirconyl chloride octahydrate ($ZrOCl_2 \cdot 8H_2O$), methanol (CH_3OH), and polyDADMAC (poly(diallyldimethylammonium chloride) or PDDA) with high molecular weight in the range of 400,000 to 500,000 — were used as starting materials. The compositions of the five solutions used are summarized in Table 4.1.

The electrodepositions were conducted at the room temperature of 25 °C using a potentiostat Autolab PGSTAT100N (Metrohm Autolab, Utrecht, The Netherlands) and the same cell and electrodes specified in Section 2.1. A cathodic pulsed current density of 3 $mA \cdot cm^{-2}$ ($t_{on} = t_{off} = 0.005$ s) was applied for different times (300, 600, 900, 1200, and 1500 s) and the coated samples were thereafter naturally air dried for 24 h. In order to investigate the differences in the electrochemical deposition processes when using each of the electrolytes listed in Table 4.1, cathodic polarization tests were carried out from the potential of 0 V to −2 V at a scanning rate of 0.001 V.

Table 4.1 – Compositions of the solutions used for electrodeposition.

Electrolytes	Composition
$ZrO(NO_3)_2$ (aq)	0.05 mol·L^{-1} $ZrO(NO_3)_2$ (aq)
$ZrOCl_2$ (aq)	0.05 mol·L^{-1} $ZrOCl_2$ (aq)
$ZrOCl_2$ (met)	0.05 mol·L^{-1} $ZrOCl_2$ + 100 g·L^{-1} H_2O (met)
$ZrOCl_2$ + polyDADMAC (aq)	0.05 mol·L^{-1} $ZrOCl_2$ + 1.0 g·L^{-1} polyDADMAC (aq)
$ZrOCl_2$ + polyDADMAC (met)	0.05 mol·L^{-1} $ZrOCl_2$ + 100 g·L^{-1} H_2O + 1.0 g·L^{-1} polyDADMAC (met)

4.2.3 Characterization of coatings

Structural and morphological characterizations of the deposited films were also performed using SEM/EDX, XRD, and AFM techniques. Probe analyses were performed over at least three different places along the length of the wires on two samples of each condition to assess the uniformity of the coatings. The surface roughness was measured over 10 scanning areas of 5 μm × 5 μm and expressed in terms of the average (Ra) and peak-to-valley (Rpv) roughness.

4.2.4 Corrosion resistance test

The corrosion resistance was evaluated using the same potentiostat, cell, and electrodes specified in Section 2.2. Potentiodynamic polarization curves were obtained in Hank's simulated physiological solution at a constant temperature of 37 °C (pH = 7.4), prepared with the following composition: 0.14 g·L^{-1} $CaCl_2 \cdot 2H_2O$, 0.4 g·L^{-1} KCl, 0.06 g·L^{-1} KH_2PO_4, 8.0 g·L^{-1} NaCl, 0.35 g·L^{-1} $NaHCO_3$, 0.06 g·L^{-1} $MgSO_4$, 0.05 g·L^{-1} Na_2HPO_4, and 1.0 g·L^{-1} D-Glucose. The measurements were made at a scan rate of 0.005 V·s-1, starting at −0.25 V from open circuit potential, stabilized for 60 min, up to +1.2 V. The corrosion potential (E_{corr}) and corrosion current density (i_{corr}) were calculated using the Tafel extrapolation method, whereas the breakdown potential (E_b) was obtained from the rapid increase of the current density in the polarization curve.

4.3 Theory of ZrO_2 electrochemical deposition

Cathodic electrodeposition is a widely used process for obtaining nanostructured films that offer important advantages, such as strict control of the thickness of the deposited film, good uniformity and purity, and high deposition rates. ZrO_2 coatings have been obtained via electrochemical deposition on various metallic substrates [11-14,17,18,23-25], but only a few studies of the deposition mechanism have been conducted [14,26-28]. The mechanism generally proposed for the formation of ZrO_2 using aqueous electrolytes of zirconyl salts is based on the electrosynthesis of zirconium hydroxide particles on the surface of the substrate. Initially, the salts dissolve in water, releasing the zirconyl cations (ZrO^{2+}), that are solvated forming the tetramer $[Zr_4(OH)_8(H_2O)_{16}]^{8+}$ [28,29]. The solutions of zirconyl salts are highly acidic due to the tendency of these solvated species to release protons [28,30]:

$$[Zr_4(OH)_8(H_2O)_{16}]^{8+} \rightleftharpoons [Zr_4(OH)_{2+x}.(4-x)(H_2O)]_4^{8-4x} + 4xH^+ \quad (1)$$

The cathodic reactions occurring during the electrodeposition process increase the pH value near the cathode surface, and colloidal particles of zirconium hydroxide precipitate at the NiTi surface. On a subsequent step, this hydroxide is dehydrated leading to the formation of ZrO_2 [27,28]. The OH^- ions, which allow the formation of colloidal particles on the surface of the substrate, can be generated by several cathodic reactions, including the reduction of water, dissolved oxygen, and nitrate ions [28]:

$$2H_2O + 2e^- \rightarrow H_2 + 2OH^- \quad (2)$$

$$O_2 + 2H_2O + 4e^- \rightarrow 4OH^- \quad (3)$$

$$NO_3^- + H_2O + 2e^- \rightarrow NO_2^- + 2OH^- \quad (4)$$

$$NO_3^- + 7H_2O + 8e^- \rightarrow NH_4^+ + 10OH^- \quad (5)$$

In methanolic solutions, CH_3OH reduction can also be considered:

$$2CH_3OH + 2e^- \rightarrow C_2H_6 + 2OH^- \quad (6)$$

Hydrogen reduction, as well as other concurrent reactions without the generation of OH^-, could also occur at the cathode, inhibiting the deposition of ZrO_2:

$$2H^+ + 2e^- \rightarrow H_2 \quad (7)$$

The cathodic reactions and rate of OH^- generation are determinants of the electrodeposition processes. A rate generation faster than the consumption of OH^- by the hydrolysis reactions would result in a fraction of the OH^- ions being transported away by the electric current and diffusion, moving the high pH boundary away from the surface of the cathode, and compromising the adhesion of the coating [31].

4.4 Results and discussion

4.4.1 Substrate characterization and surface preparation

The average phase transformation temperatures were determined as 15.8 °C for martensite start (Ms), 2.9 °C for martensite finish (Mf), 3.3 °C for austenite start (As), and 22.6 °C for austenite finish (Af). XRD analysis revealed the B2 austenite as the only constituent present at 25 °C. Thus, considering the temperature of Af and the XRD results, the NiTi wires used in this study were expected to be in a fully austenitic state at room temperature.

The surface preparation of the substrate is a critical step to produce coatings with higher corrosion resistance. Electropolishing is an inexpensive surface treatment, capable of selectively dissolve superficial irregularities even in objects of complex shapes [9]. A 3.5 $mol \cdot L^{-1}$ H_2SO_4 methanolic solution, which had previously demonstrated good results for the surface preparation of NiTi wires in the austenitic state [32], was chosen for the electrolytic polishing. The applied potential of 7 V was determined based on the limiting current density plateau in the anodic polarization curve. In this region, the process is controlled by mass transport, limited by the diffusion of anions dissolved from the metal surface through the passivated layer, and the polishing conditions are ideal [33]. The most uniform surface was observed via SEM after electrolytic polishing for 360 s and thus, longer polishing times were unnecessary.

Figure 4.1 shows the surface morphology of the as-received NiTi wires and after electrolytic polishing for 360 s. Several scratch marks and other defects, formed probably during mechanical polishing, were present on the commercially available NiTi wire. After electropolishing, the surface showed a martensite-like aspect, which has been reported as a pseudo-martensitic relief structure revealed owing to shearing during thermal induced phase transformations [34,35]. Some inclusions were also detected throughout the surface of the polished sample. These inclusions, as indicated by EDX microanalysis, were mainly particles of TiC, which usually form during the melting processes of NiTi alloys in carbon crucibles [36]. Semi-quantitative EDX microanalysis on the surface of the NiTi wire showed an average chemical composition statically similar before and after electropolishing. The average surface roughness (Ra) of the as-received surface was 195 ± 9 nm whereas after electrolytic polishing, the roughness was reduced to 20 ± 1 nm. The real surface area of the electropolished samples, calculated from AFM data, was higher than its geometrical area by only 0.3% and its influence on the current density applied during electrodeposition can be neglected.

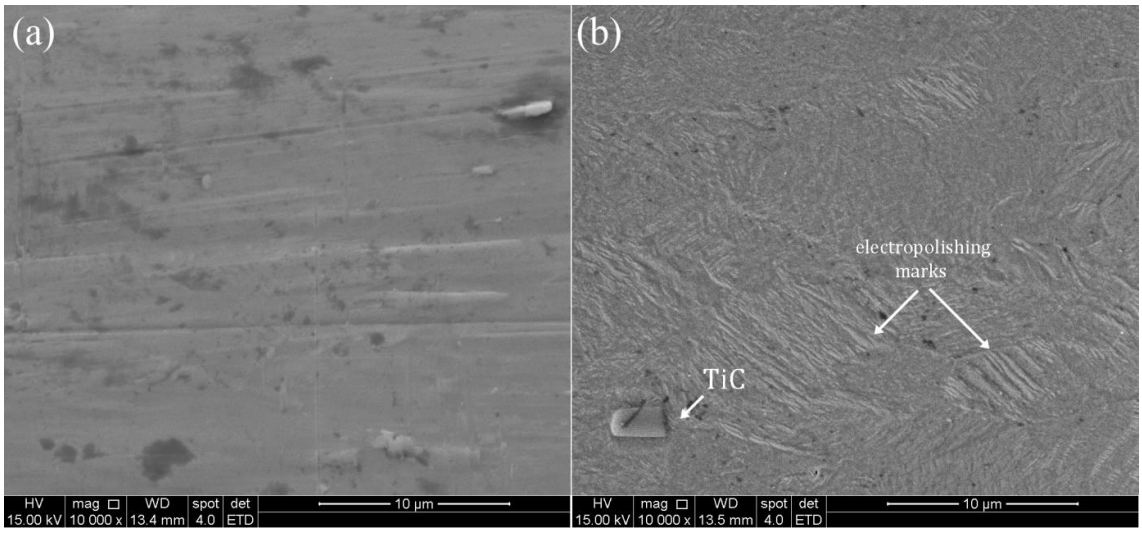

Figure 4.1 – Surface morphology of NiTi wires: (a) as received and (b) after electrolytic polishing in H_2SO_4.

4.4.2 Electrochemical deposition

Polarization tests were performed in aqueous electrolytes and methanolic electrolytes. The cathodic polarization curves of NiTi wires in 0.05 mol L^{-1} $ZrO(NO_3)_2$ (aq) and 0.05 mol L^{-1} $ZrOCl_2$ (aq) are shown in Figure 4.2a. Both curves can be divided into two stages. First, as the potential is swept to the cathodic region, there is a sharp increase in current density from potentials of approximately −0.5 V and −0.8 V for the $ZrO(NO_3)_2$ (aq) and $ZrOCl_2$ (aq) solutions, respectively. This current can be related to several reactions. Prior to the H^+ reduction reaction (Eq. 7) it is likely that both O_2 reduction [14,37] in acidic media (Eq. 8) and NO_3^- reduction (Eq. 4) occur [27], although there is no study demonstrating the reduction of NO_3^-.

$$O_2 + 4H^+ + 4e^- \rightarrow 2H_2O \quad (8)$$

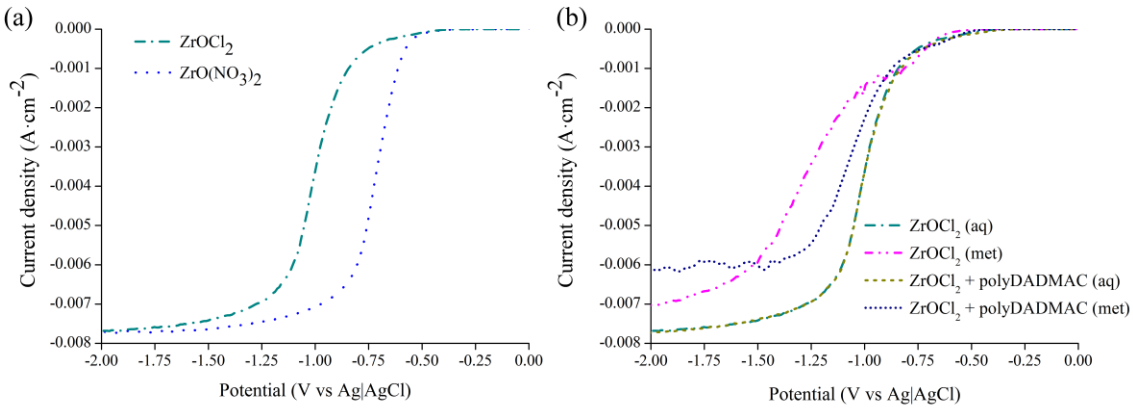

Figure 4.2 – Cathodic polarization curves of the NiTi wires in the electrolytes evaluated in this study: (a) $ZrO(NO_3)_2$ or $ZrOCl_2$ aqueous electrolytes, and (b) solutions with methanol and polyDADMAC additions.

In our polarizations tests, it was not possible to observe any feature that indicated the reduction of O_2 or NO_3^- as the currents related to the reduction of these species were much smaller than the current of the H^+ reduction and, consequently, the higher rate of this reaction overlapped other possible reactions. Figure 4.2a also shows a higher overpotential in the H^+ reduction in the presence of chloride than in the presence of nitrate. As shown by Yen [14] in a previous study, the addition of NO_3^- accelerates the reduction of H^+. This faster hydrogen evolution can explain the higher surface roughness in the deposits obtained from $ZrO(NO_3)_2$, as will be discussed later. In the

second stages of the polarizations curves, which starts at the potentials of −1.5 V and −1.75 V for the $ZrO(NO_3)_2$ and $ZrOCl_2$ solutions, respectively, a limiting current density is observed and it can be attributed to the reduction of H^+ ions [14].

The cathodic polarization curves of the solutions of $ZrOCl_2$ salt in aqueous and methanolic media are shown in Figure 4.2b. These curves can also be divided into two stages as previously discussed. The first stage starts at approximately −0.5 V where the current increases due to the reduction of H^+ and O_2, according to equations (7) and (8). The second stage starts when the curves reach the current density plateau related to the limiting current density of H^+. These current densities are the same for the aqueous electrolytes (approximately $-0.0078\ A \cdot cm^{-2}$). However, the $ZrOCl_2$ (met) solution resulted in lower H^+ limiting current density, most likely due to the lower diffusion rate of H^+ ions in the methanolic solution. The addition of polyDADMAC to the $ZrOCl_2$ (met) solution further reduced the limiting current density to approximately $-0.006\ A \cdot cm^{-2}$. The presence of polyDADMAC did not affect the polarization curve in aqueous solutions, as expected, as it does not deposit on the cathode [13,27]. However, in a mixed methanol–water solvent, the polymer can be adsorbed onto the surface of the colloidal particles [13] and it is likely that the presence of polyDADMAC on the electrode interface causes a reduction in the mass transport of H^+. This would explain the lower limiting current density in a methanol–water polyDADMAC solution. Regarding the difference in the slope of the polarizations curves in methanolic and aqueous solutions, the lower slope in methanolic solutions can be attributed to an increase in the charge transfer resistance.

4.4.3 Coating characterization

4.4.3.1 Deposition from aqueous solutions

Studies wherein the ZrO_2 coatings were prepared from pure aqueous $ZrO(NO_3)_2$ or $ZrOCl_2$ solutions systematically reported low current efficiencies, low adhesion, and high incidence of cracks [11–14,17,18,27,31]. Low adhesion has been associated with the electrostatic repulsion of negatively charged colloidal particles formed at the cathode surface [28] and low current efficiency is attributed to the reduction reactions that do not produce hydroxyl ions or the consumption of hydroxyl ions by H^+ ions

generated at the anode and present in the bulk solution [27]. The coating cracks are often attributed to drying shrinkage during the dehydration of the hydroxide via annealing or natural drying in air [12,18,25] and are more accentuated on thick coatings[31].

The morphologies of the NiTi surfaces after electrodeposition using the aqueous solutions of $ZrO(NO_3)_2$ and $ZrOCl_2$ are shown in Figure 4.3. The coating obtained using $ZrO(NO_3)_2$ covered the electropolishing surface marks but was considerably more heterogeneous than the one obtained using $ZrOCl_2$. From AFM analyses (Figure 4.4), it can be observed that the surface roughness measured after the electrodeposition with $ZrO(NO_3)_2$ was lower than at the initial electropolished NiTi surface. Furthermore, the deposition using the $ZrOCl_2$ electrolyte systematically resulted in a more pronounced reduction in the roughness at all deposition times. From X-ray analyses, no peaks corresponding to ZrO_2 phases were observed possibly owing to the low thickness or the amorphous state of the coating, as suggested by other studies [18,25]. According to the literature, crystallization of the ZrO_2 coating is observed only after annealing [25].

The corrosion resistance of NiTi components strongly relies on its surface condition, and smoother surfaces are usually associated with higher corrosion and wear resistances [9,38]. A low surface roughness is desirable for many applications, such as in stents and orthodontic wires [39,40]. Therefore, the $ZrOCl_2$ solution was chosen for further investigations on the addition of methanol and polyDADMAC.

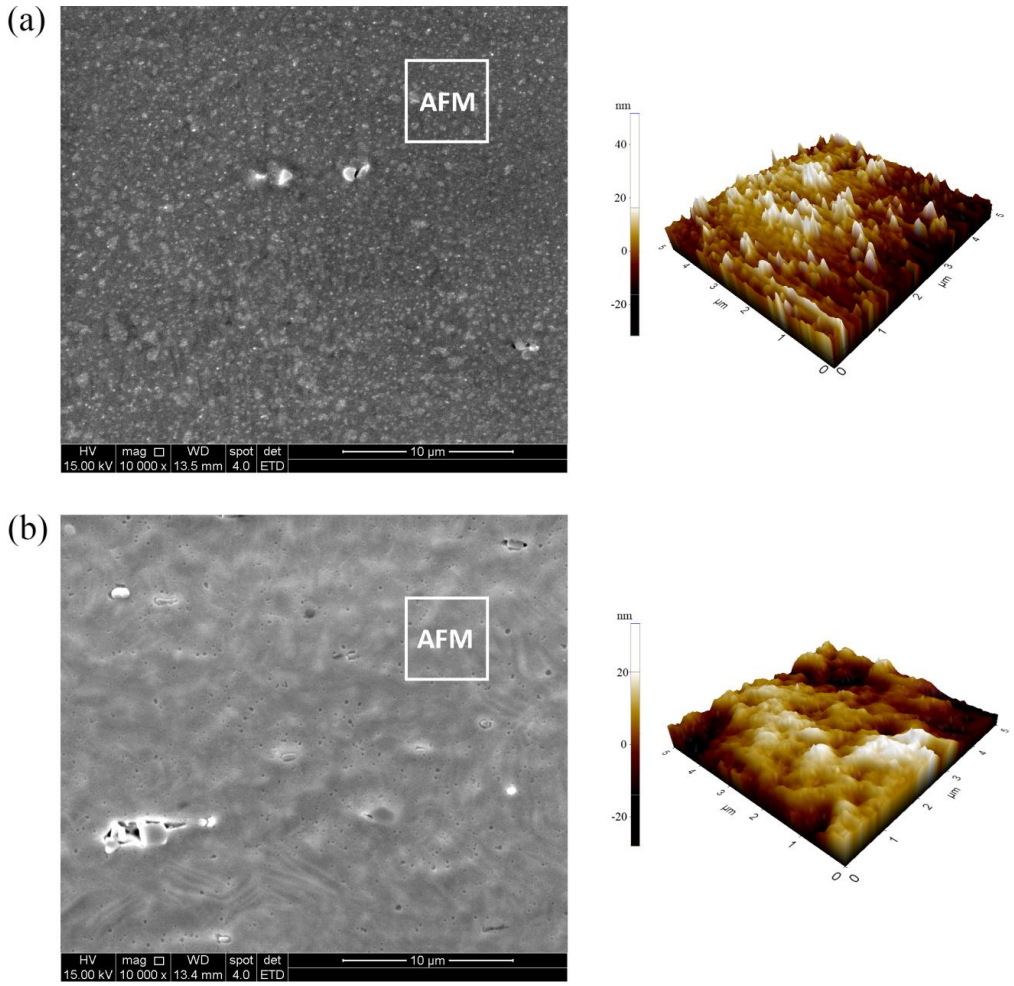

Figure 4.3 – SEM and AFM 3D surface images of NiTi wires after electrodeposition for 1200 s using aqueous electrolytes: (a) $ZrO(NO_3)_2$ and (b) $ZrOCl_2$.

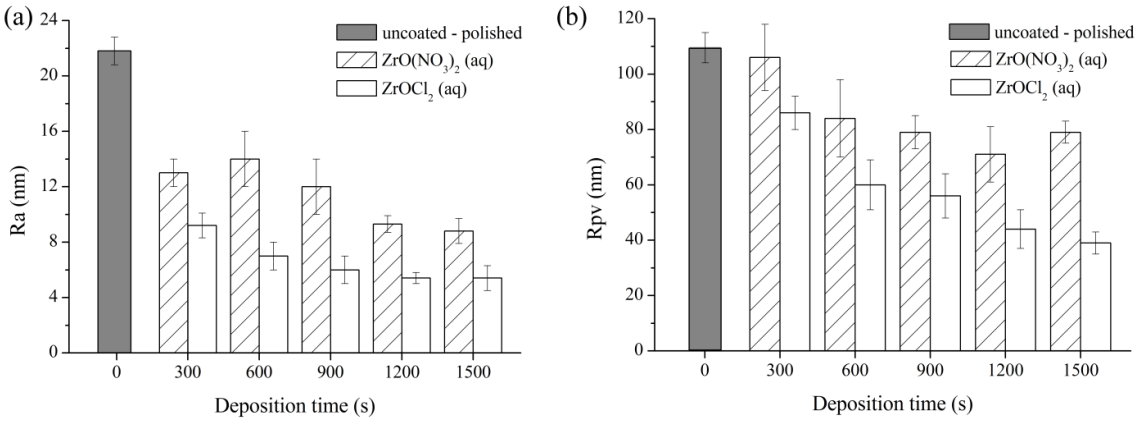

Figure 4.4 – Roughness measured using AFM analysis of NiTi wires before and after electrodeposition using the $ZrO(NO_3)_2$ and $ZrOCl_2$ aqueous electrolytes: (a) average surface roughness; and (b) peak-to-valley roughness.

4.4.3.2 Deposition from methanolic solution

The use of methanol–water solutions have been found to be efficient at reducing cracking and porosity in electrolytic deposits and enhancing the deposition rate [28]. The addition of alcohols to aqueous solutions reduces the total dielectric constant of the solvent, decreases the double layer, and promotes particle coagulation. A reduction in the dielectric constant also reduces the solubility of the deposit layer. Nevertheless, in electrodeposition, a sufficient amount of water for base generation in cathodic reactions is always necessary [41].

Figure 4.5 shows the surface morphology of the film deposited on the NiTi wire using the $ZrOCl_2$ methanolic electrolyte. As shown in these SEM images, there is a high deposit accumulation adjacent to the TiC precipitates (dark regions), due to charge concentration effects. The cracks in the film, indicated by white arrows, are also evident in the image. The same characteristics were observed in the films for all the electrodeposition times applied.

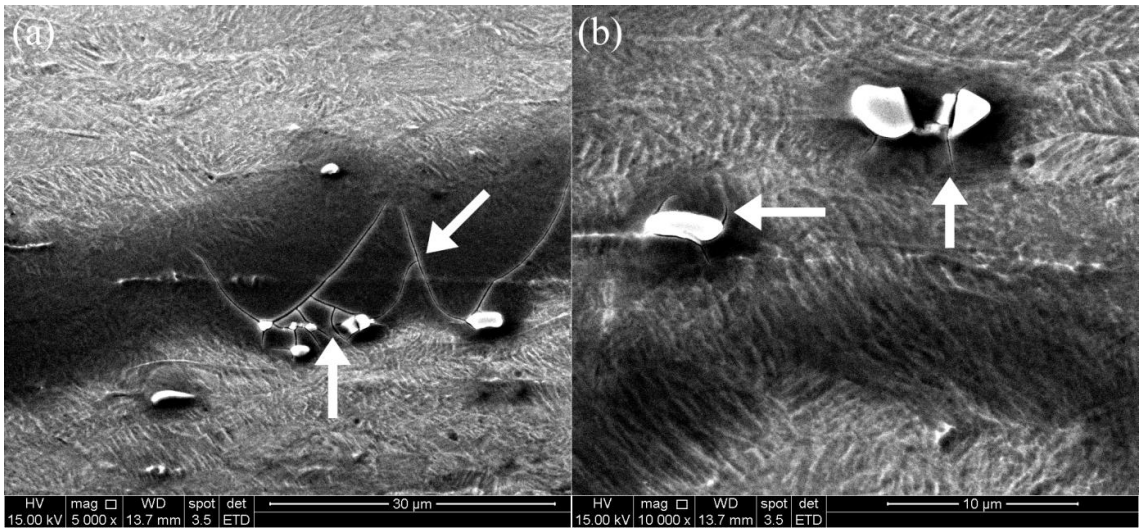

Figure 4.5 – SEM surface images of NiTi wire after electrodeposition using the $ZrOCl_2$ methanolic electrolyte for: (a) 900 s with the original magnification of 5000×; and (b) 1200 s with the original magnification of 10000×.

4.4.3.3 Deposition using polyDADMAC

PolyDADMAC is a strong cationic polyelectrolyte with inherent binding properties, which can be used to increase the adherence of the deposit and prevent cracking. It compresses the double layer of zirconium hydroxide particles at the surface, resulting in particle flocculation and an increase in the deposition efficiency. Moreover, the polymer particles are adsorbed onto the hydroxide colloidal particles and an organoceramic composite can be formed [31]. According to Zhitomirsky [28], ZrO_2 deposits obtained without polyDADMAC have low adhesion. However, at higher concentrations, the polyelectrolyte can cause a shielding effect preventing the formation of colloidal particles of zirconium hydroxide [31].

The morphologies of NiTi surfaces after electrodeposition using the $ZrOCl_2$ + polyDADMAC aqueous and methanolic electrolytes for 1200 s are shown in Figure 4.6. For both electrolytes, the addition of polyDADMAC resulted in a uniform surface morphology and the electropolishing marks were less evident. The values of surface roughness before and after electrodeposition using the $ZrOCl_2$ aqueous and $ZrOCl_2$ + polyDADMAC aqueous and methanolic electrolytes are shown in Figure 4.7. It can be observed that, when adding polyDADMAC to the $ZrOCl_2$ aqueous electrolyte, the film obtained exhibited values of Ra — which corresponds to the arithmetic average of the height deviations from the mean profile — either inferior or equal to the values of Ra obtained from $ZrOCl_2$ aqueous electrolytes. Furthermore, the values of Rpv — which is the average of the five highest peaks and the five deepest valleys — were statistically inferior ($p = 0.01$) for all deposition times. Although the peak-to-valley roughness can be strongly affected by the chosen region of the analyses, it is an important parameter as it is sensitive to coating defects and can influence the friction and wear.

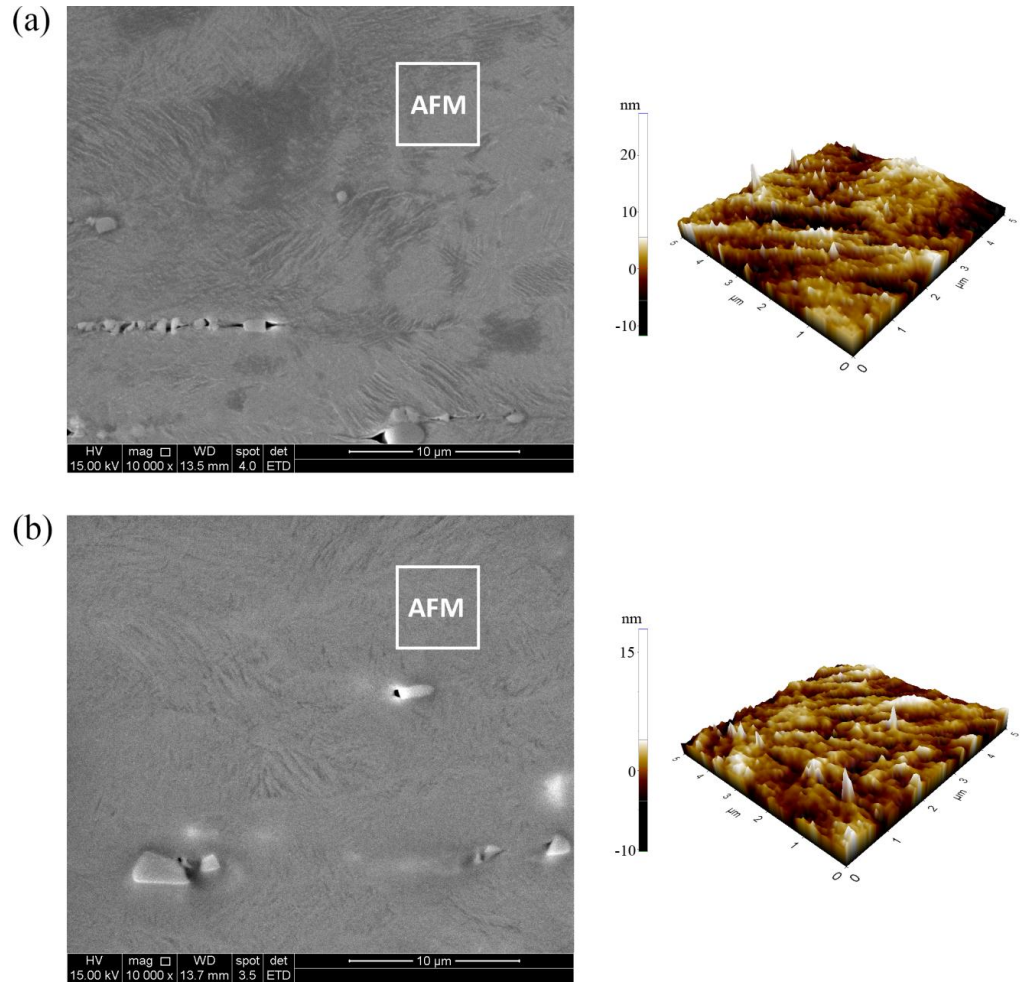

Figure 4.6 – SEM and AFM 3D surface images of NiTi wires after electrodeposition using the $ZrOCl_2$ + polyDADMAC (a) aqueous and (b) methanolic electrolytes.

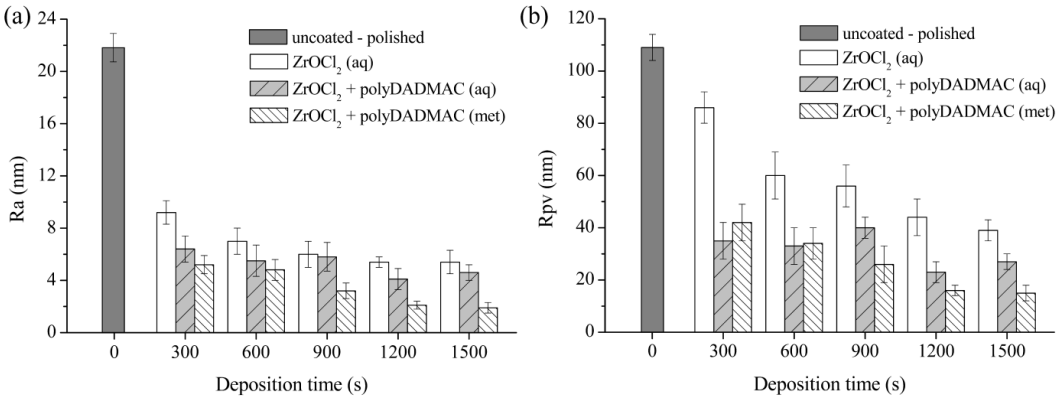

Figure 4.7 – Roughness measured using the AFM analysis of NiTi wires before and after electrodeposition using the $ZrOCl_2$ aqueous and $ZrOCl_2$ + polyDADMAC aqueous and methanolic electrolytes: (a) average surface roughness; and (b) peak-to-valley roughness.

For the coating obtained from the $ZrOCl_2$ + polyDADMAC methanolic electrolyte, roughness values were statistically significant and systematically inferior to those obtained using the $ZrOCl_2$ aqueous electrolyte. When compared to the $ZrOCl_2$ + polyDADMAC aqueous electrolyte, for deposition times up to 600 s, the surface roughness was statistically similar. After 900 s, both Ra and Rpv were inferior in the case of the $ZrOCl_2$ + polyDADMAC methanolic electrolyte and the minimum surface roughness was achieved after 1200 s of electrodeposition (Ra = 2.1 ± 0.3 nm; Rpv = 15 ± 2 nm). No significant difference was observed in the surface roughness between 1200 s and 1500 s of deposition.

Zhitomirsky and Petric [31], using a 0.005 $mol \cdot L^{-1}$ $ZrOCl_2$ aqueous solution with the addition of polyDADMAC of 0.1 $g \cdot L^{-1}$, and the galvanostatic current density of 10 $mA \cdot cm^{-2}$, determined, via thermogravimetric analysis, that the deposits obtained on Ni foils were mainly composed of zirconium hydroxide and a small amount of polyDADMAC. However, the deposits obtained with the addition of 1.0 $g \cdot L^{-1}$ of polyDADMAC contained 51 wt.% of the organic phase. The authors stated that, for small amounts the polyDADMAC acts as a binder, preventing cracking and increasing deposit adhesion, and at higher concentrations, organoceramic deposits can be obtained. Similarly, Pang et. al [13] using a 0.005 $mol \cdot L^{-1}$ $ZrOCl_2$ methanolic electrolyte (5 vol.% water), and the galvanostatic current density of 5 $mA \cdot cm^{-2}$, determined, that the amount the organic phase was 41.5 and 60.8 wt.% in the deposits on stainless steel that were prepared from the solutions containing, respectively, 0.5 and 1.0 $g \cdot L^{-1}$ of polyDADMAC. Considering the polyDADMAC addition ratio used in our study (0.05 $mol \cdot L^{-1}$ $ZrOCl_2$ and 1.0 $g \cdot L^{-1}$ polyDADMAC), it is more likely that our deposit will not contain the organic phase. The presence of polyDADMAC on the deposits could not be confirmed using DSC or XRD analyses due owing to its low thickness. Analogous to the coatings obtained from the $ZrOCl_2$ aqueous electrolyte, XRD only detected the NiTi austenite phase on the wires after deposition using the $ZrOCl_2$ + polyDADMAC aqueous or methanolic electrolytes, also likely as a result of its low thickness or amorphous state [13,27]. However, the coatings obtained when the polyDADMAC was added to the electrolyte were more homogeneous and smoother, and are more likely to enhance the corrosion resistance than the coating obtained using the $ZrOCl_2$ aqueous electrolyte.

4.4.4 Corrosion resistance

Figure 4.8 shows the potentiodynamic polarization curves in Hank's solution at 37 °C of NiTi wires as received, electropolished, and after electrodeposition for 1200 s for each deposition solution evaluated in this study. The electrochemical parameters extracted from the curves are given in Table 4.2. It can be observed that the as-received NiTi wire exhibited the lowest corrosion resistance, with a corrosion potential of −0.256 V, corrosion current density of 1.3×10^{-8} A·cm^{-2}, and breakdown potential of 0.284 V. Electrolytic polishing of the NiTi wire sample resulted in a slightly more noble corrosion potential (−0.220 V) and a similar corrosion current density. However, the polished sample did not exhibit breakdown at potentials below the oxygen evolution, evidencing that the polished wire is less prone to localized corrosion than the as-received NiTi wire, which is consistent with previous studies on the corrosion resistance in Hank's solution of electropolished NiTi alloys [32,42].

Compared to the uncoated, as-received, and polished samples, the corrosion potential of the wires coated using $ZrO(NO_3)_2$ and $ZrOCl_2$ aqueous electrolytes was higher, indicating the improvement of corrosion resistance. The corrosion current of the sample coated using the $ZrO(NO_3)_2$ aqueous solution electrolyte was marginally higher than that coated using the $ZrOCl_2$ aqueous solution. With the addition of polyDADMAC to the $ZrOCl_2$ aqueous electrolyte, the corrosion potential of the coated wire increased by 0.080 V. It can also be observed that the corrosion potentials of the wires coated using methanolic electrolytes were the most positives. The sample coated using the $ZrOCl_2$ methanolic electrolyte exhibited the corrosion potential of 0.159 V, which changed to 0.194 V after the polymer addition.

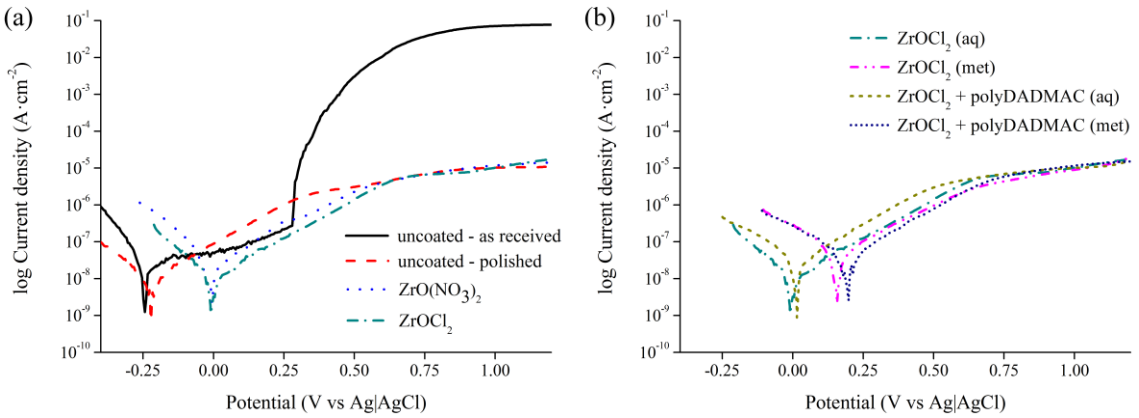

Figure 4.8 – Potentiodynamic polarization curves of NiTi wires in Hank's solution: (a) uncoated wires, as received and polished, and polished wires coated using $ZrO(NO_3)_2$ and $ZrOCl_2$ aqueous electrolytes, and (b) polished wires coated using $ZrOCl_2$ electrolytes with methanol and polyDADMAC additions.

Table 4.2 – Corrosion parameters obtained from the potentiodynamic polarization curves of the NiTi wires in Hank's solution.

	E_{corr} [V]	**i_{corr} [A·cm^{-2}]**	**E_b [V]**
uncoated - as received	−0.256	1.3 ×10^{-8}	0.284
uncoated - polished	−0.220	1.1 ×10^{-8}	-
$ZrO(NO_3)_2$ (aq)	−0.068	2.1 ×10^{-8}	-
$ZrOCl_2$ (aq)	−0.002	0.9 ×10^{-8}	-
$ZrOCl_2$ (met)	0.159	2.4 ×10^{-8}	-
$ZrOCl_2$ + polyDADMAC (aq)	0.008	2.0 ×10^{-8}	-
$ZrOCl_2$ + polyDADMAC (met)	0.194	2.1 ×10^{-8}	-

Briefly, the results obtained for the coated samples indicate that the deposition shifted the corrosion potential values toward noble potentials for all compositions of the electrolytes evaluated in this study. The corrosion current densities of the coated samples were similar, and no breakdown potential was observed. The highest corrosion resistance was obtained using the $ZrOCl_2$ methanolic electrolyte with the addition of polyDADMAC.

It is interesting to note that the coating deposition was sufficient to protect the NiTi substrate from localized corrosion even when no prior electropolishing was used, as presented in Figure 4.9 and Table 4.3. The only exception was the $ZrOCl_2$ methanolic, which exhibited a breakdown potential at 0.564 V. As observed on the polished wires, the addition of polyDADMAC to the electrolytes resulted in the improvement of corrosion potential, and the highest corrosion resistance was observed using the $ZrOCl_2$ + polyDADMAC methanolic solution. Moreover, for the methanolic electrolytes, the combination of electrolytic polishing and deposition resulted in higher corrosion resistance.

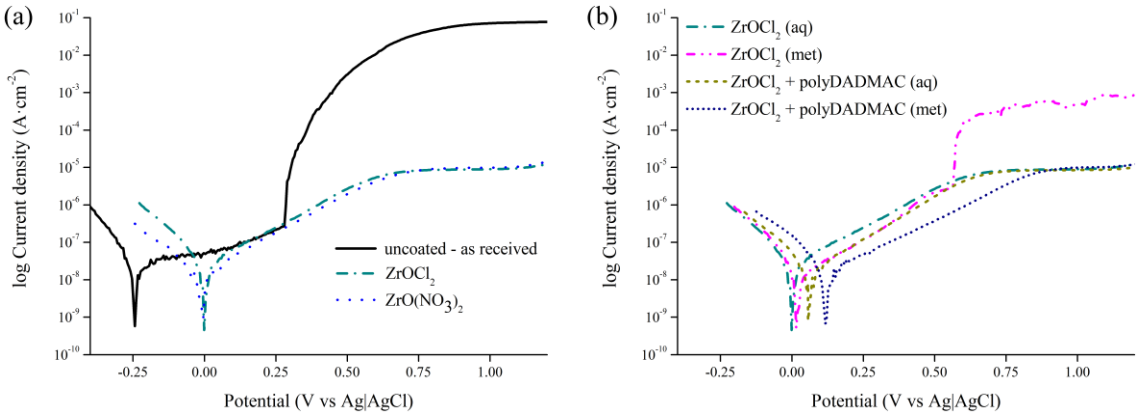

Figure 4.9 – Potentiodynamic polarization curves in Hank's solution of NiTi unpolished wires after deposition using different electrolytes: (a) as-received uncoated wires coated using $ZrO(NO_3)_2$ and $ZrOCl_2$ aqueous electrolytes, and (b) wires coated using $ZrOCl_2$ electrolytes with methanol and polyDADMAC additions.

Table 4.3 – Corrosion parameters obtained from the potentiodynamic polarization curves in Hank's solution of the unpolished NiTi wires coated using different electrolytes.

	E_{corr} [V]	i_{corr} [A·cm^{-2}]	E_b [V]
$ZrO(NO_3)_2$ (aq)	−0.011	1.3×10^{-8}	-
$ZrOCl_2$ (aq)	0.000	1.4×10^{-8}	-
$ZrOCl_2$ (met)	0.026	1.4×10^{-8}	0.564
$ZrOCl_2$ + polyDADMAC (aq)	0.060	1.4×10^{-8}	-
$ZrOCl_2$ + polyDADMAC (met)	0.127	1.4×10^{-8}	-

Based on the results of the present study, it is evident that ZrO_2 coatings can improve the properties of NiTi alloys intended for biomedical applications. Deposition using aqueous solutions of $ZrOCl_2$ and $ZrO(NO_3)_2$ reduced the surface roughness and improved the corrosion resistance of superelastic NiTi wires. However, cracks were observed in the deposited coating when a methanolic electrolyte of $ZrOCl_2$ was used. The addition of PolyDADMAC to both aqueous and methanolic electrolytes of the $ZrOCl_2$ resulted in more uniform coating surface, with lower roughness and higher corrosion resistance in Hank's solution. Moreover, it can be seen that the deposition of ZrO_2 protects the NiTi substrate from localized corrosion even when no prior electropolishing is used, for all electrolytes evaluated, with the exception of the $ZrOCl_2$ methanolic solution. The optimal condition for the electrodeposition of ZrO_2 on NiTi superelastic wires, i.e. when the coated sample showed the lowest surface roughness and highest corrosion resistance, was achieved when the NiTi wire was coated using the $ZrOCl_2$ + polyDADMAC methanolic electrolyte.

These results demonstrate that the ZrO_2 coating is a good alternative for the improvement of corrosion resistance of NiTi superelastic alloys used in biomedical applications, owing to its capability to act as a barrier, blocking the electron transfer between the electrolyte and metal substrate. Additionally, the ZrO_2 coating obtained in this study can potentially reduce nickel release to the human body, avoiding cytotoxicity, and can diminish premature failures caused by fatigue in biomedical devices of NiTi alloys, for example vascular stents and endodontic instruments [1,9]. Also, due the good tribological properties or the ZrO_2, its application on NiTi alloys can improve wear resistance, expanding its use in load-bearing applications such as orthopedic implants and scaffolds [15,16].

4.5 Conclusions

ZrO_2 coating was deposited on the surface of a NiTi superelastic wire via pulsed cathodic electrodeposition using different solutions. Two aqueous solutions of $ZrO(NO_3)_2$ and $ZrOCl_2$ were evaluated, and also electrolytes with the addition of methanol and polyDADMAC. SEM and AFM analyses showed that the deposited film significantly reduced the surface roughness of the NiTi wires. Coatings obtained with

the $ZrOCl_2$ electrolyte were smoother than those obtained with $ZrO(NO_3)_2$. When a $ZrOCl_2$ methanolic electrolyte was used, the deposition was heterogeneous and cracks were observed. With the addition of polyDADMAC to both the aqueous and methanolic $ZrOCl_2$ electrolytes, a more uniform and smoother surface was obtained. From XRD analyses, no ZrO_2 phases could be identified possibly owing to low thickness or amorphous state of the deposit. The corrosion polarization tests in Hank's solution at 37°C showed that, for all the electrolyte compositions evaluated in this study, the coatings deposited on electropolished wires enhanced the corrosion potential to noble potentials and no breakdown potential was observed. The coating deposition was sufficient to protect the NiTi substrate from localized corrosion even when no prior electropolishing was used, with the exception of the $ZrOCl_2$ methanolic solution. The highest corrosion resistance was observed when the NiTi wire was coated using the $ZrOCl_2$ + polyDADMAC methanolic electrolyte, which also resulted in lower surface roughness and can be considered the optimal condition for the electrodeposition of ZrO_2 on NiTi superelastic wires. The results of this study indicate that the ZrO_2 coating is a good alternative for the improvement of corrosion of NiTi superelastic wires and can potentially improve the wear resistance, reduce nickel release to the human body, and avoid its premature failure in biomedical applications.

ACKNOWLEDGMENTS

The authors acknowledge Conselho Nacional de Desenvolvimento Científico e Tecnológico (CNPq), Fundação de Amparo à Pesquisa do Estado de Minas Gerais (FAPEMIG), and Coordenação de Aperfeiçoamento de Pessoal de Nível Superior (CAPES/PROEX) for supporting this research.

4.6 References

1. Q. Chen, G.A. Thouas, Metallic implant biomaterials, Materials Science and Engineering R: Reports. 87 (2015) 1–57. doi:10.1016/j.mser.2014.10.001.
2. M. Es-Souni, M. Es-Souni, H. Fischer-Brandies, Assessing the biocompatibility of NiTi shape memory alloys used for medical applications, Analytical and Bioanalytical Chemistry. 381 (2005) 557–567. doi:10.1007/s00216-004-2888-3.
3. G. Rondelli, Corrosion resistance tests on NiTi shape memory alloy, Biomaterials. 17 (1996) 2003–2008. doi:10.1016/0142-9612(95)00352-5.
4. E. Denkhaus, K. Salnikow, Nickel essentiality, toxicity, and carcinogenicity, Critical Reviews in Oncology/Hematology. 42 (2002) 35–56. doi:10.1016/S1040-8428(01)00214-1.
5. J. Ryhänen, E. Niemi, W. Serlo, E. Niemelä, P. Sandvik, H. Pernu, T. Salo, Biocompatibility of nickel-titanium shape memory metal and its corrosion behavior in human cell cultures, Journal of Biomedical Materials Research. 35 (1997) 451–457. doi:10.1002/(SICI)1097-4636(19970615)35:4<451::AID-JBM5>3.0.CO;2-G.
6. N. Figueira, T.M. Silva, M.J. Carmezim, J.C.S. Fernandes, Corrosion behaviour of NiTi alloy, Electrochimica Acta. 54 (2009) 921–926. doi:10.1016/j.electacta.2008.08.001.
7. N. Ohtsu, S. Suginishi, M. Hirano, Antibacterial effect of nickel-titanium alloy owing to nickel ion release, Applied Surface Science. 405 (2017) 215–219. doi:10.1016/j.apsusc.2017.02.037.
8. I. Milošev, B. Kapun, The corrosion resistance of Nitinol alloy in simulated physiological solutions, Materials Science and Engineering: C. 32 (2012) 1087–1096. doi:10.1016/j.msec.2011.11.007.
9. S. Shabalovskaya, J. Anderegg, J. Van Humbeeck, Critical overview of Nitinol surfaces and their modifications for medical applications, Acta Biomaterialia. 4 (2008) 447–467. doi:10.1016/j.actbio.2008.01.013.
10. J. Chevalier, What future for zirconia as a biomaterial?, Biomaterials. 27 (2006) 535–43. doi:10.1016/j.biomaterials.2005.07.034.

11. I. Espitia-Cabrera, H. Orozco-Hernández, R. Torres-Sánchez, M.E. Contreras-García, P. Bartolo-Pérez, L. Martínez, Synthesis of nanostructured zirconia electrodeposited films on AISI 316L stainless steel and its behaviour in corrosion resistance assessment, Materials Letters. 58 (2004) 191–195. doi:10.1016/S0167-577X(03)00443-9.

12. E. Setare, K. Raeissi, M.A. Golozar, M.H. Fathi, The structure and corrosion barrier performance of nanocrystalline zirconia electrodeposited coating, Corrosion Science. 51 (2009) 1802–1808. doi:10.1016/j.corsci.2009.05.004.

13. X. Pang, I. Zhitomirsky, M. Niewczas, Cathodic electrolytic deposition of zirconia films, Surface and Coatings Technology. 195 (2005) 138–146. doi:10.1016/j.surfcoat.2004.08.216.

14. S. Yen, Mechanism of electrolytic ZrO2 coating on commercial pure titanium, Materials Chemistry and Physics. 63 (2000) 256–262. doi:10.1016/S0254-0584(99)00232-1.

15. E. Zalnezhad, Effect of structural evolution on mechanical properties of ZrO2 coated Ti-6Al-7Nb-biomedical application, Applied Surface Science. 370 (2016) 32–39. doi:10.1016/j.apsusc.2016.02.113.

16. S. Saleem, R. Ahmad, R. Ayub, U. Ikhlaq, W. Jin, P.K. Chu, Investigation of nano-structured Zirconium oxide film on Ti6Al4V substrate to improve tribological properties prepared by PIII&D, Applied Surface Science. 394 (2017) 586–597. doi:10.1016/j.apsusc.2016.09.091.

17. S.K. Yen, M.J. Guo, H.Z. Zan, Characterization of electrolytic ZrO2 coating on Co–Cr–Mo implant alloys of hip prosthesis, Biomaterials. 22 (2001) 125–133. doi:10.1016/S0142-9612(00)00133-2.

18. F.C. Giacomelli, C. Giacomelli, A.G. De Oliveira, A. Spinelli, Effect of electrolytic ZrO2 coatings on the breakdown potential of NiTi wires used as endovascular implants, Materials Letters. 59 (2005) 754–758. doi:10.1016/j.matlet.2004.11.015.

19. D. Qiu, A. Wang, Y. Yin, Characterization and corrosion behavior of hydroxyapatite/zirconia composite coating on NiTi fabricated by electrochemical

deposition, Applied Surface Science. 257 (2010) 1774–1778. doi:10.1016/j.apsusc.2010.09.014.

20. J.H. Sui, W. Cai, Formation of ZrO2 coating on the NiTi alloys for improving their surface properties, Nuclear Instruments and Methods in Physics Research Section B: Beam Interactions with Materials and Atoms. 251 (2006) 402–406. doi:10.1016/j.nimb.2006.06.028.
21. K.W. Ng, H.C. Man, T.M. Yue, Corrosion and wear properties of laser surface modified NiTi with Mo and ZrO2, Applied Surface Science. 254 (2008) 6725–6730. doi:10.1016/j.apsusc.2008.04.076.
22. I. Gurrappa, L. Binder, Electrodeposition of nanostructured coatings and their characterization—A review, Science and Technology of Advanced Materials. 9 (2008) 43001. doi:10.1088/1468-6996/9/4/043001.
23. P. Stefanov, D. Stoychev, M. Stoycheva, J. Ikonomov, T. Marinova, XPS and SEM characterization of zirconia thin films prepared by electrochemical deposition, Surface and Interface Analysis. 30 (2000) 628–631. doi:10.1002/1096-9918(200008)30:1<628::AID-SIA800>3.0.CO;2-7.
24. B. Liu, J. Hu, J.S. Foord, Electrochemical deposition of zirconia films on diamond electrodes, Electrochemical and Solid-State Letters. 14 (2011) D20. doi:10.1149/1.3518453.
25. S.K. Yen, T.Y. Huang, Characterization of the electrolytic ZrO2 coating on Ti-6A1-4V, Materials Chemistry and Physics. 56 (1998) 214–221. doi:10.1016/S0254-0584(98)00178-3.
26. I. Valov, D. Stoychev, T. Marinova, Study of the kinetics of processes during electrochemical deposition of zirconia from nonaqueous electrolytes, Electrochimica Acta. 47 (2002) 4419–4431. doi:10.1016/S0013-4686(02)00482-6.
27. L. Gal-Or, I. Silberman, R. Chaim, Electrolytic ZrO2 coatings, Journal of The Electrochemical Society. 138 (1991) 1939. doi:10.1149/1.2085904.
28. I. Zhitomirsky, Cathodic electrodeposition of ceramic and organoceramic materials. Fundamental aspects., Advances in colloid and interface science. 97 (2002) 279–317. doi:10.1016/S0001-8686(01)00068-9.

29. M.A. Blesa, A.J.G. Maroto, S.I. Passaggio, N.E. Figliolia, G. Rigotti, Hydrous zirconium dioxide: interfacial properties, the formation of monodisperse spherical particles, and its crystallization at high temperatures, Journal of Materials Science. 20 (1985) 4601–4609. doi:10.1007/BF00559350.

30. A. Clearfield, The mechanism of hydrolytic polymerization of zirconyl solutions, Journal of Materials Research. 5 (1990) 161–162. doi:10.1557/JMR.1990.0161.

31. I. Zhitomirsky, A. Petric, Electrolytic deposition of zirconia and zirconia organoceramic composites, Materials Letters. 46 (2000) 1–6.

32. N.I.A. Lopes, L.A.O. Silva, L.A. Santos, V.T.L. Buono, Surface characterization of NiTi superelastic and shape memory alloys after electrolytic polishing, Materials Research. (2017) 1–8. doi:10.1590/1980-5373-mr-2016-0933.

33. L. Neelakantan, A.W. Hassel, Rotating disc electrode study of the electropolishing mechanism of NiTi in methanolic sulfuric acid, Electrochimica Acta. 53 (2007) 915–919. doi:10.1016/j.electacta.2007.08.007.

34. M. Pohl, C. Heßing, J. Frenzel, Electrolytic processing of NiTi shape memory alloys, Materials Science and Engineering A. 378 (2004) 191–199. doi:10.1016/j.msea.2003.11.080.

35. L. Neelakantan, M. Valtiner, G. Eggeler, A.W. Hasse, Surface chemistry and topographical changes of an electropolished NiTi shape memory alloy, Physica Status Solidi (A) Applications and Materials Science. 207 (2010) 807–811. doi:10.1002/pass.200983312.

36. J. Frenzel, Z. Zhang, K. Neuking, G. Eggeler, High quality vacuum induction melting of small quantities of NiTi shape memory alloys in graphite crucibles, Journal of Alloys and Compounds. 385 (2004) 214–223. doi:10.1016/j.jallcom.2004.05.002.

37. I. Zhitomirsky, A. Petric, Cathodic electrodeposition of polymer films and organoceramic films, Materials Science and Engineering B: Solid-State Materials for Advanced Technology. 78 (2000) 125–130. doi:10.1016/S0921-5107(00)00535-3.

38. K. Holmberg, H. Ronkainen, A. Matthews, Tribology of thin coatings, Ceramics International. 26 (2000) 787–795. doi:10.1016/S0272-8842(00)00015-8.

39. G. Tepe, J. Schmehl, H.P. Wendel, S. Schaffner, S. Heller, M. Gianotti, C.D. Claussen, S.H. Duda, Reduced thrombogenicity of nitinol stents - In vitro evaluation of different surface modifications and coatings, Biomaterials. 27 (2006) 643–650. doi:10.1016/j.biomaterials.2005.06.004.

40. A. Wichelhaus, M. Geserick, R. Hibst, F.G. Sander, The effect of surface treatment and clinical use on friction in NiTi orthodontic wires., Dental materials : official publication of the Academy of Dental Materials. 21 (2005) 938–45. doi:10.1016/j.dental.2004.11.011.

41. N.B. Dahotre, T.S. Sudarshan, Intermetallic and ceramic coatings, Marcel Dekker, 1999.

42. B.G. Pound, Susceptibility of nitinol to localized corrosion, Journal of Biomedical Materials Research - Part A. 77 (2006) 185–191. doi:10.1002/jbm.a.30584.

5. Desempenho do material recoberto

RESISTÊNCIA À CORROSÃO E ESTABILIDADE DE UM REVESTIMENTO NANOESTRUTURADO DE ZrO_2 EM FIO NiTi SUPERELÁSTICO PARA APLICAÇÕES BIOMÉDICAS

Neste trabalho, buscou-se avaliar a resistência à corrosão de fios superelásticos de NiTi, recobertos com o filme fino de zircônia, analisando a estabilidade do revestimento após imersão em solução fisiológica artificial e após testes de comportamento mecânico. Os testes foram escolhidos para se aproximarem de condições frequentemente encontradas em aplicações biomédicas. Dispositivos biomédicos de NiTi, como *stents* e instrumentos endodônticos, por exemplo, são frequentemente submetidos a dobramentos severos e a carregamentos cíclicos que podem causar degradação de suas propriedades e levar à fratura por fadiga. Em instrumentos endodônticos, a amplitude de deformação na região da curvatura máxima do canal pode chegar a 6% e falhas prematuras por fadiga são comuns. Para este estudo, utilizou-se novamente o fio de NiTi superelástico com Af nominal igual a 20°C e a eletrodeposição de ZrO_2 foi feita nas condições que apresentaram os melhores resultados de rugosidade superficial e de resistência à corrosão no estudo mostrado no capítulo 4. Buscou-se ainda avaliar a influência do uso do polimento eletrolítico, apresentado no capítulo 3, como tratamento de superfície na morfologia do revestimento de zircônia. Os resultados mostraram que a homogeneidade do filme e a resistência à corrosão do fio aumentaram quando o pré-tratamento foi aplicado. Após imersão em *Hank's solution* à 37°C, por até 12 meses, tanto as amostras revestidas como as não revestidas mostraram uma camada de fosfato de cálcio cobrindo suas superfícies, indicando bioatividade. Além disso, o teor de níquel liberado em solução foi insignificante. Os testes de comportamento mecânico mostraram que, apesar de algumas trincas no filme serem visíveis, sua delaminação foi mínima, indicando boa adesão ao substrato. Além disso, o revestimento de zircônia manteve sua capacidade de proteção contra a corrosão localizada, mesmo após o trincamento induzido pela deformação.

Submetido para publicação em **Corrosion Science**

CORROSION RESISTANCE AND COATING STABILITY OF ZrO_2 THIN FILMS OBTAINED ON SUPERELASTIC NiTi ALLOY FOR BIOMEDICAL APPLICATIONS

ABSTRACT

Thin ZrO_2 films were produced using pulsed cathodic electrodeposition on superelastic NiTi wires with and without prior surface treatment. The coating morphology was assessed by scanning electron microscopy with energy dispersive X-ray spectrometry, transmission electron microscopy, atomic force microscopy, X-ray diffraction and time of flight secondary ion mass spectrometry. The corrosion resistance of the coated wires was evaluated using potentiodynamic polarization tests and long-term immersion in simulated physiological solution at 37°C. The adhesion of the coating to the NiTi substrate, i.e. the coating stability when subject to mechanical stresses, was assessed by fatigue and three-point bending tests. Characterization results show that a nanostructured coating, continuous and free of defects, was obtained on the NiTi wire. Film homogeneity increased using electropolishing as a surface pretreatment. Potentiodynamic polarization tests showed that the coated wires are less vulnerable to corrosion in Hank's solution at 37°C than untreated NiTi wires. After immersion in Hank's solution both coated and uncoated samples showed a calcium-phosphate layer covering the surface, a good indicator of bioactivity. Three-point-bending and fatigue tests showed that, although some cracks are visible on ZrO_2 films after deformation to the strain level of 4%, the delamination was minimal, indicating a good adhesion to the NiTi substrate. Therefore, the ZrO_2 film applied on superelastic NiTi wires remains satisfactorily stable in simulated physiological environment, with negligible nickel releasing, and when subject to mechanical stresses, without significant delamination or impact on its corrosion protection properties.

Keywords: *Biomaterials; corrosion; fatigue; nickel-titanium alloys; nanocoatings; zirconia.*

5.1 Introduction

The earliest use of NiTi for biomedical applications was reported in 1973, however, it only became widespread in the mid-1990s, when commercial intra-vascular stent made their medical breakthrough [1]. The unique thermomechanical properties of NiTi alloys with near-equiatomic composition, i.e. shape memory effect and superelasticity, make them preferred over conventional implant materials, like titanium alloys and stainless steel, for various specific applications [2,3]. Nevertheless, biological response and fatigue life of NiTi biomedical devices are still a concern, especially due to the systemic toxicity of nickel ion release and the risk of failure of the devices [4–6].

In biomedical applications, NiTi alloys are often submitted to irregular cyclic loading that can induce functional and structural fatigue, i.e. degradation of properties and microstructure damage followed by crack nucleation and growth leading to fracture, respectively [7]. For example, a stent placed in a popliteal artery, located under the knee joint, may experience deformations of 90° and, overall, stents implanted into blood vessels can be subjected to approximately 37 million loading cycles per year [1,8]. The cumulative incidence of stent fractures range from 2% to 65%, a rate equivalent to 0.6 to 60/1000 person/month [9]. Additionally, NiTi endodontic instruments used for preparing curved root canals are bend and submitted to strain cycles in the region of the canal curvature with amplitudes of 5% that can give rise to fatigue failure of the instruments [10].

Along with the mechanical demands, NiTi biomedical devices are exposed to physiological fluids, a corrosive environment especially due to the presence of ionic salts such as chloride [1]. Corrosion of NiTi alloys results in the diffusion of nickel ions from the substrate, inducing undesirable biological responses, and can cause or contribute to fatigue and premature failure [11,12]. The corrosion behavior of NiTi alloys relies highly on their surface conditions and numerous modification techniques have been proposed to improve their properties [13]. Coatings of ZrO_2 have been deposited on several alloys intended for biomedical applications, successfully improving wear and corrosion resistances of the substrates [14–20]. Furthermore, the application of ZrO_2 coatings on NiTi alloys can potentially reduces corrosion and nickel

release to the human body, and also reduce premature failures caused by fatigue in NiTi biomedical devices.

To the best of our knowledge, few attempts to coat NiTi alloys with ZrO_2 have been reported. Giacomelli et al. [21] performed electrodeposition to improve the breakdown potentials of the NiTi wires in artificial saliva, but numerous cracks were evident. In a study by Sui and Cai [22], a 200-nm-thick coating that lowered the surface friction coefficient and improved the corrosion resistance of a NiTi sheet in Hank's solution was obtained using plasma immersion ion implantation and deposition.

The aim of this study was to evaluate the corrosion resistance and the integrity of a ZrO_2 thin film deposited on a NiTi superelastic wire when subjected to simulated physiological environment and to mechanical stresses. The film was obtained using pulsed cathodic electrodeposition and was characterized using scanning electron microscopy with energy dispersive X-ray spectrometry (SEM/EDX), transmission electron microscopy (TEM), atomic force microscopy (AFM), X-ray diffraction (XRD) and time of flight secondary ion mass spectrometry (ToF-SIMS). The effects of surface preparation using electrolytic polishing on the morphology of the deposited coating were also evaluated. The corrosion resistance of the NiTi wire coated with ZrO_2 and its stability were assessed using potentiodynamic polarization tests, and immersion in Hank's simulated physiological solution. Fatigue and three-point bending tests were also performed and the tested samples were reevaluated using potentiodynamic polarization test and SEM.

5.2 Experimental procedure

5.2.1 Surface preparation and coating deposition

The investigations were carried out on commercially available superelastic NiTi wires with a diameter of 1.0 mm (Confluent Medical Technologies, Fremont, CA, USA). Details of the characterization of the substrate and of the investigations to define the optimal conditions for the preparation of the coating are provided elsewhere [23]. Briefly, the electrolytic deposition was conducted using a cathodic pulsed current density of 3 $mA.cm^{-2}$ (t_{on} = t_{off} = 0.005 s), applied for 1200 s, using a potentiostat

Autolab PGSTAT100N (Metrohm Autolab, Utrecht, The Netherlands). A standard electrochemical cell with a platinum grid as counter electrode and a saturated calomel electrode (SCE) was as reference. All potentials mentioned in this work refer to this electrode at 298 K.

The electrolyte was prepared using 16.1 $g \cdot L^{-1}$ of zirconyl chloride octahydrate ($ZrOCl_2 \cdot 8H_2O$), 1.0 $g \cdot L^{-1}$ of poly(diallyldimethylammonium chloride) — polyDADMAC (molecular weight = 400,000–500,000) in methanol. All the reagents were analytical grade chemicals produced by Sigma-Aldrich with a minimum purity of 99.0%. To guarantee the OH^- generation in the cathode, 100 $g.L^{-1}$ of high purity deionized water was added to the solution [14]. After deposition, the coated samples were naturally air dried for 24 hours.

For comparison, the electrodeposition was performed on NiTi wires as received, ultrasonically cleaned with acetone and deionized water, and on wires that were previously electropolished with 3.5 $mol \cdot L^{-1}$ H_2SO_4 solution at 25°C [24], also cleaned in ultrasonic bath.

5.2.2 Coating characterization

5.2.2.1 Surface morphology

The surface morphology was evaluated via SEM (Inspect S50, FEI, Hillsboro, USA), equipped with X-ray Energy Spectroscopy - EDX (Genesis, EDAX Inc., Mahwah, USA), and via AFM (XE–70, Park System, Suwon, Korea), operating in tapping mode, with the scanning rate of 1 Hz. The surface roughness was measured in three different areas of 30 μm × 30 μm per sample using the average surface roughness (Ra) and peak-to-valley roughness (Rpv) parameters. The SEM and AFM analyses were performed over at least three different places along the length of the surface of the wires, on two samples of each condition, to assess the uniformity of the coatings.

5.2.2.2 Cross-section TEM analysis

Thin foils of the coated NiTi wires were prepared by focused ion beam (FIB) milling in a dual beam FIB/SEM system (STRATA DB 235, FEI, Eindhoven, The Netherlands).

The samples were prepared using *in situ* welding lift-out technique, with deposition of a platinum layer on the surface to protect the ZrO_2 coating, followed by specimen thinning until reaching electron transparency. TEM analysis of the cross-sections was performed with a CM30 microscope (Philips/FEI, Eindhoven, The Netherlands) operating at 300 kV.

5.2.2.3 X-ray diffraction

The crystallographic phase investigation was conducted via XRD (Empyrean, PANalytical, Almelo, The Netherlands) using Cu-Kα radiation at 40 kV and 30 mA, with a step size of 0.01° and time per step of 3.0 s.

5.2.2.4 Time of Flight Secondary Ion Mass Spectrometry (ToF-SIMS)

Elemental depth profiles of the coated NiTi wires were obtained on a ToF-SIMS V instrument (IONTOF GmbH, Münster, Germany). A pulsed primary bismuth ion beam, operating with a 25 keV, was used for analysis over a 75 µm × 75 µm area. Sputtering was performed with a 1 keV oxygen beam over a 400 µm × 400 µm area. The spectra were recorded in positive polarity and the acquired data were processed using the Measurement Explorer IONTOF software.

5.2.3 Corrosion behavior in simulated body fluid and coating stability

The corrosion resistance of NiTi alloys, hence the coating stability during application, is crucial for its biocompatibility. To investigate the corrosion behavior of the coated NiTi wires in physiological conditions, polarization tests were performed in Hank's solution at a constant temperature of 37°C (pH nearly 7.2). The solution was prepared with analytical grade reagents (Sigma-Aldrich) in the following composition: 0.185 $g \cdot L^{-1}$ $CaCl_2 \cdot 2H_2O$, 0.4 $g \cdot L^{-1}$ KCl, 0.06 $g \cdot L^{-1}$ KH_2PO_4, 8.0 $g \cdot L^{-1}$ NaCl, 0.35 $g \cdot L^{-1}$ $NaHCO_3$, 0.097 $g \cdot L^{-1}$ $MgSO_4$, 0.048 $g \cdot L^{-1}$ Na_2HPO_4, and 1.0 $g \cdot L^{-1}$ D-Glucose.

In order to assess the coating stability, immersion in Hank's solution, three-point bending and fatigue tests were also performed. After the tests, the samples were reevaluated via polarization tests and SEM/EDX.

5.2.3.1 Potentiodynamic polarization test

The corrosion resistance evaluation was performed with the same potentiostat, cell, and electrodes used for the electrolytic deposition, specified at section 5.2.1. Potentiodynamic polarization curves were obtained at a scan rate of 0.005 $V \cdot s^{-1}$, starting at −0.25 V from open circuit potential (OCP), after stabilization for 60 minutes, and finishing at +1.2 V. The corrosion potential (E_{corr}) and corrosion current density (i_{corr}) were calculated using the Tafel extrapolation method, whereas the breakdown potential (E_b) was obtained from the rapid increase of the current density in the polarization curve.

5.2.3.2 Immersion test

In order to determine the nickel ion release rate in Hank's solution, uncoated and coated wires, with the exposed surface area of 0.95 cm^2, were immersed in 30 mL of Hank's solution at 37 °C for periods of 3, 6, and 12 months. The concentrations of nickel ion in the solutions were determined, in duplicate, using an ICP-OES (Optima 7300DV, Perkin Elmer, Boston, USA). After the immersion periods, the samples were removed from the solution, rinsed with deionized water, and analyzed via SEM/EDX and potentiodynamic polarization test.

5.2.3.3 Three-point bending test

Three-point bending tests were carried using three wires of each condition (as received and as received and coated), at room temperature of 25°C, loading rate of 2 mm/min, and bending strain of 4%, in a tensile testing apparatus (AN8032, Analogica, Belo Horizonte, MG, Brazil). After the bending tests, the samples outer surface was examined through SEM and the tested wires were analyzed by potentiodynamic polarization test.

5.2.3.4 Fatigue test

Fatigue tests were performed at the temperature of 37°C, bending strain level of 4%, and 30 rpm in a rotating-bending apparatus produced by Analogica (Belo Horizonte, MG, Brazil). Fatigue resistance was evaluated measuring the number of cycles until

failure (Nf) of ten NiTi wires of each condition, i.e. as received and as received and coated. To assess the coating stability, three wires of each condition were tested until its fatigue half-live was reached (400 cycles). After cycling, the outer surfaces of the wires, where the bending strain level is the highest, were then examined by SEM. Polarization tests were also performed in cycled specimens.

5.3 Results and discussion

5.3.1 Coatings characterization

Surface morphologies of the as received NiTi wire coated with the ZrO_2 thin film and the electropolished and coated wire are shown in Figure 5.1. Scratch marks and other defects on the commercially available NiTi wire, formed probably during mechanical polishing, were smoothed but are still visible after coating (Figure 5.1a). On the electrolytically polished surface, the ZrO_2 coating covered most of the surface marks and partially covered the inclusions of TiC particles present throughout the surface. Semi-quantitative EDX microanalysis on the surface of the coated wires showed zirconium and oxygen related peaks with a composition close to stoichiometry, which suggests a uniform deposition of ZrO_2 on both as received and electropolished NiTi wires. The ZrO_2 occurrence on the surface film could not be confirmed by X-ray analyses, possibly due to its low thickness or to its amorphous state, as suggested in other studies [21,25]. The surface roughness parameters measured via AFM are shown in Table 5.1. Both average and peak-to-valley surface roughness were reduced after coating deposition on the as received sample, as well as after electrolytic polishing. Moreover, the electrolytic polishing followed by the ZrO_2 deposition resulted in the lowest roughness values.

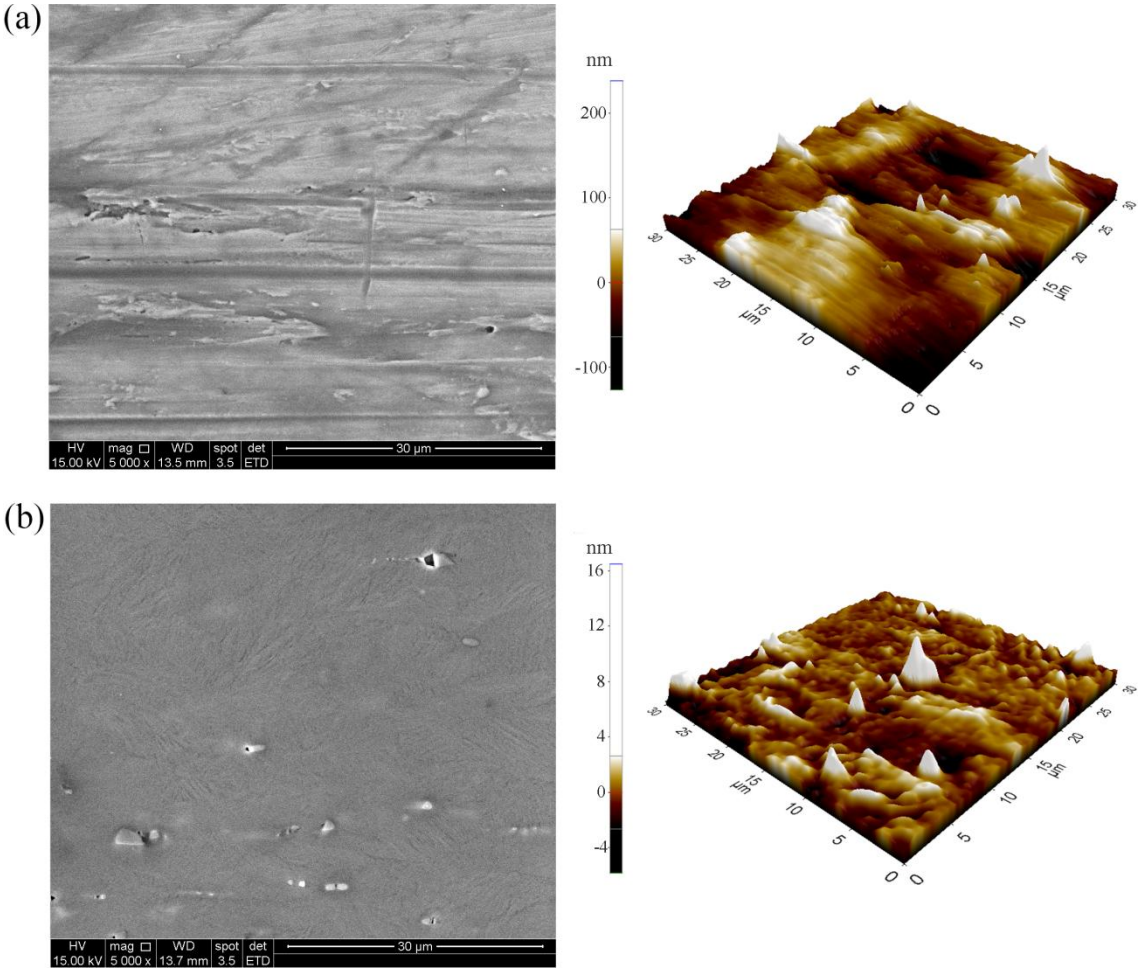

Figure 5.1 – SEM and AFM 3D surface images of NiTi wires (a) as received and coated; and (b) electropolished and coated.

Table 5.1 – Average and peak-to-valley surface roughness of the NiTi wires obtained from AFM analyses**.**

	Ra [nm]	Rpv [nm]
as received	195 ± 9	900 ± 100
as received and coated	27 ± 1	299 ± 5
electropolished	20 ± 1	254 ± 25
electropolished and coated	15 ± 3	176 ± 11

The cross-section micrographs of the coated wires are shown in Figure 5.2. The ZrO_2 coating deposited on the as received NiTi wire showed an average thickness of 54 ± 6 nm and a microstructure constituted of apparently equiaxed, nanostructured crystallites. A thin TiO_2 layer, with a thickness of about 8 ± 1 nm can also be seen between the ZrO_2 coating layer and the NiTi substrate (as indicated in Figure 5.2a). When electrolytic polishing was applied prior to coating deposition, a more homogeneous film was obtained, with an average thickness of 61.7 ± 2.1 nm ZrO_2 (Figure 5.2b). In this case, the coating layer was apparently amorphous, or constituted of extremely small crystallites, and no intermediary TiO_2 layer was evident. For both samples, there were no noticeable defects or cracks throughout the coating as well as no evidence of delamination. This is an indication of good coating adhesion and high coating quality.

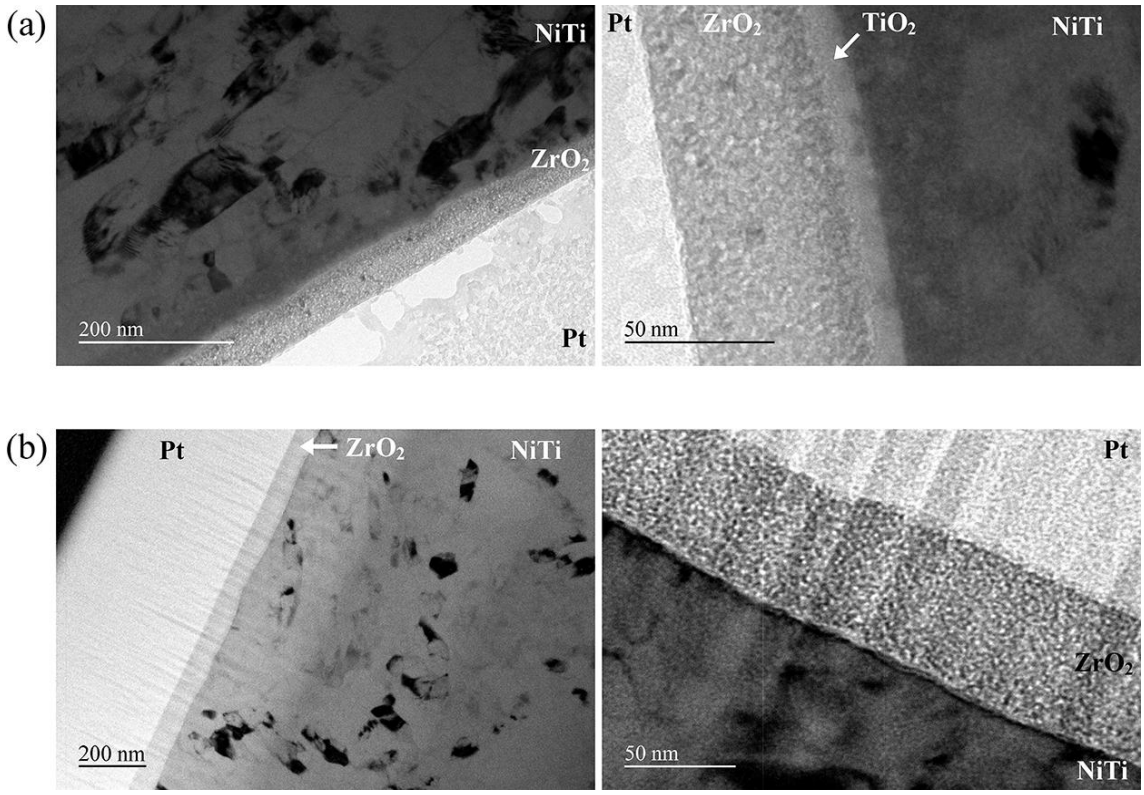

Figure 5.2 – TEM cross-section micrographs of the coated wires: (a) as received and coated; (b) electropolished and coated.

The composition depth profiling of the deposited coating was investigated by ToF-SIMS analyses. The sinal intensity of ZrO^+, Ti^+ and Ni^+ ions fragments, monitored as a

function of the sputtering time are presented in Figure 3. These profiles show the influence of the surface treatment on the coating layer thickness and uniformity. As can be seen, electrolytic polishing increased the oxide layer thickness and gave rise also to a higher coating uniformity.

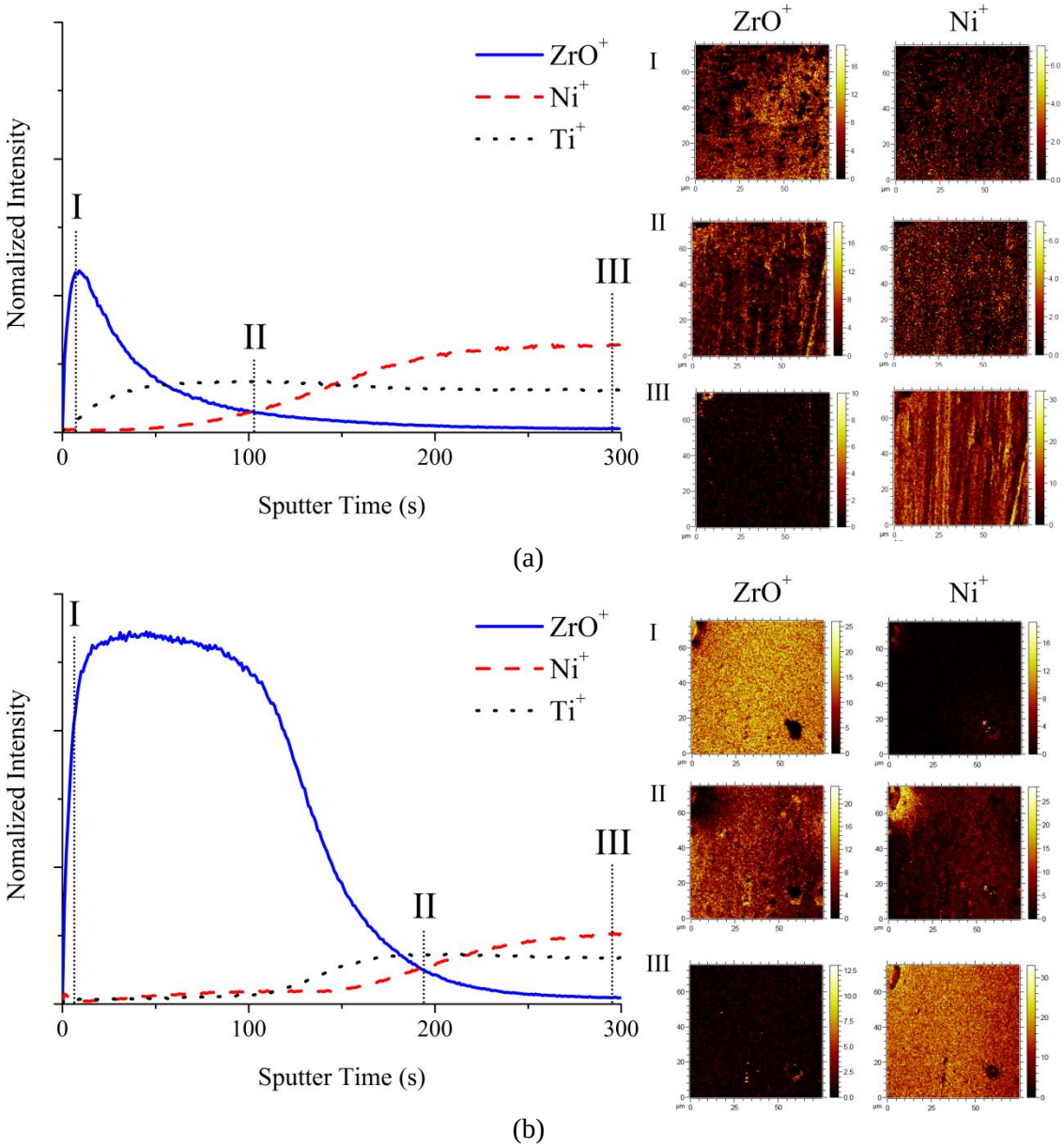

Figure 5.3 – ToF-SIMS depth profiling of the coated wires: (a) as received and coated; (b) electropolished and coated.

ToF-SIMS is a powerful technique which provides high mass and depth resolution and allows the detection and characterization of additives and contaminants at the sub

monolayer level [26]. Reports in the literature show that the most intense peaks generated from polyDADMAC analysis in ToF-SIMS are from $C_3H_8N^+$, $C_2H_4N^+$ and $C_2H_3^+$ ions [27,28]. None of these ions was detected on the coated samples throughout the entire depth profiling acquisition in significant concentrations. This indicates that, although the polyDADMAC addition plays an important role in the ZrO_2 electrolytic deposition on NiTi wires [19,29], its co-deposition did not occur in the conditions reported in our study.

5.3.2 Corrosion behavior in simulated body fluid and coating stability

5.3.2.1 Potentiodynamic polarization

The polarization curves in Hank's solution at 37°C of the uncoated NiTi wires (as received and electropolished) and of the coated samples, with and without prior electropolishing, are shown in Figure 4. Among these samples, the NiTi wire in the as-received condition showed the lowest corrosion potential (E_{corr} = -0.301 V), a passivation range starting at -0.2 V, and a breakdown potential of 0.239 V. Electropolishing resulted in a slightly more noble corrosion potential of -0.265 V; however, the polished sample did not show breakdown at potentials below 1.2 V, suggesting that the polished wire is less prone to localized corrosion than the as received NiTi wire.

The corrosion potentials of the coated wires were significantly higher than those of the corresponding substrates, revealing an improvement on the corrosion resistance. The wire as received and coated showed a corrosion potential of 0.082 V, whereas in the polished and coated wire it was 0.149 V. The coated samples also showed a continuous increase of current density up to 1 V, where stabilization occurs. The coating deposition was sufficient to protect the NiTi substrate from localized corrosion even when no prior electropolishing was used, as a result of the improvement on the uniformity and homogeneity of the coating on them.

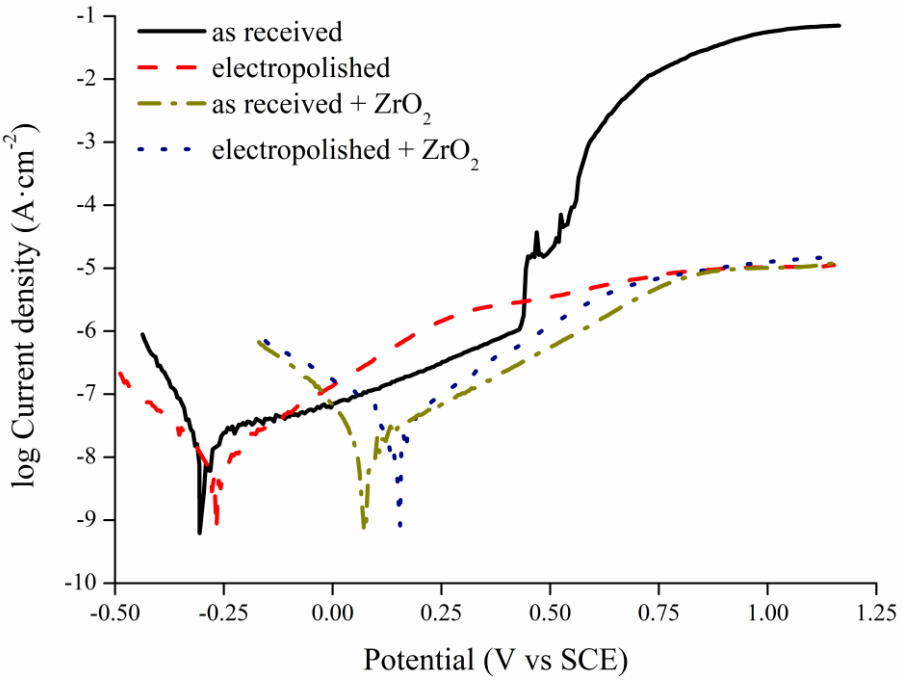

Figure 5.4 – Potentiodynamic polarization curves in Hank's solution at 37°C of coated and uncoated NiTi wires, with and without electrolytic polishing.

5.3.2.2 Immersion test

Examples of SEM surface micrographs and EDX analysis of the coated and as received NiTi wires after 12 months immersion in Hank's solution at 37 °C are shown in **Erro! Fonte de referência não encontrada.**. After immersion, the wires exhibited flake-like crystals distributed uniformly throughout the surface and some spherical clusters randomly spread. EDX analyses showed the presence of calcium and phosphorous, hydroxyapatite constituents. Growth of a calcium-phosphate layer is also observed after 3 and 6 months immersion in Hanks' solution, for both uncoated and coated wires. The morphology of the particles was similar to others reported for hydroxyapatite and related calcium-phosphates formed naturally on NiTi and other alloys after immersion in simulated body fluids [30–32]. The ability to form calcium-phosphates on the surface when immersed in simulated body fluids is an important indicator of biocompatibility and bioactivity of the material [33,34]. From EDX microanalysis, the intensity of the peaks corresponding to calcium and phosphate in the spectra indicates that the deposited layer becomes thicker for longer immersion times. Also, the layer formed on the coated wires was slightly thicker than the uncoated wires, most likely as a result of surface

roughness and chemical composition differences that affect formation of calcium-phosphates [34].

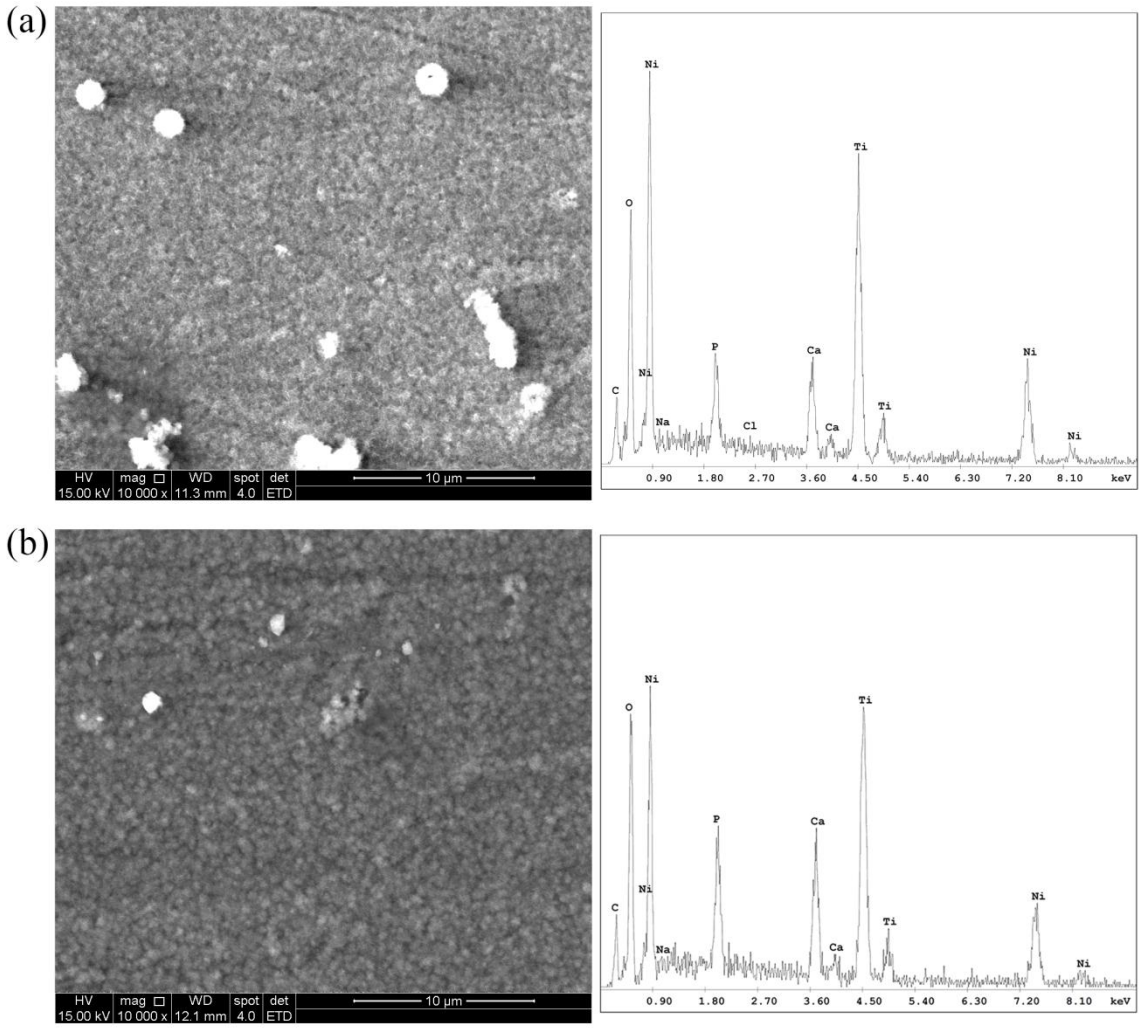

Figure 5.5 – SEM surface micrographs of NiTi wires after 12 months of immersion in Hank's solution at 37 °C: (a) as received uncoated; (b) as received and coated.

Additionally, the amount of nickel released from the as received NiTi wire and the as received NiTi coated with ZrO_2 after immersion for 3, 6, and 12 months, analyzed by ICP-OES, were statically similar and close to the detection limit of the equipment. The maximum nickel content measured was about 10 ppb, after 12 months of immersion in Hank's solution. This nickel content is insignificant when compared to the average daily intake of nickel in human diet and to reference values in serum and urine [6,35].

After immersion tests, the corrosion behavior in Hank's solution at 37°C of the NiTi wires coated and as received were reevaluated using potentiodynamic polarization tests (Figure 6). From the results, it was observed that the passive current of the samples after 12-month immersion is unstable, implying in a poor stability of the calcium phosphate layer, however, and no breakdown is observed up to 1.2 V.

These results indicate that the calcium phosphate layer formed during immersion acts as a further protective barrier, along with TiO_2 and ZrO_2 layers, against corrosion and nickel releasing therefore explaining the ICP-OES results of nickel releasing from the as received, and as received coated with ZrO_2, wires after immersion tests. Since the main reason for the mitigation of nickel diffusion seems to be formation of a calcium phosphate layer, the direct effect of ZrO_2 application on nickel releasing could not be established.

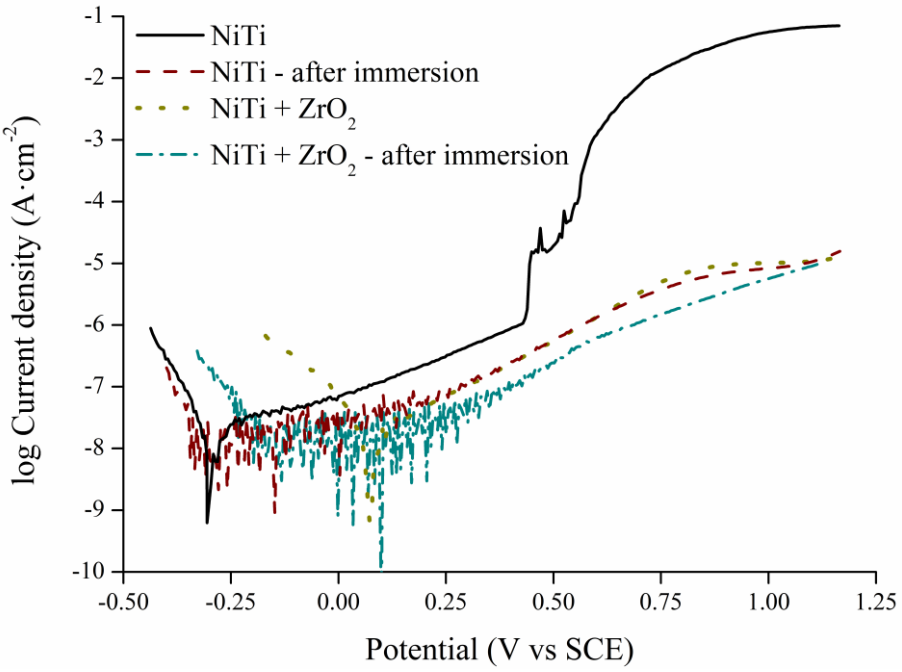

Figure 5.6 – Potentiodynamic polarization curves in Hank's solution at 37°C of the NiTi wires after 12-month immersion test.

5.3.3 Three-point bending test

The surface morphology of the NiTi wires after three-point bending tests is shown in Figure 5.7. Although some cracks are evident on the ZrO_2 coating (Figure 5.7b), no delamination was observed after deformation to the strain level of 4%, indicating a good bonding strength between the ZrO_2 thin film and the NiTi substrate.

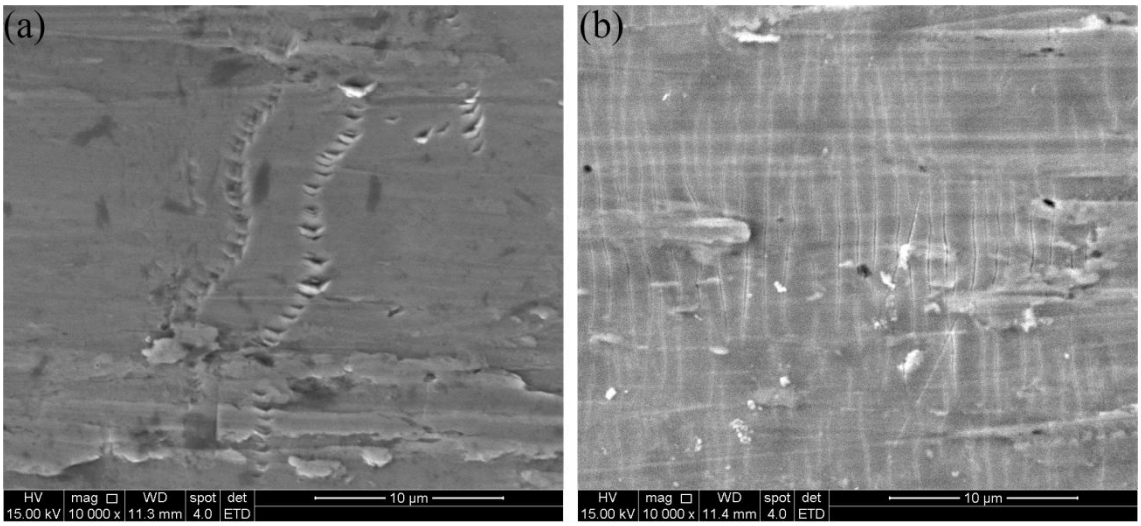

Figure 5.7 – SEM surface micrographs of NiTi wires after three-point bending test: (a) as received uncoated; (b) as received and coated.

The potentiodynamic polarization curves in Hank's solution at 37°C of the NiTi wires after three-point-bending tests are shown in Figure 5.8. It can be noted that the bending induced a current instability on both coated and uncoated wires, due to cracking of the ZrO_2 thin film and of the TiO_2 oxide layer, respectively. It is also observed that the bending stress was detrimental to the corrosion resistance of the uncoated NiTi wires, causing a decrease of breakdown potential. The ZrO_2 coated NiTi after bending showed a passivation region between 0.5 V and 0.8 V, when the breakdown of the film occurs and current increases.

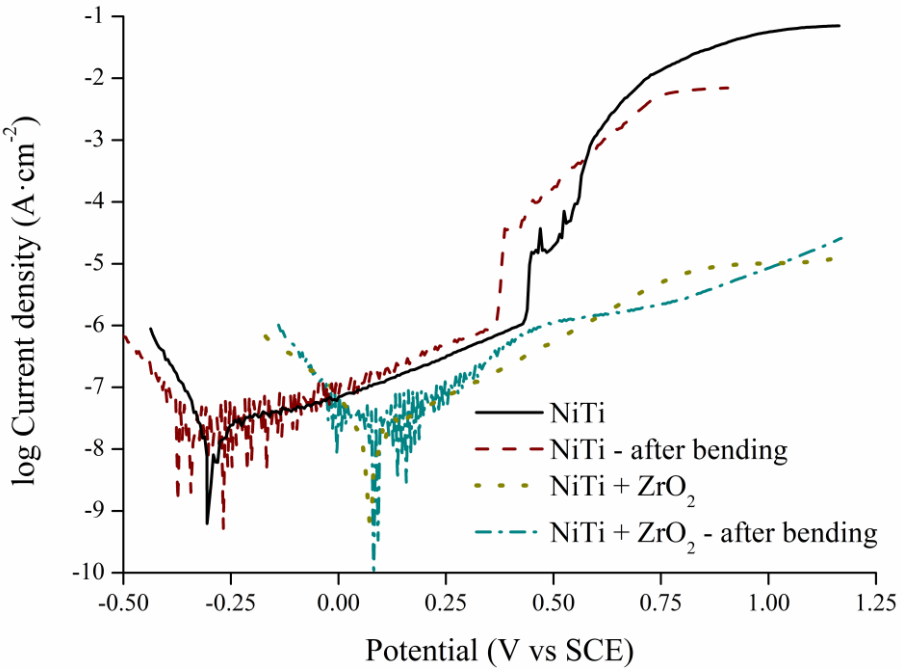

Figure 5.8 – Potentiodynamic polarization curves in Hank's solution at 37°C of the NiTi wires after three-point-bending tests.

5.3.4 Fatigue test

SEM micrographs of the wires surface subjected to a bending strain level of 4% and 400 cycles are show in Figure 5.9. Although cracking of the ZrO_2 film is evident in the coated wire, delamination was minimum, indicating good adhesion strength and, therefore, a fatigue resistance enhancement could be expected. However, results from the fatigue tests showed a noteworthy data dispersion and no statistical difference, within a confidence level of 95%, could be observed between the average number of cycles until fracture of the wires as received (Nf = 942 ± 116) and the wires as received and coated with ZrO_2 (Nf = 1068 ± 203).

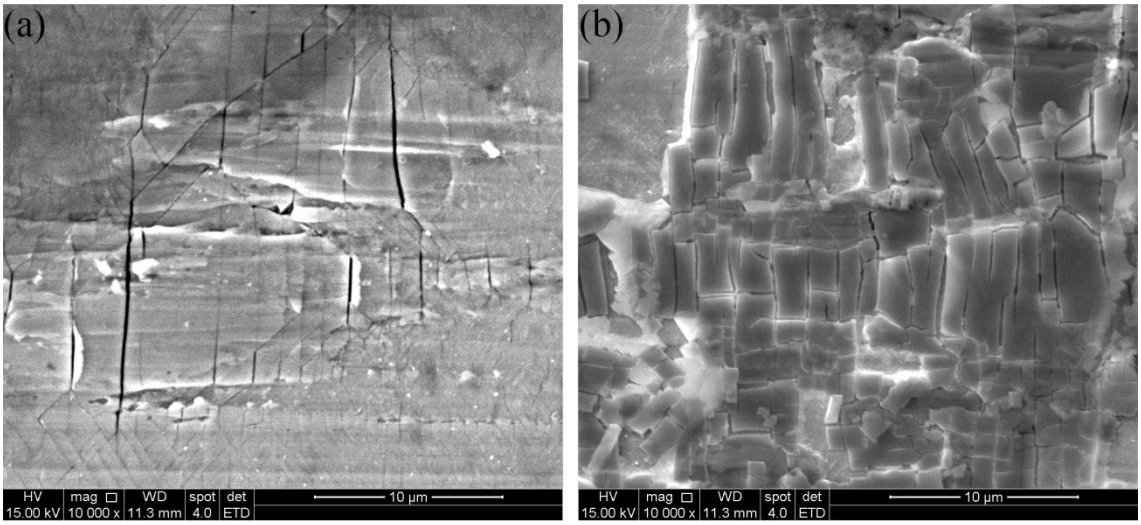

Figure 5.9 – SEM surface micrographs of NiTi wires after fatigue test: (a) as received uncoated; (b) as received and coated.

It has been shown that cracks tend to deviate towards inclusions and precipitates [10,36] and this can explain the high dispersion of the Nf data, since numerous inclusions and other defects are randomly distributed on the surface of the NiTi as received wire, that are still dominant on the mechanism of fracture, even after coating deposition. Moreover, Figueiredo et al. [36] showed that NiTi superelastic wires have an unusual fatigue behavior for strain amplitudes higher than about 4%, i.e., the fatigue life increases with increasing strain level. For strain amplitudes lower than 4% and for values above 8%, the fatigue behavior is the expected for typical metallic materials and the number of cycles until failure decreases for higher strain levels. Consequently, further studies are needed to investigate the fatigue behavior of NiTi wires coated with ZrO_2 thin films, at various strain levels.

The results of potentiodynamic polarization tests in Hank's solution at 37°C of the NiTi wires after fatigue tests are given in Figure 5.10. In a similar way to that observed after the bending tests, fatigue induced a current instability, due to cracking of the ZrO_2 film, but no breakdown is observed on the coated wire, contrary to the uncoated NiTi wire. Moreover, the fatigue stress decreased the breakdown potential of the NiTi uncoated wire, indicating a reduction of its corrosion resistance. The ZrO_2 coated wire after fatigue showed a small passivation region between 0.5 and 0.7 V, and the current density increases, with no stabilization, up to 1.2 V.

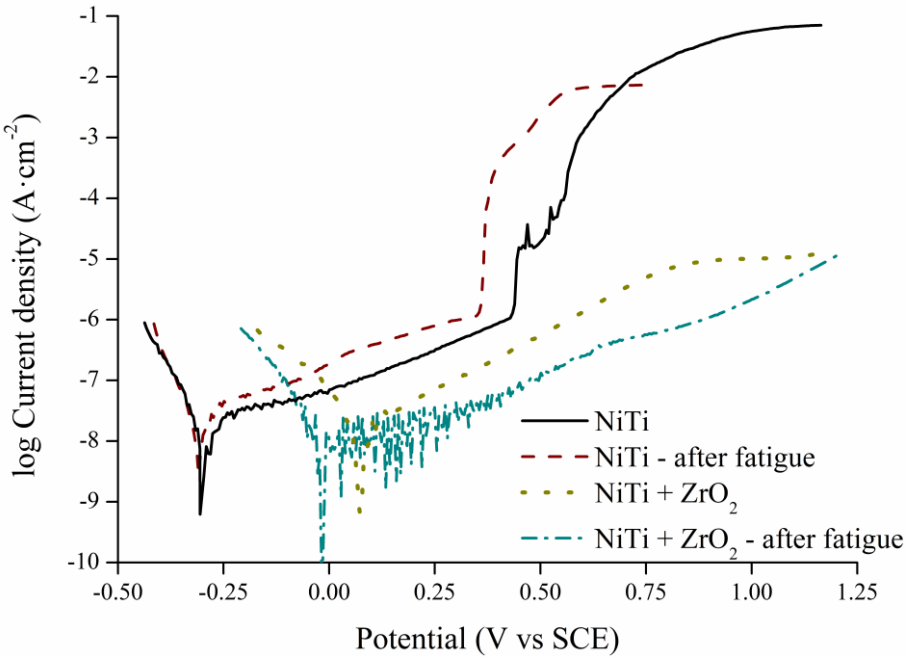

Figure 5.10 – Potentiodynamic polarization curves in Hank's solution at 37°C of the NiTi wires after fatigue tests.

The results of the present research demonstrate that the electrodeposition of a ZrO_2 thin film on NiTi alloy improves its corrosion properties, increasing the corrosion potential and decreasing the values of the anodic current density. NiTi wires coated with ZrO_2 can withstand mechanical stresses and environment conditions similar to those of biomedical applications. After long-term immersion in Hank's solution at 37 °C both coated and uncoated NiTi wires were integrally covered by a calcium-phosphate layer. Although the biocompatibility of NiTi and ZrO_2 components is often attributed to its bioinertness, the spontaneous growth of a calcium-phosphate layer demonstrates the bioactivity of the materials [6,18]. Hence, NiTi alloys coated with ZrO_2 can be considered as a good candidate to orthopedic implant applications, particularly in joints. Being bioactive, it can bond to hard and soft tissues, and ally the excellent tribological properties of ZrO_2 compounds to the extraordinary mechanical behavior of NiTi alloys.

The calcium-phosphate layer, together with the TiO_2 oxide layer present on the wire as received and the ZrO_2 thin film deposited, also act as a barrier and block electron transfers and nickel diffusion from the NiTi substrate. Studies concerning nickel releasing on NiTi devices and the induced biological response are controversial. While some state that the release is insignificant, others report serious systemic toxicity of

nickel ion release. The controversies are caused by differences the surface chemistry and morphology of the NiTi alloys, since these vary extremely according to the surface treatments applied [6,37,38]. In our study, the nickel releasing of both coated and uncoated wires was insignificant after immersion in Hank's solution at 37 °C up to 12 months, mostly due to the formation of a calcium-phosphate layer.

The evaluation of the corrosion behavior in Hank's solution at 37°C showed that the application of the ZrO_2 film significantly improves the corrosion resistance of NiTi wires, increasing the corrosion potential and reducing anodic current densities. When electrolytic polishing is applied before the deposition, a more homogeneous coating is obtained and, consequentially, a higher corrosion resistance is achieved.

After three-point-bending and fatigue tests, it is clear that even with cracking occurrence, the delamination is not extensive. In the potentiodynamic polarization performed after the tests, the ZrO_2 coated wires showed a passivation region and the passive current density only increased slightly at higher potentials, while the uncoated wires show a breakdown potential bellow 0.5 V.

It is important to note that the susceptibility to localized corrosion (pitting) is of vital importance in biomedical applications. This form of corrosion, especially when associated with cyclic loads and tensile stresses, can provoke severe damage on implants and biomedical devices that will lead to premature failure and nickel releasing [1,2]. In *in vivo* environments, the potentials of implanted materials can be as high as 0.5 V [39]. Our results show that the uncoated NiTi wires are susceptible to pitting corrosion at potentials bellow this value. However, the wires coated with ZrO_2 films are resistant to localized corrosion. This suggests that NiTi devices coated with ZrO_2 thin film are suitable for biomedical applications. However, further investigations regarding cell adhesion and proliferation are necessary to guarantee its biocompatibility and bioactivity.

5.4 Conclusions

The corrosion properties of a NiTi superelastic wire coated with a ZrO_2 thin film obtained using pulsed cathodic electrodeposition with and without prior surface preparation have been investigated. The coating integrity when subjected to simulated physiological environment and to mechanical stresses was also evaluated. The thin ZrO_2 coating applied did not show noticeable defects or cracks, reduced the surface roughness and improved the corrosion resistance of the NiTi wire. When electrolytic polishing was used as surface pretreatment, a more uniform and slightly thicker ZrO_2 film was obtained, leading to lower surface roughness and higher corrosion resistance. No significant nickel releasing was observed from the as received and coated NiTi wires after immersion up to 12 months. Moreover, after immersion the surface of the wires was completely covered by a calcium-phosphate layer, indicating biocompatibility and bioactivity. After bending and fatigue tests, although cracks on the ZrO_2 film are present, no significant delamination was observed. Although further investigation is needed to guarantee its biocompatibility, NiTi alloys coated with ZrO2 thin film are potentially suitable materials for a variety of biomedical applications, including vascular stents, orthopedic implants, scaffolds and others.

ACKNOWLEDGEMENTS

This research has been funded by Conselho Nacional de Desenvolvimento Científico e Tecnológico (CNPq), Fundação de Amparo à Pesquisa do Estado de Minas Gerais (FAPEMIG), and Coordenação de Aperfeiçoamento de Pessoal de Nível Superior (CAPES/PROEX). The financial support of the European Commission in the framework of Erasmus Mundus and within the project IBRASIL is also gratefully acknowledged. The authors are also particularly grateful to Nicolas Nuns (UCCS/Lille University, France), for the ToF-SIMS analyses, and to LAQ-DEMET/UFMG, INCT-Acqua, for the ICP-OES analyses.

5.5 References

1. Q. Chen, G.A. Thouas, Metallic implant biomaterials, Materials Science and Engineering R: Reports. 87 (2015) 1–57. doi:10.1016/j.mser.2014.10.001.
2. T. Duerig, A. Pelton, D. Stöckel, An overview of nitinol medical applications, Materials Science and Engineering: A. 273–275 (1999) 149–160. doi:10.1016/S0921-5093(99)00294-4.
3. J. Mohd Jani, M. Leary, A. Subic, M.A. Gibson, A review of shape memory alloy research, applications and opportunities, Materials & Design (1980-2015). 56 (2014) 1078–1113. doi:10.1016/j.matdes.2013.11.084.
4. M.J. Mahtabi, N. Shamsaei, M.R. Mitchell, Fatigue of Nitinol: The state-of-the-art and ongoing challenges. Journal of the mechanical behavior of biomedical materials. 50 (2015) 228–254. doi:10.1016/j.jmbbm.2015.06.010.
5. N. Figueira, T.M. Silva, M.J. Carmezim, J.C.S. Fernandes, Corrosion behaviour of NiTi alloy, Electrochimica Acta. 54 (2009) 921–926. doi:10.1016/j.electacta.2008.08.001.
6. M. Es-Souni, M. Es-Souni, H. Fischer-Brandies, Assessing the biocompatibility of NiTi shape memory alloys used for medical applications, Analytical and Bioanalytical Chemistry. 381 (2005) 557–567. doi:10.1007/s00216-004-2888-3.
7. G. Eggeler, E. Hornbogen, A. Yawny, A. Heckmann, M. Wagner, Structural and functional fatigue of NiTi shape memory alloys, Materials Science and Engineering A. 378 (2004) 24–33. doi:10.1016/j.msea.2003.10.327.
8. M. Vodˇ, J. Kubásek, P. Novák, P. Sedá, A. Michalcová, D. Vojtěch, M. Voděrová, J. Kubásek, P. Novák, P. Šedá, A. Michalcová, J. Fojt, J. Hanuš, O. Mestek, Effects of short-time heat treatment and subsequent chemical surface treatment on the mechanical properties, low-cycle fatigue behavior and corrosion resistance of a Ni-Ti (50.9at.% Ni) biomedical alloy wire used for the manufacture of stents, Materials Science and Engineering A. 528 (2011) 1864–1876. doi:10.1016/j.msea.2010.10.043.

9. J. Rits, J.A. van Herwaarden, A.K. Jahrome, D. Krievins, F.L. Moll, The Incidence of Arterial Stent Fractures with Exclusion of Coronary, Aortic, and Non-arterial Settings, European Journal of Vascular and Endovascular Surgery. 36 (2008) 339–345. doi:10.1016/j.ejvs.2008.05.005.

10. M.G.A. Bahia, B.M. Gonzalez, V.T.L. Buono, Fatigue behaviour of nickel-titanium superelastic wires and endodontic instruments, Fatigue & Fracture of Engineering Materials and Structures. 29 (2006) 518–523. doi:10.1111/j.1460-2695.2006.01021.x.

11. Y. Okazaki, E. Gotoh, Metal release from stainless steel, Co-Cr-Mo-Ni-Fe and Ni-Ti alloys in vascular implants, Corrosion Science. 50 (2008) 3429–3438. doi:10.1016/j.corsci.2008.09.002.

12. G. Rondelli, Corrosion resistance tests on NiTi shape memory alloy, Biomaterials. 17 (1996) 2003–2008. doi:10.1016/0142-9612(95)00352-5.

13. I. Milošev, B. Kapun, The corrosion resistance of Nitinol alloy in simulated physiological solutions, Materials Science and Engineering: C. 32 (2012) 1087–1096. doi:10.1016/j.msec.2011.11.007.

14. I. Zhitomirsky, Cathodic electrodeposition of ceramic and organoceramic materials. Fundamental aspects, Advances in colloid and interface science. 97 (2002) 279–317. doi:10.1016/S0001-8686(01)00068-9.

15. J. Chevalier, What future for zirconia as a biomaterial?, Biomaterials. 27 (2006) 535–43. doi:10.1016/j.biomaterials.2005.07.034.

16. S. Yen, Mechanism of electrolytic ZrO2 coating on commercial pure titanium, Materials Chemistry and Physics. 63 (2000) 256–262. doi:10.1016/S0254-0584(99)00232-1.

17. I. Espitia-Cabrera, H. Orozco-Hernández, R. Torres-Sánchez, M.E. Contreras-García, P. Bartolo-Pérez, L. Martínez, Synthesis of nanostructured zirconia electrodeposited films on AISI 316L stainless steel and its behaviour in corrosion resistance assessment, Materials Letters. 58 (2004) 191–195. doi:10.1016/S0167-577X(03)00443-9.

18. E. Setare, K. Raeissi, M.A. Golozar, M.H. Fathi, The structure and corrosion barrier performance of nanocrystalline zirconia electrodeposited coating, Corrosion Science. 51 (2009) 1802–1808. doi:10.1016/j.corsci.2009.05.004.

19. X. Pang, I. Zhitomirsky, M. Niewczas, Cathodic electrolytic deposition of zirconia films, Surface and Coatings Technology. 195 (2005) 138–146. doi:10.1016/j.surfcoat.2004.08.216.

20. S.K. Yen, M.J. Guo, H.Z. Zan, Characterization of electrolytic ZrO2 coating on Co–Cr–Mo implant alloys of hip prosthesis, Biomaterials. 22 (2001) 125–133. doi:10.1016/S0142-9612(00)00133-2.

21. F.C. Giacomelli, C. Giacomelli, A.G. De Oliveira, A. Spinelli, Effect of electrolytic ZrO2 coatings on the breakdown potential of NiTi wires used as endovascular implants, Materials Letters. 59 (2005) 754–758. doi:10.1016/j.matlet.2004.11.015.

22. J.H. Sui, W. Cai, Formation of ZrO2 coating on the NiTi alloys for improving their surface properties, Nuclear Instruments and Methods in Physics Research Section B: Beam Interactions with Materials and Atoms. 251 (2006) 402–406. doi:10.1016/j.nimb.2006.06.028.

23. N.I.A. Lopes, N.H.J. Freire, P.D. Resende, L.A. Santos, V.T.L. Buono, Electrochemical deposition and characterization of ZrO2 ceramic nanocoatings on superelastic NiTi alloy, Applied Surface Science. (2018). Accepted for publication.

24. N.I.A. Lopes, L.A.O. Silva, L.A. Santos, V.T.L. Buono, Surface characterization of NiTi superelastic and shape memory alloys after electrolytic polishing, Materials Research. (2017) 1–8. doi:10.1590/1980-5373-mr-2016-0933.

25. S.K. Yen, T.Y. Huang, Characterization of the electrolytic ZrO2 coating on Ti-6A1-4V, Materials Chemistry and Physics. 56 (1998) 214–221. doi:10.1016/S0254-0584(98)00178-3.

26. D. Briggs, Secondary Ion Mass Spectrometry of Polymers, Nuclear Instruments and Methods. ([s.d.]).

27. P. Fardim, B. Holmbom, ToF-SIMS imaging: A valuable chemical microscopy technique for paper and paper coatings, Applied Surface Science. 249 (2005) 393–407. doi:10.1016/j.apsusc.2004.12.041.

28. Y.Y. Lua, L. Yang, C.A. Pew, F. Zhang, W.J.J. Fillmore, R.T. Bronson, A. Sathyapalan, P.B. Savage, J.D. Whittaker, R.C. Davis, M.R. Linford, Polyelectrolytes as new matrices for secondary ion mass spectrometry, Journal of the American Society for Mass Spectrometry. 16 (2005) 1575–1582. doi:10.1016/j.jasms.2005.05.007.

29. I. Zhitomirsky, A. Petric, Cathodic electrodeposition of polymer films and organoceramic films, Materials Science and Engineering B: Solid-State Materials for Advanced Technology. 78 (2000) 125–130. doi:10.1016/S0921-5107(00)00535-3.

30. D.J. Wever, A.G. Veldhuizen, J. de Vries, H.J. Busscher, D.R.A. Uges, J.R. van Horn, Electrochemical and surface characterization of a nickel–titanium alloy, Biomaterials. 19 (1998) 761–769. doi:10.1016/S0142-9612(97)00210-X.

31. X. Liu, P.K. Chu, C. Ding, Surface modification of titanium, titanium alloys, and related materials for biomedical applications, Materials Science and Engineering R: Reports. 47 (2004) 49–121. doi:10.1016/j.mser.2004.11.001.

32. J.X. Zhang, R.F. Guan, X.P. Zhang, Synthesis and characterization of sol-gel hydroxyapatite coatings deposited on porous NiTi alloys, Journal of Alloys and Compounds. 509 (2011) 4643–4648. doi:10.1016/j.jallcom.2011.01.196.

33. T. Kokubo, H. Takadama, How useful is SBF in predicting in vivo bone bioactivity?, Biomaterials. 27 (2006) 2907–2915. doi:10.1016/j.biomaterials.2006.01.017.

34. R.A. Surmenev, M.A. Surmeneva, A.A. Ivanova, Significance of calcium phosphate coatings for the enhancement of new bone osteogenesis - A review, Acta Biomaterialia. 10 (2014) 557–579. doi:10.1016/j.actbio.2013.10.036.

35. S. Nagaraja, S.J.L. Sullivan, P.R. Stafford, A.D. Lucas, E. Malkin, Impact of nitinol stent surface processing on in-vivo nickel release and biological response, Acta Biomaterialia. (2018). doi:10.1016/j.actbio.2018.03.036.

36. A. Figueiredo, P. Modenesi, V. Buono, Low-cycle fatigue life of superelastic NiTi wires, International Journal of Fatigue. 31 (2009) 751–758. doi:10.1016/j.ijfatigue.2008.03.014.

37. S. Shabalovskaya, J. Anderegg, J. Van Humbeeck, Critical overview of Nitinol surfaces and their modifications for medical applications, Acta Biomaterialia. 4 (2008) 447–467. doi:10.1016/j.actbio.2008.01.013.

38. D.J. Wever, a. G. Veldhuizen, M.M. Sanders, J.M. Schakenraad, J.R. van Horn, Cytotoxic, allergic and genotoxic activity of a nickel-titanium alloy, Biomaterials. 18 (1997) 1115–1120. doi:10.1016/S0142-9612(97)00041-0.

39. J.K. Liu, I.H. Liu, C. Liu, C.J. Chang, K.C. Kung, Y.T. Liu, T.M. Lee, J.L. Jou, Effect of titanium nitride/titanium coatings on the stress corrosion of nickel-titanium orthodontic archwires in artificial saliva, Applied Surface Science. 317 (2014) 974–981. doi:10.1016/j.apsusc.2014.08.132.

6. Considerações finais

6.1 Conclusões

Neste trabalho, um revestimento nanocerâmico de zircônia foi desenvolvido e aplicado, tendo como objetivo melhorar as propriedades superficiais de ligas NiTi para uso em materiais biomédicos. Com base nos resultados desta pesquisa, as seguintes conclusões principais são destacadas:

- O polimento eletrolítico utilizando uma solução de 3,5 mol·L^{-1} H_2SO_4 em metanol como eletrólito, à temperatura ambiente de 20°C, reduz efetivamente a rugosidade da superfície, remove as camadas superficiais ricas em níquel e aumenta a resistência à corrosão em *Hank's solution* à 37°C de ligas NiTi superelásticas e com memória de forma.

- O processo de polimento, nas condições descritas nesse estudo, se mostrou potencialmente apropriado para aplicação como tratamento superficial de ligas NiTi para aplicações em biomateriais e como preparação superficial antes da deposição de recobrimentos de ZrO_2.

- A eletrodeposição por corrente pulsada usando soluções aquosas 0,05 mol·L^{-1} de $ZrOCl_2$ e de $ZrO(NO_3)_2$ é eficaz na redução da rugosidade da superfície e no aumento da resistência à corrosão em *Hank's solution* à 37°C de fios superelásticos de NiTi.

- O uso do eletrólito 0,05 mol·L^{-1} de $ZrOCl_2$ em metanol leva à formação de um depósito menos uniforme, com formação de trincas, em decorrência da concentração de cargas.

- A adição de polyDADMAC aos eletrólitos de $ZrOCl_2$, tanto aquoso como metanólico, resulta em um depósito com morfologia superficial mais uniforme, com menor rugosidade e maior resistência à corrosão em *Hank's solution* à 37°C.

- Os melhores resultados de morfologia superficial e de resistência à corrosão foram obtidos usando como eletrólito a solução 0,05 mol·L^{-1} $ZrOCl_2$ + 100 g·L^{-1} H_2O +

1,0 $g \cdot L^{-1}$ polyDADMAC, com o tempo de deposição de 1200 segundos e densidade de corrente de 3 $mA \cdot cm^{-2}$, após preparação superficial dos fios de NiTi por polimento eletrolítico.

- O revestimento de zircônia é capaz de proteger o substrato de NiTi contra corrosão localizada em *Hank's solution* à 37°C, mesmo sem preparação prévia da superfície usando polimento eletrolítico.

- O revestimento de zircônia obtido no fio de NiTi como recebido possui uma espessura média de 54 ± 6 nm, com microestrutura constituída, aparentemente, por cristalitos equiaxiais nanoestruturados, com uma fina camada de TiO_2, com uma espessura de cerca de 8 ± 1 nm presente entre o revestimento e o substrato.

- Quando o polimento eletrolítico é aplicado, antes da deposição, o revestimento obtido é mais homogêneo, com espessura média de 61,7 ± 2,1 nm, aparentemente amorfo, ou constituído por cristalitos extremamente pequenos, sem camada intermediária de TiO_2 evidente.

- Após imersão *Hank's solution* à 37°C pelos períodos de 3, 6 e 12 meses, ambos os fios revestidos e não revestidos de NiTi foram integralmente cobertos por uma camada de fosfato de cálcio e a liberação de íons níquel foi insignificante.

- Ao ser submetido a solicitações mecânicas severas, o revestimento de zircônia apresenta certo grau de trincamento, no entanto, ele não sofre delaminação expressiva.

Dessa forma, revestimentos de zircônia, na forma descrita nesse estudo, podem ser considerados bons candidatos para melhoria da resistência à corrosão de ligas NiTi para aplicações biomédicas, incluindo implantes ortopédicos, *stents* vasculares, fios ortodônticos, instrumentos endodônticos e outros.

6.2 Sugestões para trabalhos futuros

Devido ao baixo coeficiente de atrito e à elevada dureza, recobrimentos de ZrO_2 apresentam grande potencial para melhorar a resistência ao desgaste por abrasão de metais. Para avaliar a capacidade do nano revestimento, obtido nas condições repostadas nesse estudo, para aumentar a resistência ao desgaste, uma avaliação tribológica completa das ligas NiTi revestidas é necessária, incluindo testes de resistência ao desgaste, nanoindentação e teste de resistência ao riscamento por esclerometria.

Espera-se que a aplicação do revestimento aumente a resistência à fadiga de baixo ciclo da liga NiTi, em que a influência da condição da superfície é determinante no comportamento do material. Testes de fadiga térmica também podem ser realizados, com o intuito de avaliar a resistência do revestimento à ciclagem térmica do NiTi.

Buscando elucidar os mecanismos envolvidos na corrosão das ligas NiTi revestidas com ZrO_2, podem ser realizados testes de espectroscopia de impedância eletroquímica. Além disso, em aplicações biomédicas, as ligas NiTi podem estar sujeitas à tribocorrosão, fenômeno em que a corrosão ocorre concomitantemente com um desgaste mecânico, formando-se um sistema complexo, em que a corrosão é acelerada pelo desgaste mecânico e, simultaneamente, o desgaste é influenciado pela corrosão. O nano recobrimento de ZrO_2, obtido neste estudo, pode minimizar os efeitos da tribocorrosão e testes simulando condições de aplicação podem ser realizados para confirmar essa hipótese.

Os resultados deste estudo indicam que o revestimento de ZrO_2 aumenta a resistência à corrosão de ligas NiTi, em condições simulando o ambiente fisiológico, e apresentam bons indicadores de biocompatibilidade e bioatividade. Entretanto, o estado da superfície, incluindo a rugosidade superficial do revestimento, exerce grande influência na adsorção de proteínas e na adesão e proliferação celular. Dessa forma, testes *in vitro* e *in vivo* ainda são necessários para garantir a completa adequação das ligas NiTi, recobertas com nano revestimento ZrO_2 para aplicações biomédicas.

Finalmente, o método de eletrodeposição descrito neste estudo poderá ser testado para aplicação do revestimento em dispositivos biomédicos de formas geométricas mais complexas, tais como *stents* vasculares, filtros de veia cava, limas endodônticas, entre outros.